

TBMCE2024

7th International Conference on
Technologies & Business Models for Circular Economy

Conference Proceedings

Sanja POTRČ

Miloš BOGATAJ

Zdravko KRAVANJA

Zorka NOVAK PINTARIČ

EDITORS



Emerging Technologies and Innovative Approaches –
**from Development Environments
to Practical Implementation**



University of Maribor Press





University of Maribor

Faculty of Chemistry and
Chemical Engineering

7th International Conference on Technologies & Business Models for Circular Economy

Conference Proceedings

Editors

Sanja Potrč

Miloš Bogataj

Zdravko Kravanja

Zorka Novak Pintarič

March 2025

Title	7th International Conference on Technologies & Business Models for Circular Economy
Subtitle	Conference Proceedings
Editors <i>Uredniki</i>	Sanja Potrč (University of Maribor, Faculty of Chemistry and Chemical Engineering) Miloš Bogataj (University of Maribor, Faculty of Chemistry and Chemical Engineering) Zdravko Kravanja (University of Maribor, Faculty of Chemistry and Chemical Engineering) Zorka Novak Pintarič (University of Maribor, Faculty of Chemistry and Chemical Engineering)
Technical editor	Jan Perša (University of Maribor, University Press)
Cover designer	Jan Perša (University of Maribor, University Press)
Graphic material	Authors of proceedings & editors
Conference	TBMCE, International Conference on Technologies & Business Models for Circular Economy
Date and location	September 4 th to September 6 th 2024, Portorož, Slovenia
Organizing Committee	Sanja Potrč (University of Maribor, Slovenia), Miloš Bogataj (University of Maribor, Slovenia), Zorka Novak Pintarič (University of Maribor, Slovenia), Nina Meglič (Chamber of Commerce and Industry of Štajerska, Slovenia), Bojana Žiberna (University of Maribor, Slovenia), Katja Kocuvan (University of Maribor, Slovenia), Samo Simonič (University of Maribor, Slovenia), Jan Drogenik (University of Maribor, Slovenia), Sabina Premrov (University of Maribor, Slovenia), Sonja Roj (University of Maribor, Slovenia), Zdravko Kravanja (University of Maribor, Slovenia)
International Scientific Committee	Zdravko Kravanja (University of Maribor, Slovenia), Zorka Novak Pintarič (University of Maribor, Slovenia), Miloš Bogataj (University of Maribor, Slovenia), Mojca Škerget (University of Maribor, Slovenia), Mariano Martín (University of Salamanca, Spain), Agustín Valera-Medina (Cardiff University, United Kingdom), Petar Uskoković (University of Beograd, Serbia), Elvis Ahmetović (University of Tuzla, Bosnia and Herzegovina), Stefan Willför (Åbo Akademi University, Finland), Adeniyi Isafiade (University of Cape Town, South Africa), Hon Loong Lam (University of Nottingham, Malaysia), Mario Eden (Auburn University, United States of America), Timothy G. Walmsley, (Waikato University, New Zealand), Tomaž Kutrašnik (University of Ljubljana, Slovenia), Blaž Likozar (National Institute of Chemistry, Slovenia), Primož Oven (University of Ljubljana, Slovenia), Dragica Marinič (Slovenian national building and civil engineering institute, Slovenia), Vilma Ducman (Slovenian national building and civil engineering institute, Slovenia), Sanja Potrč (University of Maribor, Slovenia).

Published by **University of Maribor
University Press**
Slomškovo trg 15, 2000 Maribor, Slovenija
<https://press.um.si>, zalozba@um.si

Issued by **University of Maribor
Faculty of Chemistry and Chemical Engineering**
Smetanova ulica 17, 2000 Maribor, Slovenija
<https://www.fkkt.um.si/>, fkkt@um.si

Publication type E-book

Edition 1st

Available at <http://press.um.si/index.php/ump/catalog/book/949>

Published at Maribor, Slovenia, March 2025



© **University of Maribor, University Press**
/ Univerza v Mariboru, Univerzitetna založba

Text © Authors & Potrč, Bogataj, Kravanja, Novak Pintarič, 2025

This book is published under a Creative Commons 4.0 International licence (CC BY-NC-ND 4.0). This license allows reusers to copy and distribute the material in any medium or format in unadapted form only, for noncommercial purposes only, and only so long as attribution is given to the creator.

Any third-party material in this book is published under the book's Creative Commons licence unless indicated otherwise in the credit line to the material. If you would like to reuse any third-party material not covered by the book's Creative Commons licence, you will need to obtain permission directly from the copyright holder.

<https://creativecommons.org/licenses/by-nc-nd/4.0/>



REPUBLIC OF SLOVENIA
**MINISTRY OF THE ECONOMY,
TOURISM AND SPORT**



REPUBLIC OF SLOVENIA
**MINISTRY OF COHESION
AND REGIONAL DEVELOPMENT**

The event was held under the patronage of the Ministry of the Economy, Tourism and Sport and Ministry of Cohesion and Regional Development of the Republic of Slovenia.

Co-organizers:



Sponsors:



CIP - Kataložni zapis o publikaciji
Univerzitetna knjižnica Maribor

330:502.131.1(082) (0.034.2)

INTERNATIONAL Conference on Technologies & Business Models for Circular Economy
(7 ; 2024 ; Portorož)

7th International Conference on Technologies & Business Models for Circular Economy [Elektronski vir] : conference proceedings : [emerging technologies and innovative approaches - from development environments to practical implementation : September 4th to September 6th 2024, Portorož] / editors Sanja Potrč ... [et al.]. - 1st ed. - E-zbornik. - Maribor : University of Maribor, University Press, 2025

Način dostopa (URL): <https://press.um.si/index.php/ump/catalog/book/949>

ISBN 978-961-286-959-5 (PDF)
doi: 10.18690/um.fkkt.1.2025
COBISS.SI-ID 227616771

ISBN 978-961-286-959-5 (pdf)

DOI <https://doi.org/10.18690/um.fkkt.1.2025>

Price Free copie

For publisher Prof. Dr. Zdravko Kačič,
Rector of University of Maribor

**Attribution
Citiranje** Potrč, S., Bogataj, M., Kravanja, Z., Novak Pintarič, Z.,
(eds.). (2025). *7th International Conference on Technologies &
Business Models for Circular Economy: Conference Proceedings*
Maribor: University Press. doi: 10.18690/um.fkkt.1.2025

Table of Contents

1	Rhenium Catalyzed Production of Bio-Based Acrylates From Glyceric Acid Maja Gabrič, Florian Maximilian Harth, Brigita Hočevar, Miha Grilc, Blaž Likozar	1
2	Late-Microwave Irradiation of Alkali-Activated Waste Glass Wool: Linking Dehydration Rate with Thermomechanical Behaviour Barbara Horvat, Anže Tesovnik, Branka Mušič	11
3	Circularity and Longevity of Alkali-Activated Materials: Case-Study Using Rock Wool as a Precursor Barbara Horvat, Sara Tominc	27
4	The Influence of Pearlescent Pigments Printed on Plastic Packaging on the Print Gloss Mirica Karlovits, Blaž Likozar, Uroš Novak	41
5	High-Temperature Radical Copolymerization of Dibutyl Itaconate With N-Butyl Acrylate, Methyl Methacrylate and Styrene Nino Kokol, Tomaž Pirman, Martin Očepek, Robin A. Hutchinson	51
6	Waste Converting Into Products Anita Kovač Kralj	59
7	GEORIS Pavers – A Small Scale Demonstration Within the GEORIS Project Mojca Lončnar, Lubica Kriskova, Christos Georgopoulos, Dimitra Skentzou, Anže Tesovnik, Vilma Ducman	69
8	Unlocking Value From By-Products in Slovenia's Bioeconomy Katja Makovšek, Blaž Likozar, Uroš Novak	83
9	Eco-Friendly Biobleaching: Innovative Technology for Extracting Critical Raw Materials From WEEE Dragica Marinič, Miha Štruc, Primož Oprčkal	97

10	Overview of the Impacts of Additive Production Techniques on the Environment: Production of Continuous Fibers, Direct Laser Sintering of Metals and Selective Laser Sintering Techniques Branka Mušič, Barbara Horvat	111
11	Mineral Waste Into Alkali-Activated Pavements Majda Pavlin, Kaja Zupančič, Alenka Pavlin	121
12	Sewage Sludge Drying and Heating Valorization Tim Tetičkovič, Dušan Klinar, Klavdija Rižnar	141
13	Determination of the Maximum CO₂ Sequestration Capacity of Slovenian Waste Ashes Using Thermogravimetry and Calcimetry Sara Tominc, Vilma Ducman	151
14	The Carbon Footprint of Different Construction and Demolition Waste Management Methods Janez Turk, Patricija Ostruh, Anja Kodrič, Tajda Potrč Obrecht	161
15	Evaluation of the Performance of Clay-Based Bricks With the Addition of Co-combustion Ash Lea Žibret, Ivana Carević, Nina Štirmer, Ivan Koloda, Mojca Vrčon Mihelj, Miha Kragelj, Vilma Ducman	169

RHENIUM CATALYZED PRODUCTION OF BIO-BASED ACRYLATES FROM GLYCERIC ACID

MAJA GABRIČ,¹ FLORIAN MAXIMILIAN HARTH,¹
BRIGITA HOČEVAR,¹ MIHA GRILC,^{1,2} BLAŽ LIKOZAR¹

¹ National Institute of Chemistry, Ljubljana, Slovenia
maja.gabric@ki.si, florian.harth@ki.si, brigita.hocevar@ki.si, miha.grilc@ki.si,
blaz.likozar@ki.si

² University of Nova Gorica, Vipavska cesta 13, 5000 Nova Gorica, Slovenia
miha.grilc@ki.si

Bio-based glyceric acid, an oxidation product of glycerol, was converted into acrylic acid and its esters, crucial polymer precursors, using a new catalytic approach in a sustainable manner. Avoiding gaseous H₂ or dangerous chemicals, the crucial step is Re-catalyzed deoxydehydration (DODH) in an alcoholic medium. In addition to being a solvent and hydrogen donor, alcohol also forms protective ester groups with acrylic and glyceric acids. This study examined several catalysts, alcohols, the presence of H₂, and temperatures. Acrylic acid and methyl acrylate were produced in 72 hours with a 65% combined yield using a Re/C catalyst and methanol at 150 °C under N₂. This versatile process can also be transferred to other alcohols enabling the production of various alkyl acrylates and monomers.

DOI
[https://doi.org/
10.18690/um.fkkt.1.2025.1](https://doi.org/10.18690/um.fkkt.1.2025.1)

ISBN
978-961-286-959-5

Keywords:
acrylic acid,
heterogenous catalysis,
rhenium,
deoxydehydration,
glyceric acid



University of Maribor Press

1 Introduction

Acrylic acid (AA) and acrylate esters are essential building blocks in the polymer industry. To reduce a dependency on fossil fuels, bio-based production of acrylic acid and its ester from glycerol has been explored. Various routes have been explored in review articles (Avasthi et al., 2020; Beerthuis et al., 2015; Sun et al., 2017) and detailed studies (Katryniok et al., 2011a; Wang et al., 2022a). Mainly conversion from glycerol to acrylic happen through catalytic dehydration to acrolein (Abdullah et al., 2022; Katryniok et al., 2010 or ally alcohol (Dethlefsen & Fristrup, 2015; Jentoft, 2022), which are then further oxidized to acrylic acid (Li & Zhang, 2016; Yang et al., 2016).

Another conversion route involves glycerol oxidation to lactic acid (Razali & Abdullah, 2017b) or glyceric acid (GA) (Fan et al., 2021b), followed by dehydration to acrylic acid or acrylates (Huang et al., 2023a, 2023b). Our study presents the first heterogeneously catalyzed conversion of GA into AA or esters, avoiding toxic reagents like indoline (Boucher-Jacobs & Nicholas, n.d.) and relying on solid Re catalysts.

From our previous study for DODH of mucic acid (Brigita Hočevár et al., n.d.; Harth et al., 2024) the commercial Re/C showed the most promising results and that is why it was chosen for that reaction as well. In this study different temperatures in either hydrogen or an inert atmosphere were observed over time.

2 Material and Methods

2.1 Chemicals used

Glyceric acid (GA; 20–22 wt% aqueous solution, LD-2,3-dihydroxypropanoic acid) was sourced from TCI Chemicals. Methanol (MeOH; >99.8%) was obtained from J.T. Baker, while alternative alcohols such as ethanol (99.9%, J.T. Baker), isopropanol (>99.8%, Merck), n-propanol (>99.5%, Sigma-Aldrich), n-butanol (>99.9%, Honeywell), and n-pentanol (>99%, Sigma-Aldrich) were also tested. Homogeneous catalysts, including Re_2O_7 , $(\text{NH}_4)\text{ReO}_4$, and KReO_4 ($\geq 99\%$, Sigma Aldrich), were used without pretreatment. Supported rhenium catalysts (5 wt% Re) such as Re/C, Re/TiO₂, Re/SiO₂, Re/Al₂O₃, and Re/H-ZSM-5 were procured from

Riogen Inc. and underwent pre-treatment via reductive heating at 400 °C under H₂ flow. N₂ (5.0) and H₂ gases were provided by Messer.

2.2 Reaction set up

Catalytic experiments were conducted in stainless steel high-pressure batch reactors (Parr 5000 Multi Reactor System, 75 mL capacity) (Figure 1) with magnetic stirring and independent heating. A typical experiment involved adding 500 mg of GA solution and 45.0 mL of alcohol (*e.g.*, methanol) to achieve a ~20 mM GA solution. Rhenium catalysts were added at a fixed GA-to-Re molar ratio of 25:1, corresponding to 0.04 mmol of Re. The reactor was sealed, purged three times with N₂, pressurized to 5 bar_g with N₂ or H₂, and stirred at 600 rpm. Heating was set to a ramp of 4 K min⁻¹ to the desired temperature (typically 150 °C, with additional tests at 120, 165, and 180 °C) and held isothermal for 72 hours. After the reaction, the reactor was cooled to room temperature, depressurized, purged with N₂, and opened to collect the product mixture for analysis. Samples were taken during reaction as well.



Figure 1: Parr reactor system

2.3 Analytical methods

Gas chromatography-mass spectrometry (GC-MS) analysis was performed using a Shimadzu GCMS-QP 2010 Ultra system (Kyoto, Japan) equipped with a Zebron ZB-5MSi nonpolar capillary column (length: 60 m, diameter: 0.25 mm, film thickness: 0.25 μm). Compound identification was conducted via mass spectrometry, scanning fragment ions in the range of 35–500 m/z , and matching against the NIST 17 (National Institute of Standards and Technology) library. Quantification was achieved using a flame ionization detector (FID). The analysis employed a temperature-programmed method: the column oven was initially held at 333 K for 5.5 minutes, then ramped to 563 K at a rate of 20 K min^{-1} and held constant for 8 minutes. The injector and detector were maintained at 563 K, with an injection volume of 0.5 μL and a split ratio of 5:1. Product quantification was based on FID peak areas and external calibration curves derived from commercially available reference compounds. Although GA could not be detected, probably due to its decomposition or low volatility, several products were successfully identified, including glycerate esters, acrylic acid, propanoic acid and its methyl esters — methyl acrylate and methyl propanoate.

3 Results and discussion

3.1 GCMS analysis

All results of the reaction products were analyzed by GC-MS. Figure 2 represents a typical chromatogram of product spectra.

3.2 Screening of different temperatures and gas phases

The results of the screening of different temperatures and different gas phases are represented in the Figure 2. The temperature variation shows that expectedly all reactions involved are enhanced with increasing temperature, i.e. DODH, hydrogenation and esterification, which results in other products. However, considering the market value of the unsaturated products acrylic acid and methyl acrylate, the most optimal temperature for N_2 atmosphere is 150 $^\circ\text{C}$, and yields near 60 % were obtained after 72 h.

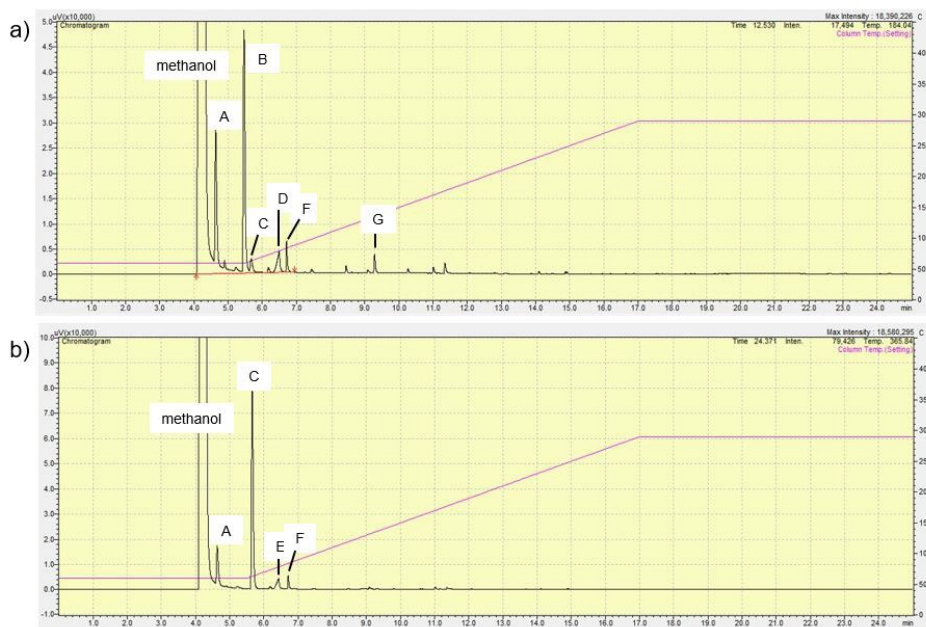


Figure 2: Representative gas chromatograms of product mixtures. Pink line represents a GC oven temperature. The main products are: A – methylal, oxidation product of methanol; B – methyl acrylate (5); C – methyl propanoate (7); D – acrylic acid (4); E – propanoic acid.

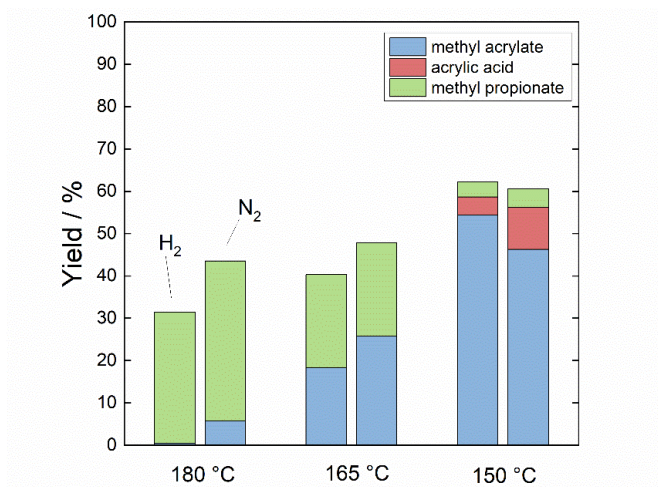


Figure 2: Yields of DODH products after 10 and 72 h of glyceric acid over Re/C in methanol at different reaction temperatures and under either inert N₂ gas or reducing H₂ gas atmosphere of 5 bar_g

The results of the screening of different temperatures and different gas phases are represented in the Figure 2. The temperature variation shows that expectedly all reactions involved are enhanced with increasing temperature, i.e. DODH, hydrogenation and esterification, which results in other products. However, considering the market value of the unsaturated products acrylic acid and methyl acrylate, the most optimal temperature for N₂ atmosphere is 150 °C, and yields near 60 % were obtained after 72 h.

3.3 Reaction over time

All samples were measured with GCMS. By stopping the reaction at shorter intervals, it becomes possible to obtain other products as well. The results are represented in the Figure 3. To gain a deeper understanding of the reaction mechanism and kinetics, microkinetic models will be employed in future studies.

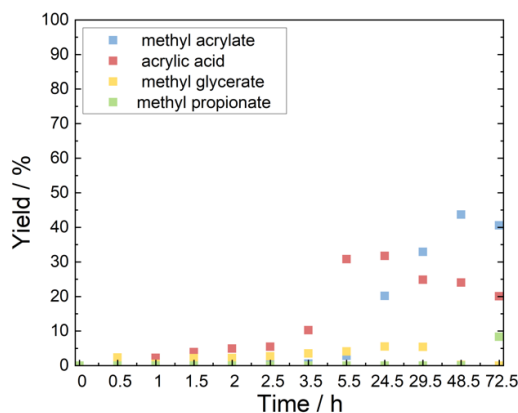


Figure 3: Example of one reaction with yields over time of deoxydehydration products over Re/C (Riogen) catalysts in methanol at T = 150°C, 5 bar_g, N₂ atmosphere. Reaction conditions: 100 mg of glyceric acid, 45.0 mL methanol, 140 mg catalyst, 150 °C, 5 bar N₂, 72 h.

4 Conclusion

This study demonstrates that the Re-catalyzed deoxydehydration (DODH) of glyceric acid is a promising and sustainable method for converting glycerol-derived glyceric acid into acrylates. The reaction was successfully carried out using Re/C,

surpassing typical homogeneous catalysts. The process, conducted in alcohols that also act as reducing agents, eliminates the need for hazardous reagents like H₂. Acrylic acid readily forms alkyl acrylates with alcohols, and different alcohols enable the production of a variety of alkyl acrylates. The highest yield of methyl acrylate (>45 %) was achieved over Re/C at 150 °C in methanol after 72 hours.

This approach not only improves acrylate production efficiency but also opens new research directions. Future work should focus on enhancing catalyst activity, selectivity, stability, and reusability, as well as applying microkinetic models to better understand and optimize acrylate formation.

Acknowledgments

This research was funded by the Slovenian Research and Innovation Agency (research projects N2–0242 and J1–3020 and research core funding P2–0152).

References

- Abdullah, A., Zuhairi Abdullah, A., Ahmed, M., Khan, J., Shahadat, M., Umar, K., & Alim, M. A. (2022). A review on recent developments and progress in sustainable acrolein production through catalytic dehydration of bio-renewable glycerol. *Journal of Cleaner Production*, *341*, 130876. <https://doi.org/10.1016/j.jclepro.2022.130876>
- Avasthi, K., Bohre, A., Grilc, M., Likozar, B., & Saha, B. (2020). Advances in catalytic production processes of biomass-derived vinyl monomers. *Catalysis Science & Technology*, *10*(16), 5411–5437. <https://doi.org/10.1039/D0CY00598C>
- Beerthuis, R., Rothenberg, G., & Shiju, N. R. (2015). Catalytic routes towards acrylic acid, adipic acid and ε-caprolactam starting from biorenewables. *Green Chemistry*, *17*(3), 1341–1361.
- Blanco, E., Loidant, S., & Pinel, C. (2016a). Valorization of Lactic Acid and Derivatives to Acrylic Acid Derivatives: Review of Mechanistic Studies. In M. Schlaf & Z. C. Zhang (Eds.), *Reaction Pathways and Mechanisms in Thermocatalytic Biomass Conversion II* (pp. 39–62). Springer, Singapore. https://doi.org/10.1007/978-981-287-769-7_3
- Blanco, E., Loidant, S., & Pinel, C. (2016b). Valorization of Lactic Acid and Derivatives to Acrylic Acid Derivatives: Review of Mechanistic Studies. In M. Schlaf & Z. C. Zhang (Eds.), *Reaction Pathways and Mechanisms in Thermocatalytic Biomass Conversion II: Homogeneously Catalyzed Transformations, Acrylics from Biomass, Theoretical Aspects, Lignin Valorization and Pyrolysis Pathways* (pp. 39–62). Springer Singapore. https://doi.org/10.1007/978-981-287-769-7_3
- Bonnotte, T., Paul, S., Araque, M., Wojcieszak, R., Dumeignil, F., & Katryniok, B. (2018a). Dehydration of Lactic Acid: The State of The Art. *ChemBioEng Reviews*, *5*(1), 34–56. <https://doi.org/10.1002/CBEN.201700012>
- Bonnotte, T., Paul, S., Araque, M., Wojcieszak, R., Dumeignil, F., & Katryniok, B. (2018b). Dehydration of Lactic Acid: The State of The Art. *ChemBioEng Reviews*, *5*(1), 34–56. <https://doi.org/10.1002/cben.201700012>
- Boucher-Jacobs, C., & Nicholas, K. M. (n.d.). *Oxo-Rhenium-Catalyzed Deoxydehydration of Polyols with Hydroaromatic Reductants*. *34*(10), 1985–1990. <https://doi.org/10.1021/acs.organomet.5b00226>

- Brigita Hočevar, Hočevar, B., Anže Prašnikar, Likozar, B., Huš, M., Matej Huš, Huš, M., & Grilc, M. (n.d.). *H 2 -Free Re-Based Catalytic Dehydroxylation of Aldaric Acid to Muconic and Adipic Acid Esters*. <https://doi.org/10.1002/ange.202010035>
- Dethlefsen, J. R., & Frstrup, P. (2015). Rhenium-Catalyzed Deoxydehydration of Diols and Polyols. *ChemSusChem*, 8(5), 767–775. <https://doi.org/https://doi.org/10.1002/cssc.201402987>
- Dodekatos, G., Schünemann, S., & Tüysüz, H. (2018). Recent Advances in Thermo-, Photo-, and Electrocatalytic Glycerol Oxidation. *ACS Catalysis*, 8(7), 6301–6333. <https://doi.org/10.1021/acscatal.8b01317>
- Fan, L., Liu, B., Liu, X., Senthilkumar, N., Wang, G., & Wen, Z. (2021a). Recent Progress in Electrocatalytic Glycerol Oxidation. *Energy Technology*, 9(2), 2000804. <https://doi.org/https://doi.org/10.1002/ente.202000804>
- Fan, L., Liu, B., Liu, X., Senthilkumar, N., Wang, G., & Wen, Z. (2021b). Recent Progress in Electrocatalytic Glycerol Oxidation. *Energy Technology*, 9(2). <https://doi.org/10.1002/ente.202000804>
- Galadima, A., & Muraza, O. (2016). A review on glycerol valorization to acrolein over solid acid catalysts. *Journal of the Taiwan Institute of Chemical Engineers*, 67, 29–44. <https://doi.org/https://doi.org/10.1016/j.jtice.2016.07.019>
- Grasselli, R. K., & Trifirò, F. (2017). Acrolein and acrylic acid from biomass. *Rendiconti Lincei*, 28(1), 59–67.
- Harth, F. M., Gabrič, M., Teržan, J., Hočevar, B., Gyergyek, S., Likozar, B., & Grilc, M. (2024). Tailoring selective de-hydroxylation/hydrogenation reactions of bio-based aldaric acids towards adipic acid derivatives by Re catalyst metal–support interactions. In *Catalysis Today* (Vol. 441). Elsevier B.V. <https://doi.org/10.1016/j.cattod.2024.114879>
- Huang, L., Wai, M. H., & Kawi, S. (2023a). On the catalytic vapor-phase dehydration of lactic acid to acrylic acid: a systematic review. *Reaction Chemistry & Engineering*, 8(3), 502–537. <https://doi.org/10.1039/D2RE00462C>
- Huang, L., Wai, M. H., & Kawi, S. (2023b). On the catalytic vapor-phase dehydration of lactic acid to acrylic acid: a systematic review. *Reaction Chemistry & Engineering*, 8(3), 502–537. <https://doi.org/10.1039/D2RE00462C>
- Jentoft, F. C. (2022). Transition metal-catalyzed deoxydehydration: missing pieces of the puzzle. *Catalysis Science & Technology*, 12(21), 6308–6358. <https://doi.org/10.1039/D1CY02083H>
- Katryniok, B., Kimura, H., Skrzyńska, E., Girardon, J.-S., Fongarland, P., Capron, M., Ducoulombier, R., Mimura, N., Paul, S., & Dumeignil, F. (2011a). Selective catalytic oxidation of glycerol: perspectives for high value chemicals. *Green Chemistry*, 13(8), 1960–1979. <https://doi.org/10.1039/C1GC15320J>
- Katryniok, B., Kimura, H., Skrzyńska, E., Girardon, J.-S., Fongarland, P., Capron, M., Ducoulombier, R., Mimura, N., Paul, S., & Dumeignil, F. (2011b). Selective catalytic oxidation of glycerol: perspectives for high value chemicals. *Green Chemistry*, 13(8), 1960. <https://doi.org/10.1039/c1gc15320j>
- Katryniok, B., Paul, S., Bellière-Baca, V., Rey, P., & Dumeignil, F. (2010). Glycerol dehydration to acrolein in the context of new uses of glycerol. *Green Chemistry*, 12(12), 2079–2098. <https://doi.org/10.1039/C0GC00307G>
- Li, X., & Zhang, Y. (2016). Highly Efficient Process for the Conversion of Glycerol to Acrylic Acid via Gas Phase Catalytic Oxidation of an Allyl Alcohol Intermediate. *ACS Catalysis*, 6(1), 143–150. <https://doi.org/10.1021/acscatal.5b01843>
- Liu, L., Ye, X. P., & Bozell, J. J. (2012). A Comparative Review of Petroleum-Based and Bio-Based Acrolein Production. *ChemSusChem*, 5(7), 1162–1180. <https://doi.org/https://doi.org/10.1002/cssc.201100447>
- Mäki-Arvela, P., Simakova, I. L., Salmi, T., & Murzin, D. Yu. (2014). Production of Lactic Acid/Lactates from Biomass and Their Catalytic Transformations to Commodities. *Chemical Reviews*, 114(3), 1909–1971. <https://doi.org/10.1021/cr400203v>

- Othman, P. N. A. M., Karim, N. A., & Kamarudin, S. K. (2021a). Research and innovation in the electrocatalyst development toward glycerol oxidation reaction. *International Journal of Energy Research*, 45(9), 12693–12727. <https://doi.org/https://doi.org/10.1002/er.6712>
- Othman, P. N. A. M., Karim, N. A., & Kamarudin, S. K. (2021b). Research and innovation in the electrocatalyst development toward glycerol oxidation reaction. *International Journal of Energy Research*, 45(9), 12693–12727. <https://doi.org/10.1002/er.6712>
- Razali, N., & Abdullah, A. Z. (2017a). Production of lactic acid from glycerol via chemical conversion using solid catalyst: A review. *Applied Catalysis A: General*, 543, 234–246. <https://doi.org/https://doi.org/10.1016/j.apcata.2017.07.002>
- Razali, N., & Abdullah, A. Z. (2017b). Production of lactic acid from glycerol via chemical conversion using solid catalyst: A review. *Applied Catalysis A: General*, 543, 234–246. <https://doi.org/https://doi.org/10.1016/j.apcata.2017.07.002>
- Singh, N., Kalbande, P. N., & Sudarsanam, P. (2022). Heterogeneous Catalytic Routes for Bio-glycerol-Based Acrylic Acid Synthesis. In *Biodiesel Production* (pp. 345–354). <https://doi.org/https://doi.org/10.1002/9781119771364.ch18>
- Sun, D., Yamada, Y., Sato, S., & Ueda, W. (2017). Glycerol as a potential renewable raw material for acrylic acid production. *Green Chemistry*, 19(14), 3186–3213.
- Talebian-Kiakalaieh, A., Amin, N. A. S., & Hezaveh, H. (2014). Glycerol for renewable acrolein production by catalytic dehydration. *Renewable and Sustainable Energy Reviews*, 40, 28–59. <https://doi.org/https://doi.org/10.1016/j.rser.2014.07.168>
- Villa, A., Dimitratos, N., Chan-Thaw, C. E., Hammond, C., Prati, L., & Hutchings, G. J. (2015). Glycerol Oxidation Using Gold-Containing Catalysts. *Accounts of Chemical Research*, 48(5), 1403–1412. <https://doi.org/10.1021/ar500426g>
- Wang, K., Yang, Z., Ma, Y., Zhao, W., Sun, J., Lu, T., & He, H. (2022a). Recent advances in the utilization of glycerol for the production of lactic acid by catalysis. *Biofuels, Bioproducts and Biorefining*, 16(5), 1428–1454. <https://doi.org/https://doi.org/10.1002/bbb.2410>
- Wang, K., Yang, Z., Ma, Y., Zhao, W., Sun, J., Lu, T., & He, H. (2022b). Recent advances in the utilization of glycerol for the production of lactic acid by catalysis. *Biofuels, Bioproducts and Biorefining*, 16(5), 1428–1454. <https://doi.org/10.1002/bbb.2410>
- Wen, L., Zhang, X., & Abdi, F. F. (2024). Photoelectrochemical glycerol oxidation as a sustainable and valuable technology. *Materials Today Energy*, 44, 101648. <https://doi.org/10.1016/j.mtener.2024.101648>
- Yang, S., Kim, M., Yang, S., Kim, D. S., Lee, W. J., & Lee, H. (2016). Production of acrylic acid from biomass-derived allyl alcohol by selective oxidation using Au/ceria catalysts. *Catalysis Science & Technology*, 6(10), 3616–3622. <https://doi.org/10.1039/C5CY02099A>

LATE-MICROWAVE IRRADIATION OF ALKALI-ACTIVATED WASTE GLASS WOOL: LINKING DEHYDRATION RATE WITH THERMOMECHANICAL BEHAVIOUR

BARBARA HORVAT,¹ ANŽE TESOVNIK,² BRANKA MUŠIČ²

¹ Milan Vidmar Electric Power Research Institute, Ljubljana, Slovenia
barbara.horvat@eimv.si

² Slovenian National Building and Civil Engineering Institute, Ljubljana, Slovenia
anze.tesovnik@zag.si, branka.music@zag.si

Building and civil engineering conventional inorganic binding materials represent a significant burden for the environment, leading to the search for more sustainable materials. One of the potential solutions is alkali-activated materials (AAMs), which can be made solely from waste materials and at lower temperatures. However, reaction rate and solidification time depend on the precursor used. To enhance the speed of solidification, the curing temperature can be increased, but from the inside out not to create the crust on the surface, which would hinder the dehydration. Therefore, three mixtures of alkali-activated glass wool, a slow-in-alkali media solidifying precursor, were irradiated with low- and high-power microwaves in the late curing stage till complete dehydration, to determine the influence of artificial volumetric solidification onto thermomechanical behaviour of the AAM. As the electromagnetic power increased, the damages in the AAM became more severe, resulting in a reduction in mechanical strength.

DOI
[https://doi.org/
10.18690/um.fkkt.1.2025.2](https://doi.org/10.18690/um.fkkt.1.2025.2)

ISBN
978-961-286-959-5

Keywords:
microwave irradiation,
electromagnetic
dehydration,
glass wool,
alkali-activated material,
mechanical performance



University of Maribor Press

1 Introduction

Building and civil engineering inorganic binding materials currently available on the market (e.g. cement, mortar, concrete, ceramics) represent a significant burden for the environment ('The Industry Creating a Third of the World's Waste', n.d.):

- Continuous consumption of raw materials (yearly almost 70 m% of the mass of Mount Everest),
- The high energy demands of production leading to a significant carbon footprint (approximately 40% of man-caused CO₂), and
- Constant waste generation (more than 30 m% of global waste).

While building materials already act as a "black hole" for various types of waste, climate change calls for an urgent transition to more sustainable alternatives, like alkali-activated materials (AAMs) (Škvára 2007; Obonyo et al. 2014). AAMs can be made solely from (local) waste materials and at lower temperatures (Pacheco-Torgal, Castro-Gomes, and Jalali 2008), which both positively affect the influence on the environment. The only requirement from the waste material is that it contains enough Si and Al in the amorphous content (Horvat and Ducman 2019), like glass wool (GW) (Horvat et al. 2018).

GW is a fibrous material that consumes at the end of its use a lot of space in landfills due to its low density (Horvat et al. 2018), therefore, using waste GW as the source of Si and Al in alkali activation for building products is an ideal solution. However, GW needs a longer time and/or higher temperature for solidification (Pavlin et al. 2021), which is a significant environmental and economic drawback.

To speed up the solidification process in AAMs based on GW without the use of conventional heat chambers and driers, surface heating can be replaced with volumetric heating. Unlike conventional surface heating, which requires hours or days, volumetric heating can finalize the AAM within minutes (Horvat et al. 2022; 2023). However, the rapid finalisation of a freshly prepared mixture of the precursor and alkali (slurry) with high-power microwaves ends as a foam and not a potential load-bearing material (Horvat et al. 2023).

Therefore, when foamed AAM is not desired, volumetric heating can be applied after the initial conventional heating (Tesovnik and Horvat 2024a; 2024b). However, low-power microwaves can lead to foamed material when the curing stage is not completely finalised (Tesovnik and Horvat 2024a), which insists that AAM can be exposed to microwaves for a period shorter than the time needed for complete dehydration.

Nonetheless, before evaluating the point to which material can be exposed to electromagnetic irradiation, it is necessary to study the exposure limit beyond which no further changes occur. Therefore, this study analysed three mixtures of alkali-activated GW irradiated with low- and high-power microwaves in the late curing stage till complete dehydration to determine the influence on the thermomechanical and structural behaviour of the AAM. The study showed that high-power microwaves lead to macro-fractures which cause a significant decrease in mechanical performance, while low-power microwaves cause less significant damage. The most important finding in this study was the existence of a critical point of microwave power, where the amount of water does not influence the time of dehydration.

2 Experimental

2.1 Materials and characterisation of the materials

The following ingredients were used in the synthesis of AAMs:

- Waste GW with organic material on its surface (loss on ignition at 550 °C is 5.7 m%) was used as a precursor. GW was milled in a vibrating disk mill (Labor-Scheibenschwingmühle TS.250, Siebtechnik GmbH) and sieved below 63 µm.
- Na-silicate solution (Geosil, 344/7, Woelner, 16.9 m% Na₂O, 27.5 m% SiO₂, 55.6 H₂O), which was used as received as the only (aqueous liquid) alkali.

In the present study, there was no theoretical limit (Horvat and Ducman 2019) on the amount of alkali added to prevent efflorescence, as GW naturally contains such a high amount of Na (Horvat et al. 2018) that efflorescence in alkali-activated GW would happen without added alkali (see Tables 1 and 2) – of course, if GW would dissolve and react in water itself. Namely, the molar ratio between amorphous

elements from the first group of the periodic table and amorphous Al is higher than 1.

To evaluate the amount of excessive alkali in the mixtures (and GW), GW (dried, milled and sieved below 63 μm) was analysed by:

- X-ray fluorescence (XRF; Thermo Scientific ARL Perform'X Sequential XRF) to determine the chemical composition (elements from fluorine to americium). The main results are collected in Table 1, raw analysis is in the open repository.
- X-ray diffraction (XRD; Empyrean PANalytical X-ray Diffractometer, Cu X-Ray source; under clean room conditions in the 2θ range from 4 to 70° and step 0.0263°) to qualitatively determine the minerals. Results are shown in Figure 1. Because the determination of the most prominent peak at $\sim 44.5^\circ$ (and a few more on the amorphous halo) might lead to a false positive result, the mostly amorphous pattern was considered as completely amorphous.

Therefore, elements present in the amorphous content, which is calculated as the difference between XRF and XRD (Horvat and Ducman 2019), are elements measured by XRF. The results of the GW evaluation are shown in Table 1.

Table 1: Mass percentage (m%) of crucial elements in alkali activation.

Elements [m%]	Na	K	Mg	Ca	Al	Si	Content [m%]
XRF	13.5	0.5	5.6	8.7	6.1	62.5	100
XRD	0	0	0	0	0	0	0*
Amorphous	13.5	0.5	5.6	8.7	6.1	62.5	100

*The one prominent peak (at $2\theta \sim 44.5^\circ$), which indicates that crystalline material is present in GW, was not enough to determine the mineral(s) present in GW. Nonetheless, their amount is insignificant.

The response of GW and all AAM samples to thermal exposure was measured in platinum crucibles using thermogravimetric analysis (TGA; TGA Q5000IR analyser, TA Instruments, New Castel, DE, United States) in constant airflow. Masses of (milled and sieved below 63 μm) materials used for analysis ranged from 6 ± 2 mg. Because the focus of TGA analysis was only on water and organic compound behaviour, which can be influenced by microwave irradiation, the temperature range was from 25 to 600 $^\circ\text{C}$. The heating rate was 5 $^\circ\text{C}/\text{min}$.

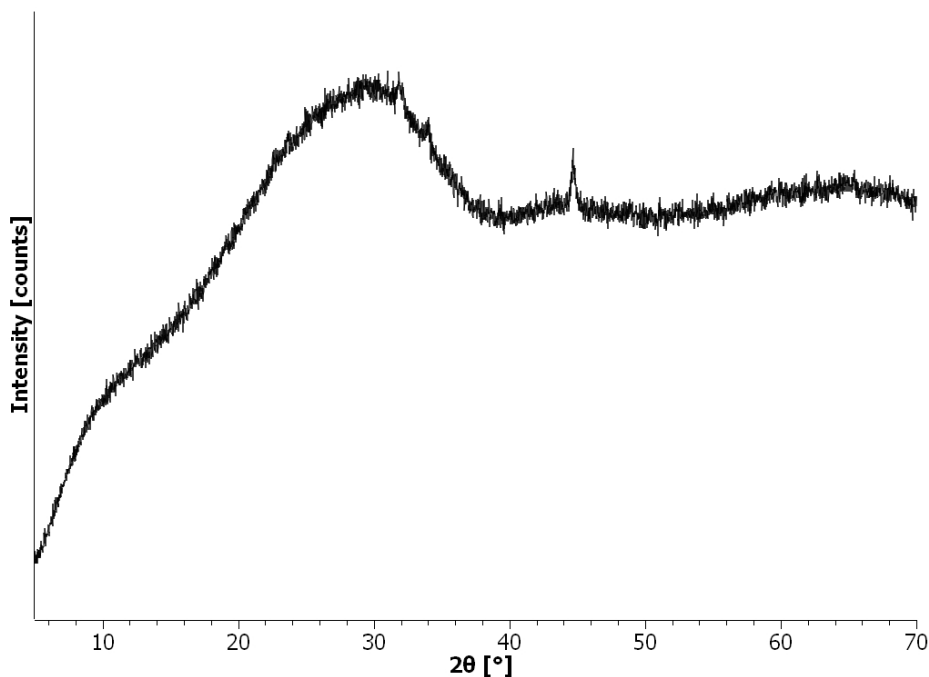


Figure 1: XRD pattern of waste GW.

Source: own.

The compressive strength, which determines if the building industry product has the potential to bear the load, was measured with the compressive and bending strength testing machine (ToniTechnik ToniNORM) on 7- and 21-day-old AAM prisms.

2.2 Synthesis of the material

AAMs were prepared in three different recipes (100-50, 100-80, and 100-100, where the numbers indicate the mass of precursor to the mass of alkali) shown in Table 2 along with their chemical compositions, which are relevant to the potential of efflorescence occurrence and compactness of AAM (Duxson et al. 2005) as follows:

- If the molar ratio between amorphous elements from the first group of the periodic table and Al (1st/Al), is higher than 1, efflorescence will eventually occur.

- If the molar ratio between amorphous Si and Al (Si/Al) is 1.9, compressive strength will be the highest, if this ratio is below 1.4, the structure will be porous, if it is above 1.9, compressive strength will be lower than when the molar ratio is 1.9.

The theoretical molar ratio of GW and AAM mixtures (shown in Table 2) was calculated using software designed in MS Excel platform, developed in project no. C3330-17-529032 “Raziskovalci-2.0-ZAG-529032” (Horvat and Ducman 2019) and upgraded in the ARIS project under grant no. J2-3035.

Table 2: Chemical composition of the samples (precursor and AAMs) with mixture recipes.

Sample	1 st /Al [mol/mol]	Si/Al [mol/mol]	Precursor [g]	Alkali [g]	H ₂ O in alkali [g]	Na in alkali [g]
GW	3.6	8.5	/	/	/	/
100-50	5.9	10.5	100	50	27.8	6.3
100-80	7.3	11.6	100	80	44.5	10.0
100-100	8.2	12.4	100	100	55.6	12.5

The prechosen masses of GW and alkali were mixed at up to 1000 rpm. Freshly mixed slurries were moulded into 2×2×8 cm³ prisms in a rubber mould, and cured for 6 days at 40 °C in the heating-drying chamber (Memmert, Universal Oven U). On day 7, prisms were demoulded and treated further: one-third of the samples was irradiated with microwaves at 100 W, the second third at 1000 W, both until complete dehydration, and the last third was left to evolve further at room conditions as a reference.

Dehydration was performed in an inverter microwave oven (Panasonic, NN-CD575M; frequency 2.45 GHz, magnetron source; working in mode with constant presence of microwaves) following the procedure shown in Figure 2:

- A ceramic plate (cooled to room temperature) was put into the centre of the microwave chamber.
- 7-day-old bulk prisms were placed individually into the centre of the ceramic plate.
- The prism on the ceramic plate was covered by a clean and dry 1000 ml beaker (cooled to room temperature) placed upside-down, without touching

the prism (the beaker cannot withstand the temperatures created in the prism by electromagnetic irradiation – the beaker explodes if it gets into contact with the heated prism). On the left and right side of the prism, a paper towel was placed to absorb condensed water to disable its absorption by the prism.

- Set-up was irradiated at the prechosen power (100 W, the lowest possible power, and 1000 W, the highest possible power) first for 30 s, then every additional irradiation for 10 s, until there was no condensed moisture seen on the beaker.
- The beaker and plate were replaced with clean, dry and cooled to room temperature beaker and plate for every additional irradiation. The time of the prism kept at the room conditions between irradiations was as minimal as possible.

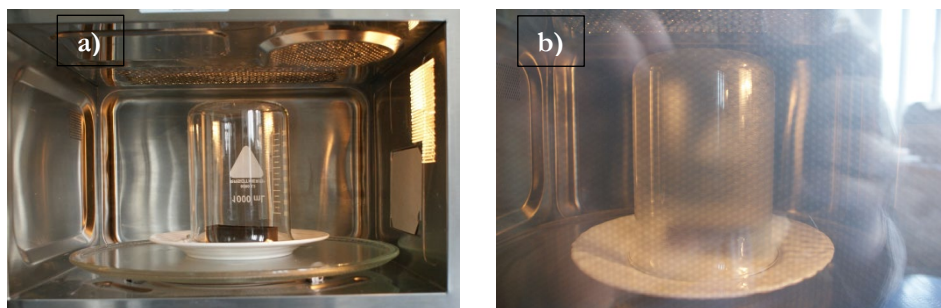


Figure 2: Dehydration set up a) before irradiation and b) during irradiation.

Source: own.

3 Results and discussion

7-day-old AAM prisms of all three mixtures are shown in Figure 3, from which it can be concluded, that the amount of liquid defines the rheology of the slurry (fresh mixture of precursor and liquid alkali) and the moulding procedure. If there is not enough liquid, AAM can end as ellipsoidal aggregates, unless the aggregates (or wetted powder) are physically pressed in the mould (mixture 100-50) into a prism or a tablet. Therefore, for this study, the mixture 100-50 was manually pressed directly into the mould (layer by layer), while both other mixtures (100-80 and 100-100) were poured into the mould. While there is no inhomogeneity obvious in the mixture 100-

50 (the sample is overall made from small spheres of the same colour), for mixtures 100-80 and 100-100 buoyancy is expressed by the lower lighter coloured part of the prism, and the upper darker part of the prism. The latter expresses a sticky nature (when touched with fingers), while the lower part is solid and “non-wet”, meaning that with alkali-reacted organic material (which is present on the surface of the GW) travels towards the top surface of the prism. Therefore, the physically optimal mixture is somewhere between 100-50 and 100-80, when buoyancy on a large scale will not occur.

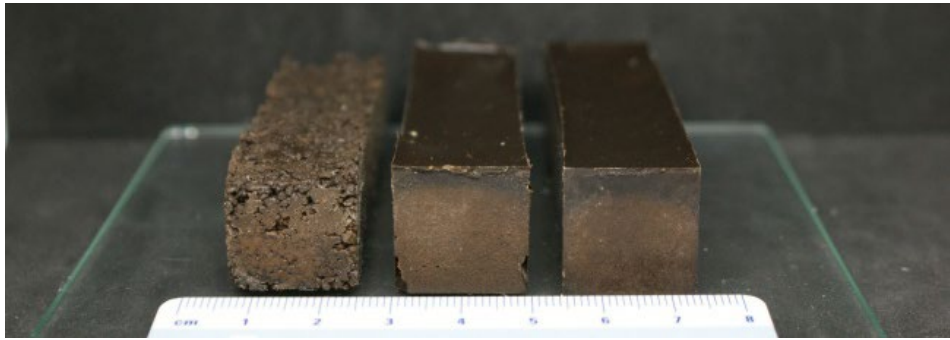


Figure 3: 7-day-old non-irradiated prisms. Mixtures from left to right: 100-50, 100-80, and 100-100.

Source: own.

From the cross-sections of the prisms, shown in Figure 4, local inhomogeneities present in samples not exposed to the microwave irradiation (cracks in the case of the mixture 100-50, and spheres in the case of the mixtures 100-80 and 100-100) are a consequence of the manual moulding. Cracks occurred because layers were not evenly pressed over the whole top-surface area, and because not all layers were pressed with the same force. Spherical bubbles, on the other hand, can occur in all AAMs that are conventionally moulded (slurry is poured into the mould) as remaining bubbles from mixing powder and liquid. While the cracks can be avoided by machine pressing, bubbles can be removed by shaking freshly moulded prisms on vibration tables for concrete.

Nonetheless, microwave irradiation induced additional spherical pores and elongated cracks. Spherical pores in irradiated samples were a consequence of 7-day-old AAMs not being completely finalised (curing at 40 °C for 6 days was not enough

to completely cure the sample), which left an open window for late volumetric foaming (Tesovnik and Horvat 2024a). However, because irradiation did not stop when induced porosity would be only spherical, but was prolonged until there was any steam coming out from the prism, the pressure in the prism increased to the point that the aluminosilicate network opened to depressurise and let the steam out through artificially formed elongated cracks (Tesovnik and Horvat 2024a). The severity of the microwave-induced porosity was visually more notable for mixtures synthesised with a higher amount of liquid (mixtures 100-80 and 100-100), ending with more spherical pores compared to the mixture 100-50. The most severe damage in the aluminosilicate network was caused by higher-power microwave irradiation (1000 W) for mixtures with more liquid (100-80 and 100-100), while the mixture with the smallest amount of liquid had no clear difference between low-power (100 W) and high-power (1000 W) irradiation.

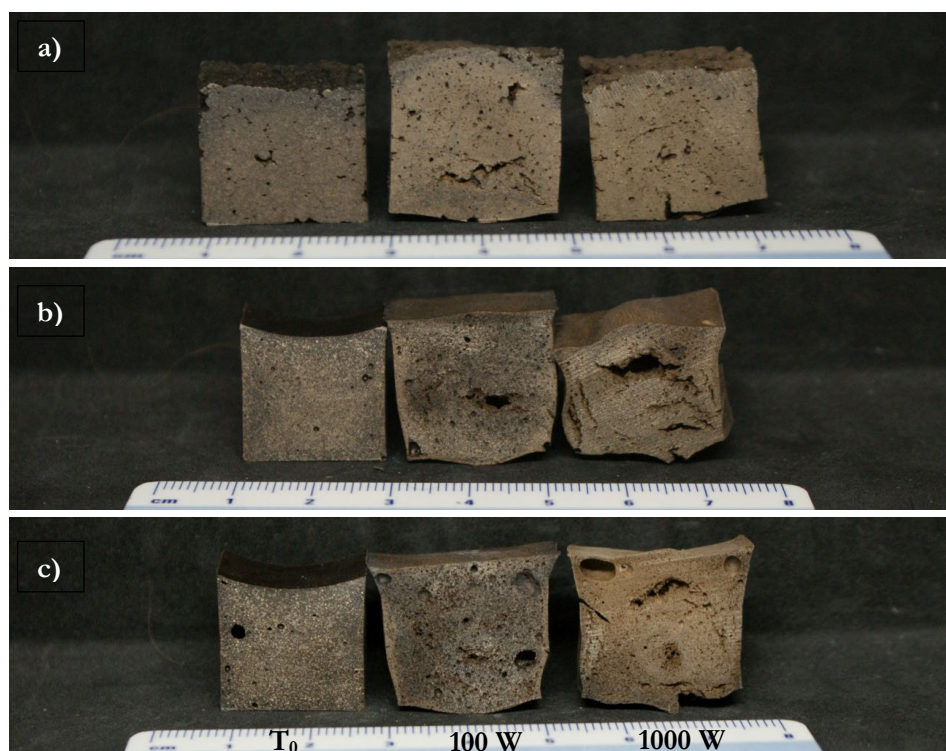


Figure 4: Cross-section of 14-day-old mixtures a) 100-50, b) 100-80, and c) 100-100, that were (from left to right) kept at room conditions, irradiated at 100 W, and at 1000 W.

Source: own.

The compressive strength, shown in Figure 5 (measurements are available in the open repository), decreased with the addition of liquid alkali, i.e. mixture 100-50 had the highest compressive strength and was the least impacted by irradiation. This phenomenon can be explained by Figure 4 where irradiated mixture 100-50 shows the highest structural integrity among the mixtures.

While the compressive strength for the non-irradiated sample slightly increased with time (Figure 5a compared to Figure 5b), for the samples irradiated with high-power microwaves the compressive strength decreased.

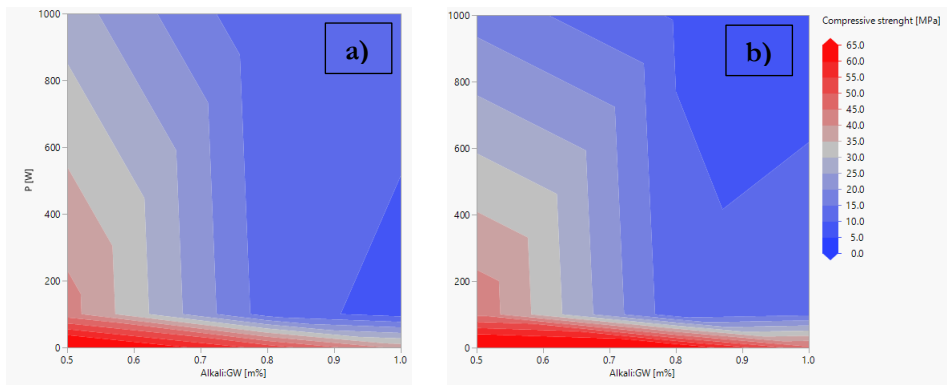


Figure 5: Delaunay triangulation of compressive strength of a) 7 and b) 21-day-old AAM prisms from GW in different mass ratios of GW and alkali (0.5, 0.8, and 1; mixtures 100-50, 100-80, 100-100, respectively).

Source: own.

The irradiation time, shown in Figure 6a, needed to reach the dehydration stage when no visible steam appears on the beaker anymore depends on: (i) the mass of water, (ii) the compactness of the irradiated material (initial cracks/voids/pores), (iii) the strength of the chemical bonds holding the material together, (iv) power of microwaves, (v) frequency of the microwaves, and (vi) the dimension of the irradiated material. While there was no option to vary the frequency of microwaves, also the dimensions of the prisms, chemical bonds and compactness of the material were assessed as comparable among the samples, and therefore a constant. The only parameters heavily influencing the outcomes of the irradiation were the mass of water and the power of microwaves.

Samples containing the same amount of water needed less time for dehydration if the power of microwaves was higher. This is the same as in conventional heat treatment, i.e. the material exposed to higher temperatures reaches higher temperatures faster. However, the dependence of the time of the irradiation till complete dehydration at a constant power is heavily dependent on the amount of water and the pre-chosen power of microwaves. In Figure 6a are presented both behaviours:

- Subcritical: at the low power of microwaves the time of irradiation increases with the amount of mass, just as in conventional heat treatment.
- Supercritical: at the high power of microwaves the time of irradiation shortens with the amount of water, which is paradoxical in the conventional heat treatment.

The reversed phenomenon at high-power microwave exposure (more water leading to a shorter time for dehydration), which cannot happen with surface heating methods, happens because more water molecules in the slurry absorb more microwaves. Water molecules can also not absorb microwaves, but if the water molecules are in the “strong part” of the electromagnetic standing wave, they try to align with the rapidly changing outer electromagnetic field, and enhance temperature by rubbing the neighbouring material. The absorbed microwaves are replaced by “new microwaves” in the microwave chamber, i.e., the inverter microwave tries to maintain the chosen output power at a constant level, meaning that there is no decrease in the source power used for the heat treatment. The more molecules that are simultaneously impacted by microwave irradiation, the faster the temperature increases inside the irradiated AAM. Water molecules that were not impacted by the microwave field are used as a heat dissipation media (cooling system), i.e., which is secondary (conventional) heating in the material. When there are more by-microwaves-impacted water molecules (acting as the inner heat sources, i.e., the secondary heating), the temperature rises faster. If there is more water, i.e., more potential heat sources, the system at high microwave power internally heats up faster.

In the presented systems (the size of the samples, compactness of the material, frequency of the microwave were constant), the critical power of microwaves (when all three mixtures need the same time for dehydration) is between 100 and 1000 W. Above the critical power the system is supercritical (1000 W: more water leads to

faster dehydration), below the critical power the system is subcritical (100 W: more water leads to slower dehydration).

As shown in Figure 6a, a mixture 100-100, which contains the highest amount of water, dehydrates at 1000 W fastest among all mixtures but just slightly faster than mixture 100-80. The fastest dehydration (for both mixtures with higher amounts of alkali) damages the material the most (Figure 4b and c: the right cross-sections have the most prominent damage) and negatively influences the compressive strength (Figure 5).

The relative changes in mass (δm), volume (δV) and geometrical density ($\delta \rho$) of AAMs, shown in Figure 6b, were calculated as the difference between the values on non-irradiated samples and their thermally treated 7-day-old counterparts, normalised to the non-irradiated values. While the mass and geometrical density of all microwave-irradiated mixtures decreased, the volumes increased. Samples containing more liquid alkali (mixture 100-100) expressed the biggest changes, which are attributed to the loss of water (loss of mass) and the creation of more voids/pores/cracks by the removal of a higher amount of liquid from the system. However, the difference in mass, volume and geometrical density between low and high-power microwave treatment is comparable. Therefore, the irradiation with high-power microwaves only notably decreased the time of dehydration, while other changes were just slightly more expressed. The smaller macro-difference in prisms between low and high-power treatment cannot have caused a severe decrease in compressive strength (Figure 5). Therefore, the cause behind the destruction of the mechanical performance of AAMs treated with high-power microwaves is the larger fractures in the micro/mili-structure of the aluminosilicate network (Figure 4). Therefore, dehydration must be performed with low-power microwaves when dehydrating samples still have to express significant mechanical performance.

The thermogravimetric behaviour of GW and 7-day-old mixtures, non-irradiated and irradiated at different powers, is shown in Figure 7. GW does not contain water, therefore there is no mass loss up to 300 °C. At 300 °C GW starts expressing approximately linear mass loss in the remaining measurement area (from 300 to 600 °C; 600 °C was the measurement limit to avoid GW melting which can cause irreversible damage to used crucibles). The thermogravimetric mass loss corresponds to the measured value of gravimetric loss on ignition (~ 6 m%).

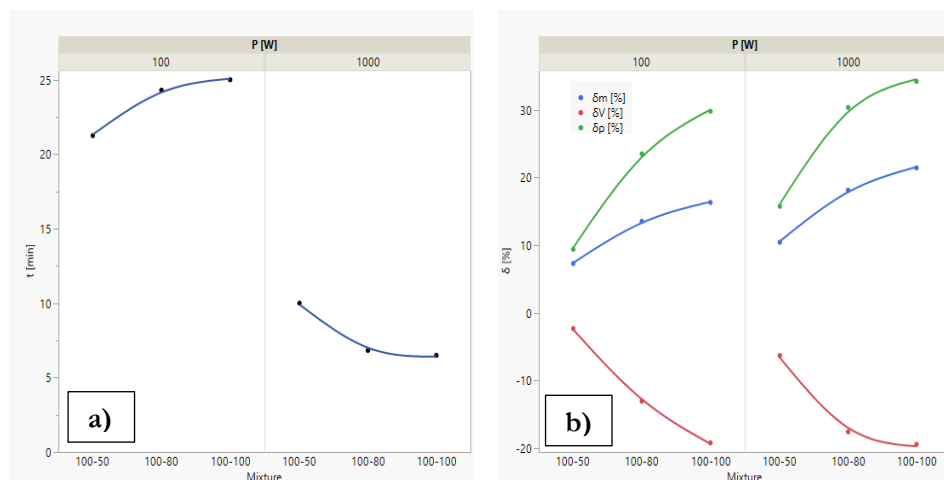


Figure 6: a) Dehydration time and b) changes in mass/volume/density ($\delta m/\delta V/\delta \rho$) of AAM prisms per irradiation power and mixture.

Source: own.

The linear mass loss is present for all alkali-activated samples in the same range as for GW. Because AAMs and GW have also a comparable mass loss rate in the higher temperature range, this loss is attributed to the thermal degradation of the remaining organic compound which did not react with alkali. Therefore, the aluminosilicate network of all AAMs can be considered thermally stable at least up to 600 °C.

The water loss is represented by the steepest slope in the lowest temperature range (from approximately 50 °C to slightly more than 100 °C). When comparing the AAMs treated in the same manner in the “water range”, the AAM with the highest amount of liquid (mixture 100-100) had the highest mass loss and the AAM with the lowest amount of liquid alkali (mixture 100-50) had the lowest mass loss. However, when comparing the behaviour of AAM mixtures that were irradiated with low-power microwaves, high-power microwaves, or were not irradiated, the mass loss in the “water range” is highest for non-irradiated samples and the smallest loss is for the irradiated with high-power microwaves samples. Nonetheless, Figure 7 shows that dehydration was either incomplete or samples should be put into a waterless environment directly after irradiation due to the hygroscopic nature of AAMs made from mineral wools.

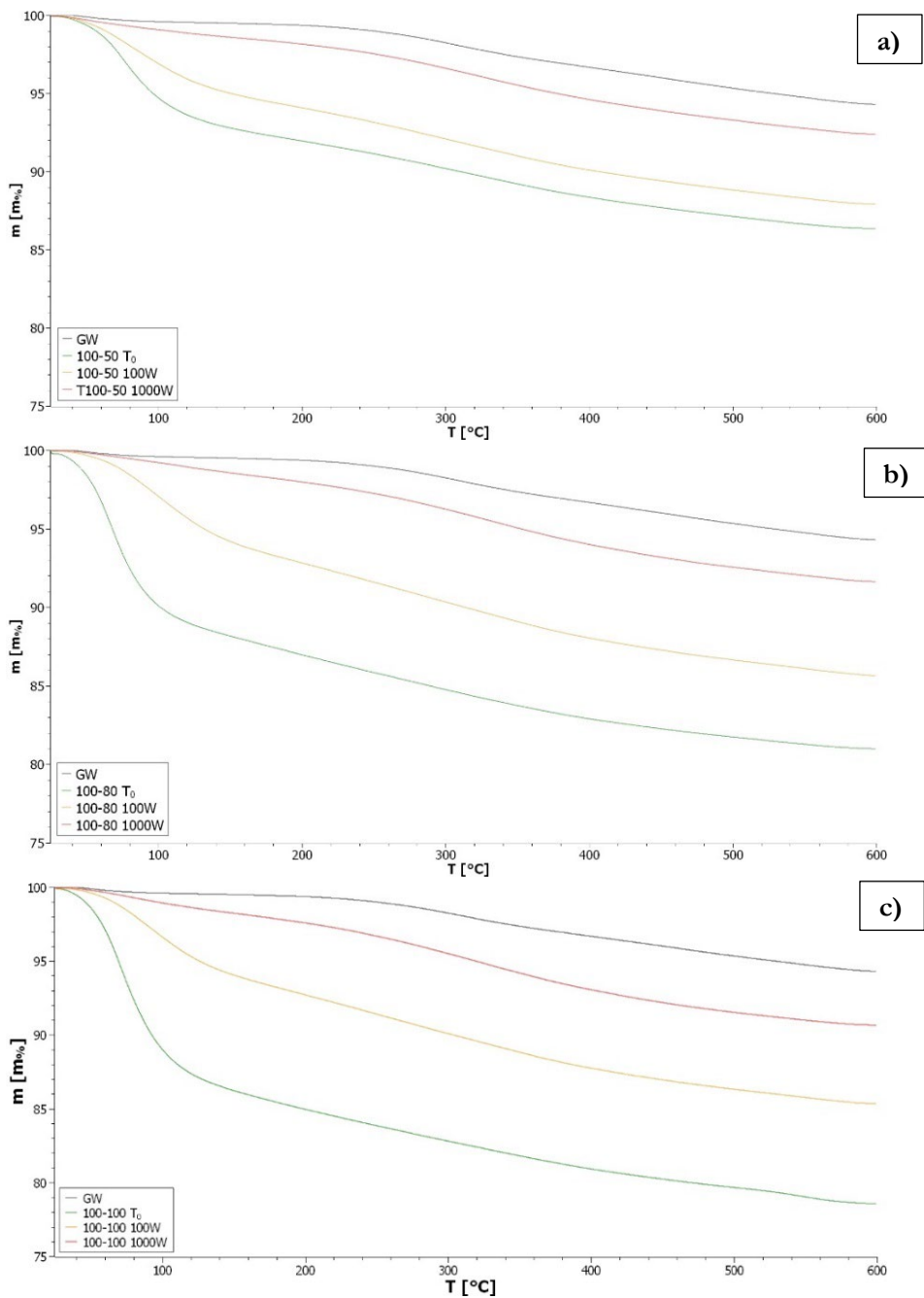


Figure 7: Thermogravimetric behaviour of GW and 7-day-old AAM (dehydrated) mixtures.

Source: own.

In the middle-temperature range (between approximately 100 °C and 300 °C), where there is no mass loss in GW, all AAMs express slightly different mass-loss rates than the rate attributed to the in-alkali-not-reacted organic compound originally present on the surface of the GW. Therefore, the mass loss in the middle range belongs to organic compounds that have at least partially reacted with alkali, which is expressed by the released scent during the reaction and release of colour when AAMs made from GW with organic material on the surface are put into water (video in the supplementary material: Tesovnik and Horvat 2024b).

4 Conclusion

Although all alkali-activated mixtures based on the waste glass wool prepared in this study will never end on the market, namely they will all eventually deteriorate because of the chemical affinity to efflorescence, they suit as an explanation of the non-trivial connection between compressive strength, microwave irradiation and time needed for dehydration of conventionally pre-cured alkali-activated mixtures. In subcritical microwave heating (lower microwave power), where a higher amount of water leads to longer dehydration time, the damage to the inner structure of the material followed by a decrease in compressive strength is smaller when compared to material irradiated in the supercritical conditions (higher microwave power), where more water leads to faster dehydration.

When the compressive strength of solidified materials should be kept as high as possible also after microwave irradiation, the irradiation should be performed in subcritical conditions. However, if the material is dehydrated solely to remove water and test chemical and mineralogical composition, supercritical conditions decrease the time for preparation: water is removed from the system faster and the compressive strength of the material becomes weaker allowing easier pulverisation.

Nonetheless, the finding that in microwave irradiation exists a critical point where the time of irradiation does not depend on the amount of water, can open a new field in research of the synthesis of materials with microwaves.

Acknowledgements

This study is part of Dr. Barbara Horvat's ARIS project and was financially supported by the Slovenian Research Agency under Grant No. J2-3035. The present study was performed at the Slovenian National Building and Civil Engineering Institute while Dr Horvat was still employed there, for which Dr. Horvat is thankful. Dr Horvat also thanks the Milan Vidmar Electric Power Research Institute for offering peer review, proofreading, and evaluation of the work by the committee.

Data availability status

The original data presented in the study are openly available in the repository Zenodo at <https://zenodo.org/records/14515939> with DOI: 10.5281/zenodo.14515939.

References

- Duxson, Peter, John L. Provis, Grant C. Lukey, Seth W. Mallicoat, Waltraud M. Kriven, and Jannie S.J. van Deventer. 2005. 'Understanding the Relationship between Geopolymer Composition, Microstructure and Mechanical Properties'. *Colloids and Surfaces A: Physicochemical and Engineering Aspects* 269 (1–3): 47–58. <https://doi.org/10.1016/j.colsurfa.2005.06.060>.
- Horvat, Barbara, Mark Češnovar, Alenka Pavlin, and Vilma Ducman. 2018. 'Upcycling with Alkali Activation Technology'. In *Technologies & Business Models for Circular Economy*. Slovenia.
- Horvat, Barbara, and Vilma Ducman. 2019. 'Potential of Green Ceramics Waste for Alkali Activated Foams'. *Materials* 12 (21): 3563. <https://doi.org/10.3390/ma12213563>.
- Horvat, Barbara, Branka Mušič, Majda Pavlin, and Vilma Ducman. 2022. 'Microwave Irradiation of Alkali-Activated Metakaolin Slurry'. Slovenia, Portorož. <https://doi.org/10.18690/um.fkkt.6.2022>.
- . 2023. 'Microwave Irradiation of Alkali-Activated Metakaolin Slurry'. 9–24. Slovenia, Portorož: University of Maribor Press. <https://doi.org/10.18690/um.fkkt.1.2023.2>.
- Obonyo, Esther, Elie Kamseu, Patrick Lemougna, Arlin Tchamba, Uphie Melo, and Cristina Leonelli. 2014. 'A Sustainable Approach for the Geopolymerization of Natural Iron-Rich Aluminosilicate Materials'. *Sustainability* 6 (9): 5535–53. <https://doi.org/10.3390/su6095535>.
- Pacheco-Torgal, Fernando, João Castro-Gomes, and Said Jalali. 2008. 'Alkali-Activated Binders: A Review. Part 2. About Materials and Binders Manufacture'. *Construction and Building Materials* 22 (7): 1315–22. <https://doi.org/10.1016/j.conbuildmat.2007.03.019>.
- Pavlin, Majda, Barbara Horvat, Ana Frankovič, and Vilma Ducman. 2021. 'Mechanical, Microstructural and Mineralogical Evaluation of Alkali-Activated Waste Glass and Stone Wool'. *Ceramics International* 47 (11): 15102–13. <https://doi.org/10.1016/j.ceramint.2021.02.068>.
- Škvára, František. 2007. 'Alkali Activated Material - Geopolymer'. *Department of Glass and Ceramics Faculty of Chemical Technology*, 16.
- Tesovnik, Anže, and Barbara Horvat. 2024a. 'Rapid Immobilisation of Chemical Reactions in Alkali-Activated Materials Using Solely Microwave Irradiation'. *Minerals* 14 (12): 1219. <https://doi.org/10.3390/min14121219>.
- . 2024b. 'Rapid Immobilisation of Chemical Reactions in Alkali-Activated Materials Using Solely Microwave Irradiation'. Chemistry and Materials Science. <https://doi.org/10.20944/preprints202410.0394.v1>.
- 'The Industry Creating a Third of the World's Waste'. n.d. Accessed 30 September 2024. <https://www.bbc.com/future/article/20211215-the-buildings-made-from-rubbish>.

CIRCULARITY AND LONGEVITY OF ALKALI-ACTIVATED MATERIALS: CASE-STUDY USING ROCK WOOL AS A PRECURSOR

BARBARA HORVAT,¹ SARA TOMINC²

¹ Milan Vidmar Electric Power Research Institute, Ljubljana, Slovenia
barbara.horvat@eimv.si

² Slovenian National Building and Civil Engineering Institute, Ljubljana, Slovenia
sara.tominc@zag.si

Alkali-activated materials (AAMs) are being envisaged as a future alternative to cements because AAMs (i) can be made solely from locally available secondary raw materials and (ii) because of their low energy consumption during synthesis. However, products that cannot be reused should never enter the market. Therefore, the circular economy viability of AAMs was studied by reusing (alkali-activated) pulverised rock wool in alkali activation synthesis until the theoretically determined limit leading to the efflorescence would be reached. While 25% of the maximal allowed liquid alkali did not offer significant mechanical performance, 50, 75 and 100% of allowed alkali ended up with 15, 20 and 20 MPa, respectively, which is only 5 MPa lower than AAM made with the same technique (pressing) in a one-step approach. Therefore, if the initial AAM does not reach the efflorescence limit, it could still be used as a precursor before it becomes waste.

DOI
[https://doi.org/
10.18690/um.fkkt.1.2025.3](https://doi.org/10.18690/um.fkkt.1.2025.3)

ISBN
978-961-286-959-5

Keywords:

rock wool,
alkali-activated materials,
microwave irradiation,
electromagnetic
dehydration,
linear model,
circular model,
longevity of AAM



1 Introduction

As is known from the field of plastic material, what cannot be recycled, should not be made ('Plastics and the Circular Economy' 2019), and even what can be recycled, should be reused ('Reusing 10% Will Stop Almost Half of Plastic Waste from Entering the Ocean. Heres' How | World Economic Forum', n.d.) to minimise the impact on the environment. This philosophy should be deeply implemented in all industries, the building sector included. Namely, conventional building and civil engineering materials represent a significant burden on the environment by:

- producing 40% of the global man-caused carbon footprint ('The Industry Creating a Third of the World's Waste', n.d.);
- exploiting raw materials in yearly amounts of two-thirds of Mount Everest ('The Industry Creating a Third of the World's Waste', n.d.); and
- the high energy consumption during their production as needed temperatures exceed 1000 °C ('Cement Production: How Hot Air Becomes Green Energy', n.d.).

To reduce the burden on the environment caused by building materials, alternative materials to cement, such as alkali-activated materials (AAMs), are being researched (Škvára 2007; Pacheco-Torgal, Castro-Gomes, and Jalali 2008a). AAMs are presented as an environmentally friendly and sustainable alternative (Obonyo et al. 2014) because:

- they require lower temperatures for their production (below 100 °C; (Pacheco-Torgal, Castro-Gomes, and Jalali 2008b));
- can be made solely from (local) secondary raw materials (Horvat and Ducman 2019);
- show good chemical resistance, i.e., are durable (Bernal, Mejía De Gutierrez, and Rodríguez 1969).

However, AAMs have several issues:

- Waste materials can contain heavy metals and other hazardous species which might not get immobilized in AAM (Sun et al. 2024).

- If the molar ratio of amorphous elements of alkali metal to amorphous Al is not equal or below 1, efflorescence will occur in the AAM and cause deterioration of the product (Horvat and Ducman 2019).
- If alkali earth metals also dissolve and interact with the aluminosilicate network (ASN; also called matrix, gel or binder), efflorescence can get additionally enhanced (if the pre-calculation of the optimal mixture is only related to alkali metal elements) (Horvat and Ducman 2019).
- If from precursor is “used” already everything that could form the ASN in AAM, AAM after its end-of-life cannot be used again as a precursor in alkali-activated synthesis but can be used only as an aggregate or go into a potential acidic reaction chain.

Therefore, if AAMs are made from chemically hazardous materials, the problematic part of the precursor should become completely immobilized in the AAM (Sun et al. 2024). One of the safe choices of the precursor is rock wool (RW) (Horvat et al. 2018; Yap et al. 2021) without organic resin on its surface (Li et al. 2021). Namely, if in alkali activation synthesis RW is without organic resin on its surface, there will be no colouration of the water when AAM from RW is immersed in it and less to no leaching issues. Otherwise, RW should not be used as the sole precursor for the synthesis of AAMs, even though RW is a perfect material for AAMs from the mineralogical and chemical point of view. This is because RW is highly amorphous, has sufficient Si and Al, and a low molar amount of chemical elements from the 1st group of the periodic table, but a high proportion of elements from the 2nd group (Horvat et al. 2018). However, the electron microscopy research confirmed that the ASN has a lower presence of elements from the 2nd group of the periodic table, which means that the elements from the 2nd group do not dissolve in the alkali medium so easily (Pavlin et al. 2021), as is shown in the Supplementary material in Figure S1. Therefore, the significant amounts of the elements from the 2nd group of the periodic table can be excluded from the calculation of the limit value of the alkali addition in the preliminary research. Hence, there is a span left for the addition of alkali to RW while trying to avoid efflorescence.

The theoretical calculation (Horvat and Ducman 2019) of the optimal mixture of the selected precursor (or a set of precursors) and the selected alkali takes into account the results from:

- Loss on ignition (LOI) of the precursor at 550 °C, with which mass percentage of the organic compound is measured gravimetrically.
- X-ray fluorescence (XRF), which determines the presence of the chemical elements (which and how much) regardless of how and to what they are bound.
- X-ray powder diffraction (XRD), which provides a fingerprint of the minerals present in the sample. Because it is unlikely that minerals play a role in alkali activation synthesis, their quantity must at least be estimated. Therefore, the XRD of the potential precursor must be measured together with the standard (internal or external) so that a Rietveld refinement analysis can be performed.

The elemental composition of the amorphous content present in the inorganic part of the sample is then calculated as the difference between XRF and XRD, which is used as the best approximation of the ideal mixture. To achieve the highest compressive strength of AAMs, the molar ratio of amorphous Si to amorphous Al is aimed to be 1.9 (Duxson et al. 2005), and to ensure the lifetime integrity of the material by avoiding efflorescence, the molar ratio of amorphous chemical elements from the 1st group of the periodic table and of amorphous Al must be ≤ 1 (considering that chemical elements from the 2nd group of the periodic table do not contribute to the alkali reaction).

However, even if the precursor used for AAMs does not lead to issues, even if efflorescence was avoided by pre-calculating the mixture, sustainability research on AAMs lacks data. While there is data on the durability of AAMs when exposed to different conditions, there is no data on the longevity of AAMs that exists for concrete (Roman concrete lasts more than 1000 years (Dean 2017), modern concrete 50 to 100 years ('The Problem with Reinforced Concrete', n.d.)). Therefore, this preliminary study focuses on the reuse of alkali-activated pulverised rock wool (RW) in the alkali-activated synthesis up to the mixture that would theoretically lead to efflorescence. AAMs synthesised in a 4-step (circular) model were compared with a 1-step (linear) model in terms of mechanical properties, as compressive strength is the most essential metric in load-bearing building industry products. While the 1st step was below the viability of the material, the AAM prepared in subsequent steps reached 15 to 20 MPa, which corresponds to 60 to 80% of the compressive strength

of the linear model. Therefore, this study demonstrates that properly designed AAMs can have extended longevity in the field itself.

2 Experimental

2.1 Materials and characterisation of the materials

The following ingredients were used in the synthesis of AAMs:

- Non-waste RW without organic material (LOI at 550 °C is ~0) on the surface, which was used as a precursor. RW was milled in a vibrating disk mill (Labor-Scheibenschwingmühle TS.250, Siebtechnik GmbH) and sieved below 63 µm;
- Na-silicate solution (Geosil, 344/7, Woelner, 16.9 m% Na₂O, 27.5 m% SiO₂, 55.6 H₂O), which was used as an aqueous liquid alkali without further manipulation.

In the present study, the limit for the addition of alkali was set to avoid efflorescence, i.e. the elements of the 1st group of the periodic table (originating from the alkali and the amorphous part of the RW) were not allowed to exceed the molar mass of the amorphous Al (present in the amorphous part of the RW). Therefore, RW (dried, milled and sieved below 125 µm) was analysed by XRF (Thermo Scientific ARL Perform'X Sequential XRF) to determine the chemical composition (elements from fluorine to americium) of RW, and by XRD (Empyrean PANalytical X-ray Diffractometer, Cu X-Ray source; under clean room conditions in the 2θ range from 4 to 70° and step 0.0263°) to determine the minerals present in RW. However, the Rietveld refinement was performed using X'Pert Highscore plus 4.1 software and an external standard (corundum, Al₂O₃) to evaluate the amount of elements present in the crystalline content. The amorphous content is then calculated as the difference between XRF and XRD per element (not per oxide). The results of the RW evaluation are presented in Table 1 and show that RW is completely amorphous.

The theoretically determined mass ratio (using software designed in MS Excel platform, developed in project no. C3330-17-529032 “Raziskovalci-2.0-ZAG-529032” (Horvat and Ducman 2019) and upgraded in ARIS project under grant no. J2-3035) between RW and liquid alkali was 1:0.5.

Table 1: Mass percentage (m%) of crucial elements in alkali activation.

Elements [m%]	Na	K	Mg	Ca	Al	Si	Content [m%]
XRF	1.63	0.34	11.66	16.90	18.61	42.39	100
XRD	0	0	0	0	0	0	0
Amorphous	1.63	0.34	11.66	16.90	18.61	42.39	100

The compressive strength, the most crucial parameter for the load-bearing materials, was measured with the compressive and bending strength testing machine (ToniTechnik ToniNORM) on 1-day-old AAM cylinders.

2.2 Synthesis of the material

The AAMs were prepared in two life-cycle models, i.e. linear and circular (Table 2 and Figure 1):

- The linear life-cycle model (L) was performed as a one-step synthesis (as a reference) where the optimal ratio of alkali to precursor, which should not be exceeded, was calculated using XRF and XRD on rock wool. The mass ratio of rock wool to alkali was 1 to 0.5, and this ratio was defined as the limiting value for the alkali.
- The circular life-cycle model (C) was simulated as a cyclic-stepwise synthesis, where in each cycle 25 m% of the limiting value of the alkali was added to the (1st cycle: α) rock wool and in each next cycle (50 m% β , 75 m% γ , 100 m% δ) to the microwave-dried and milled AAM from the previous cycle until the sum of the added alkali was equal to the alkali used in the linear model.

Table 2: Chemical composition of the samples (precursor and AAMs) with mixture recipes.

Sample	1st/Al [mol/mol]	Si/Al [mol/mol]	Precursor	Precursor [g]	Alkali [g]	H ₂ O in alkali [g]	Na in alkali [g]
RW	0.21	1.94	/	/	/	/	/
C _{α}	0.40	2.09	RW	100	12.5	6.9	1.6
C _{β}	0.59	2.25	C _{α}	105.6	12.5	6.9	1.6
C _{γ}	0.77	2.41	C _{β}	111.1	12.5	6.9	1.6
C _{δ}	0.96	2.56	C _{γ}	116.7	12.5	6.9	1.6
L	0.96	2.56	RW	100	50	27.8	6.3

RW and alkali were mixed at up to 1000 rpm. 25 g of the freshly prepared homogeneous mixture was pressed in a cylindrical metal mould with a diameter of 3 cm and a force of 10 kN. The cylinders were cured for 1 day at 70 °C.

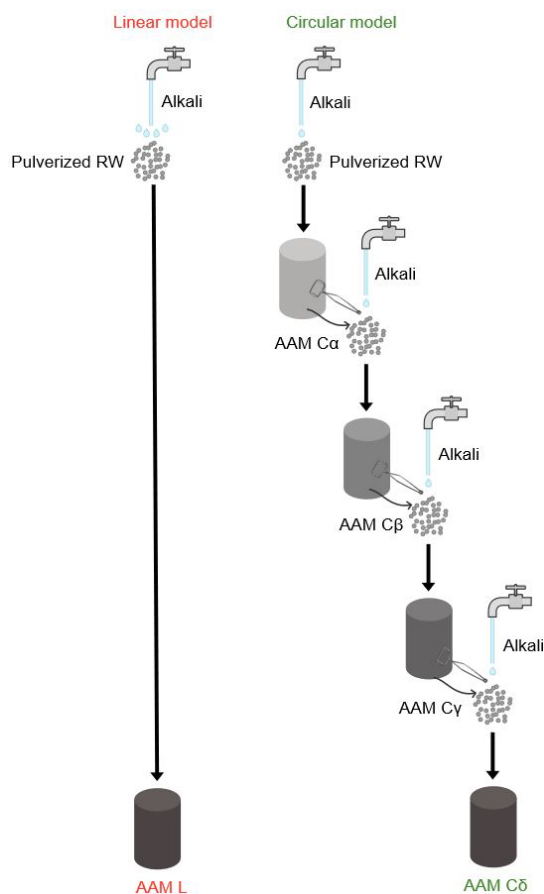


Figure 1: Synthesis scheme.

Source: own.

2.3 Evaluation of longevity of the AAM

The longevity of AAMs, i.e. the lifespan of AAMs during which they can be reused in alkali activation without theoretically causing efflorescence, with the compressive strength of more than 5 MPa (lowest concrete grade available on the market ('Different Types of Concrete Grades and Their Uses | Base Concrete' 2023)), was

compared between the two life-cycle models (linear and circular) in two implementation models (design-used and purpose-used):

- Design-used implementation model: All products were used for the purpose they can withstand for time a , after which they were replaced.
- Purpose-used implementation model: All products have been used for the same purpose. Therefore, their lifespan can be assessed on the basis of their physical properties. Assuming that the durability and conditions are the same for all products, the longevity is only influenced by the compressive strength. Therefore, all products were replaced after time $\frac{\sigma_{CS}}{\sigma_1} \cdot a$, where σ_{CS} is the compressive strength of the AAM (in MPa), σ_1 is 1 MPa (to make the measured compressive strength dimensionless), and a is the time.

After the first replacement, the product from the linear model went either to the grave or to another recycling route, while the product in the circular model was reused as the precursor in alkali activation until the total amount of alkali was the same as in the linear model.

3 Results and discussion

All freshly prepared samples in a circular model were sufficiently dry, which means that no liquid was squeezed out of the cylinders by pressing (Figure 2a). In contrast, the samples prepared in a linear model were visibly inhomogeneous (Figure 2b). Inhomogeneity results in parts that have an excessive amount of alkali, where efflorescence forms, and parts that do not have enough alkaline reagent and liquid for complete dissolution of the amorphous content and for diffusion of the dissolved building blocks that rearrange into the ASN of the AAM during dehydration and polymerisation.

The compressive strength (Table 2 and Figure 3) of the samples prepared according to the circular model did not reach the compressive strength of the sample prepared according to the linear model, although they were inhomogeneous (imperfect) immediately after pressing. Because inhomogeneity can never affect the final mechanical properties with an increased value, the compressive strength of the sample prepared in the linear model may not have reached its full potential.

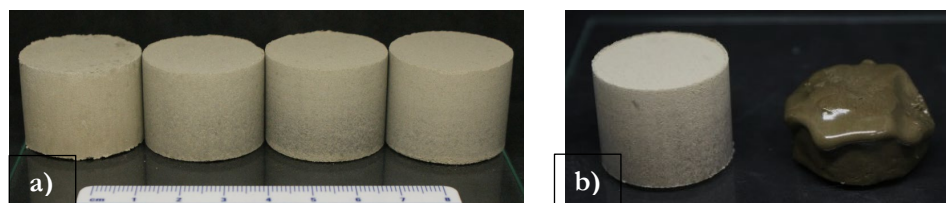


Figure 2: Pressed, freshly prepared mixtures of a) from left to right C_α , C_β , C_γ , C_δ , and b) from left to right C_δ and L.

Source: own.

Table 2: Compressive strength and standard deviation of cylindrical 1-day-old samples.

Sample	Compressive strength [MPa]	Standard deviation [MPa]	Concrete strength
C_α	1.66	1.05	/
C_β	15.94	1.32	Low
C_γ	21.10	2.66	Medium
C_δ	20.45	0.93	Medium
L	27.31	2.51	High

However, the samples prepared in the 2nd to 4th step (C_β , C_γ , C_δ) reached 60% (C_β) and almost 80% (C_γ , C_δ) of the 27 MPa of the linear model sample, which when compared to the concrete can be used for ('Strong Foundations: Mix The Perfect Concrete Every Time' 2013):

- Low-strength concrete (C_β): non-reinforced house foundations, boundary walls, freestanding retaining walls.
- Medium-strength concrete (C_γ , C_δ): reinforced foundations, footpaths, driveways, patios, steps, driveways.
- High-strength concrete (L): suspended structural beams, heavy-duty floors.

While aiming to have the compressive strength at least equal to the lowest value of concrete (5 MPa ('Different Types of Concrete Grades and Their Uses | Base Concrete' 2023)), the circular production of AAMs from RW (cradle) requires skipping C_α directly and supplying the market with C_β first, which should be reused for the production of C_γ , which should be reused for the production of C_δ , before the need to search for an alternative solution to grave: recycling as aggregates in other binding materials in the building industry, as crushed stone-like materials for

fences, as alkaline reagents that react with acids and end up in acid-activated materials that do not yet exist, etc.

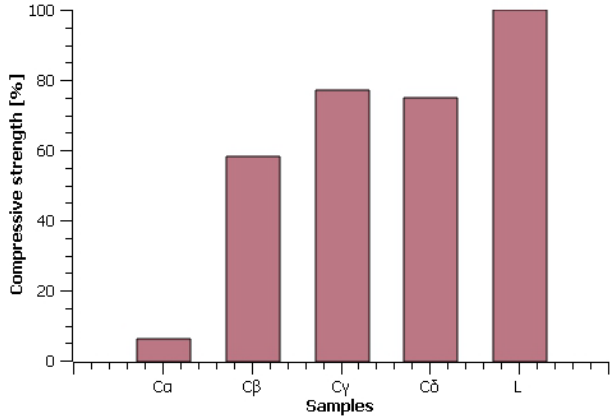


Figure 3: Compressive strength normalised to the compressive strength of the sample from the linear model.

Source: own.

The comparison of the implementation models (design-used and purpose-used) for both life-cycle models (linear and circular), shown in Figure 4, shows the superiority of the circular model. If the product is used as intended (designed), the longevity of the product in the circular model is 3 times higher than that of the material in the linear model. However, if the product is used for a selected purpose regardless of its design (potential), the longevity of the product in the circular model is only 2.1 times higher.

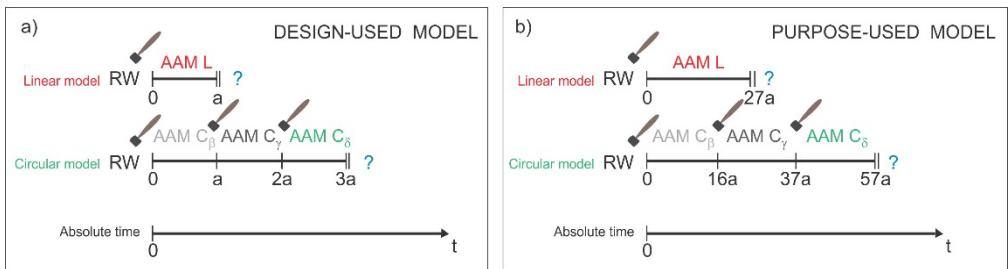


Figure 4: Longevity of the product with marked manufacturing events (hammer), grave or other recycling path (blue waymark) and the current AAM material in the timeline.

Source: own.

4 Conclusion

In this study, the potential of AAM from RW for reuse in alkali-activated synthesis was investigated by assessing the compressive strength and longevity. If efflorescence is avoided in all cases and no other issues occur, the circular model starting at 50% of the maximum allowable alkali extends the use phase of AAM beyond the linear model, regardless of whether the material was used for its intended purpose or not.

Adding 50% of the theoretical limit value of alkali can be compared to low-strength concrete, while adding 75% of the theoretical alkali maximum to medium-strength concrete. However, AAMs in this study were not performed on a pilot product scale comparable to concrete test samples, and concrete cannot be prepared in sample sizes in this study and still be representative.

The fresh alkali-activated slurry can only be pressed until the samples are homogeneous. When liquid is squeezed out from the tablet, slurry has to be moulded and not pressed, just like the liquid can be added to the pulverised precursor up to the point, when buoyancy is equal to forces acting against it in the moulded slurry.

Acknowledgements

This study is part of Dr. Barbara Horvat's ARIS project and was financially supported by the Slovenian Research Agency under Grant No. J2-3035. The present study was performed at the Slovenian National Building and Civil Engineering Institute while Dr Horvat was still employed there, for which Dr. Horvat is thankful. Dr Horvat also thanks the Milan Vidmar Electric Power Research Institute for offering peer review, proofreading, and evaluation of the work by the committee.

Supplementary materials

A polished, uncoated sample of AAM based on rock wool was evaluated using a scanning electron microscope (SEM) and energy-dispersive X-ray spectroscopy (EDXS) under low vacuum conditions (Figure S1) to determine the elemental composition of the ASN (the darkest shade of grey in Figure S1). EDXS mapping showed that Na and Ca were separately concentrated in the unreacted rock wool fibres, that the presence of Na in the ASN was significant (can be attributed to the Na-based alkali used in the reaction), while Ca was notably scarce.

However, regardless of the dissolution rate of Na and Ca present in the rock wool, the lack of Ca in the ASN supports the assumption that excluding elements from the 2nd group of the periodic table in the theoretical calculation is valid (in 1st approximation).

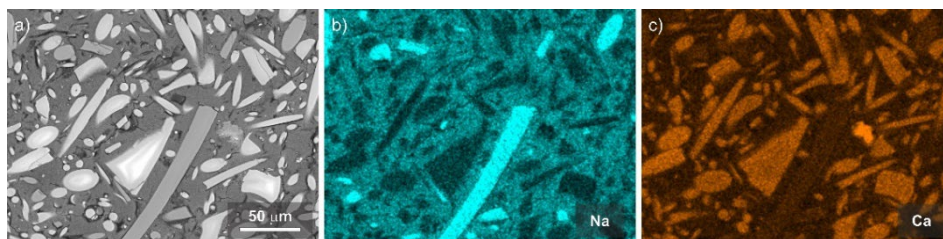


Figure S1: a) SEM micrograph of polished AAM sample based on mineral wool, with EDXS mapping of b) Na and c) Ca.

Source: own.

References

- Bernal, Susan A., Ruby Mejía De Gutierrez, and Erich D. Rodríguez. 1969. 'Alkali-Activated Materials: Cementing a Sustainable Future'. *INGENIERÍA Y COMPETITIVIDAD* 15 (2). <https://doi.org/10.25100/iyv.v15i2.2608>.
- 'Cement Production: How Hot Air Becomes Green Energy'. n.d. Accessed 30 September 2024. <https://insights.thyssenkrupp-polysius.com/story/cement-production-how-hot-air-becomes-green-energy/>.
- Dean, Amy M. 2017. 'Scientists Research as to Why Roman Concrete Lasts Millennia, While Modern-Day Concrete Lasts a Half Century'. *International Society for Concrete Pavements* (blog). 12 July 2017. <https://www.concretepavements.org/2017/07/11/scientists-research-as-to-why-roman-concrete-lasts-millennia-while-modern-day-concrete-lasts-a-half-century/>.
- 'Different Types of Concrete Grades and Their Uses | Base Concrete'. 2023. 1 September 2023. <https://www.baseconcrete.co.uk/different-types-of-concrete-grades-and-their-uses/>.
- Duxson, Peter, John L. Provis, Grant C. Lukey, Seth W. Mallicoat, Waltraud M. Kriven, and Jannie S.J. van Deventer. 2005. 'Understanding the Relationship between Geopolymer Composition, Microstructure and Mechanical Properties'. *Colloids and Surfaces A: Physicochemical and Engineering Aspects* 269 (1–3): 47–58. <https://doi.org/10.1016/j.colsurfa.2005.06.060>.
- Horvat, Barbara, Mark Češnovar, Alenka Pavlin, and Vilma Ducman. 2018. 'Upcycling with Alkali Activation Technology'. In *Technologies & Business Models for Circular Economy*. Slovenia.
- Horvat, Barbara, and Vilma Ducman. 2019. 'Potential of Green Ceramics Waste for Alkali Activated Foams'. *Materials* 12 (21): 3563. <https://doi.org/10.3390/ma12213563>.
- Li, Zhenming, Irving Alfredo Flores Beltran, Yun Chen, Branko Šavija, and Guang Ye. 2021. 'Early-Age Properties of Alkali-Activated Slag and Glass Wool Paste'. *Construction and Building Materials* 291 (July):123326. <https://doi.org/10.1016/j.conbuildmat.2021.123326>.
- Obonyo, Esther, Elie Kamseu, Patrick Lemougna, Arlin Tchamba, Uphie Melo, and Cristina Leonelli. 2014. 'A Sustainable Approach for the Geopolymerization of Natural Iron-Rich Aluminosilicate Materials'. *Sustainability* 6 (9): 5535–53. <https://doi.org/10.3390/su6095535>.
- Pacheco-Torgal, Fernando, João Castro-Gomes, and Said Jalali. 2008a. 'Alkali-Activated Binders: A Review Part 1. Historical Background, Terminology, Reaction Mechanisms and Hydration Products'. *Construction and Building Materials* 22 (7): 1305–14. <https://doi.org/10.1016/j.conbuildmat.2007.10.015>.
- . 2008b. 'Alkali-Activated Binders: A Review. Part 2. About Materials and Binders Manufacture'. *Construction and Building Materials* 22 (7): 1315–22. <https://doi.org/10.1016/j.conbuildmat.2007.03.019>.
- Pavlin, Majda, Barbara Horvat, Ana Frankovič, and Vilma Ducman. 2021. 'Mechanical, Microstructural and Mineralogical Evaluation of Alkali-Activated Waste Glass and Stone Wool'. *Ceramics International* 47 (11): 15102–13. <https://doi.org/10.1016/j.ceramint.2021.02.068>.

- 'Plastics and the Circular Economy'. 2019. 16 September 2019.
<https://www.ellenmacarthurfoundation.org/plastics-and-the-circular-economy-deep-dive>.
- 'Reusing 10% Will Stop Almost Half of Plastic Waste from Entering the Ocean. Here's How | World Economic Forum'. n.d. Accessed 11 November 2024.
<https://www.weforum.org/stories/2021/07/reusing-plastic-waste-pollution-economy-value/>.
- Škvára, František. 2007. 'Alkali Activated Material - Geopolymer'. *Department of Glass and Ceramics Faculty of Chemical Technology*, 16.
- 'Strong Foundations: Mix The Perfect Concrete Every Time'. 2013. Sans 10400 - Building Regulations. 13 March 2013. <https://sans10400.org.za/concrete-mixes/>.
- Sun, Zengqing, Xiaoyu Li, Min Gan, Zhiyun Ji, Xiaohui Fan, and Jinxin Xing. 2024. 'Converting Municipal Solid Waste Incineration Fly Ash and Municipal Sludge into Environmentally Compatible Alkali-Activated Material'. *Sustainability* 16 (18): 7912.
<https://doi.org/10.3390/su16187912>.
- 'The Industry Creating a Third of the World's Waste'. n.d. Accessed 30 September 2024.
<https://www.bbc.com/future/article/20211215-the-buildings-made-from-rubbish>.
- 'The Problem with Reinforced Concrete'. n.d. Accessed 1 October 2024.
<https://www.unsw.edu.au/newsroom/news/2016/06/the-problem-with-reinforced-concrete0>.
- Yap, Zhen Shyong, Nur Hafizah A. Khalid, Zaiton Haron, Azman Mohamed, Mahmood Md Tahir, Saloma Hasyim, and Anis Saggaff. 2021. 'Waste Mineral Wool and Its Opportunities—A Review'. *Materials* 14 (19): 5777. <https://doi.org/10.3390/ma14195777>.

THE INFLUENCE OF PEARLESCENT PIGMENTS PRINTED ON PLASTIC PACKAGING ON THE PRINT GLOSS

MIRICA KARLOVITS, BLAŽ LIKOZAR, UROŠ NOVAK

National Institute of Chemistry, Ljubljana, Slovenia
mirica.karlovits@ki.si, blaz.likozar@ki.si, uros.novak@ki.si

This study investigates the influence of pearlescent pigments printed on polypropylene (PP) packaging on print gloss, focusing on different viewing angles and background colors. Pearlescent pigments, known for their special luster and interference properties, are increasingly used in the packaging industry to increase visual appeal and differentiate products on the shelf. Five different pearlescent pigments (gold, polar white, green, blue and lilac) with the same particle size were used in the study. All pigments consist of thin platelets of the natural material mica, which are coated with a wafer-thin layer of metal oxide. The pigments were overprinted on black background color on printing material (Yupo) using the offset printing process. The print gloss was measured at three different angles (20°, 60°, 85°) using a multi-angle glossmeter, and the pigments were also examined using a scanning electron microscope (SEM). The results show that the background color significantly affects the final appearance of pearlescent pigments, with gloss being higher when printed on a black background than on a white background.

DOI
[https://doi.org/
10.18690/um.fkkt.1.2025.4](https://doi.org/10.18690/um.fkkt.1.2025.4)

ISBN
978-961-286-959-5

Keywords:
pearlescent pigment,
print gloss,
optical effect,
luster,
packaging

1 Introduction

The special effect pigments are used in various areas, e.g. in security applications to protect against counterfeiting and in aesthetic applications such as printing, coating, painting, cosmetic formulations, etc. (Chen, 2019). They are divided into two primary categories: metal effect pigments and pearlescent pigments, also known as nacreous or interference pigments (Buxbaum, 2005). The pearlescent pigments, which are either natural or synthetic, are distinguished by their iridescent color effect, brilliance, and shine, which are based on optically thin layers. Pearlescent pigments simulate the lustre of natural pearls and give the materials additional colour effects, such as the angular dependence of the colour. The light is reflected and scattered across tiny layers to create this optical appearance (Pfaff, 2008). All of these pigments consist of small, thin platelets which, when aligned in parallel in application systems (e.g. in coatings, plastics, printing inks, cosmetic formulations), exhibit strong lustrous effects (Klein, 2010). Most pearlescent pigments consist of at least three layers of two different materials with different refractive indices. The pearlescent effect is created by the specular reflection of light on the many surfaces of the platelets at different depths of the coating film. Light that hits the platelet is partly reflected and partly transmitted through the platelet; the pearlescent effect is created by the dependence of the reflection on the viewing angle. Alumina-based pigments have a strong pearlescent effect compared to mica-based pigments because they are easy to produce, have a very narrow thickness distribution and very smooth surfaces. Alumina-based pigments have the well-known advantages of mica pigments and, thanks to their controlled thickness and chemical purity, offer the possibility of achieving unique optical effects (Rossi, 2020).

Gloss is one of the basic elements of our visual appearance, both in terms of colour and texture. The geometry-dependent characteristics of a surface are described by the gloss perception.

The visual appearance attribute known as specular gloss describes the perceived luminance created by specular reflection on the surface. A typical example of a surface with a high gloss level is a mirror (Kehren, 2013).

Four optical processes can take place when light strikes a pigmented ink layer. These include light scattering and absorption within the ink film as well as light reflection and refraction at the film's surface. All four processes occur to a greater or lesser extent. If the surface of the ink film is smooth and mirror-like, the incident light is reflected in a specular manner, which obeys the small laws of reflection. The film then appears glossy. If the surface is rough, the light is reflected diffusely in all directions and the gloss decreases (Thompson, 2004).

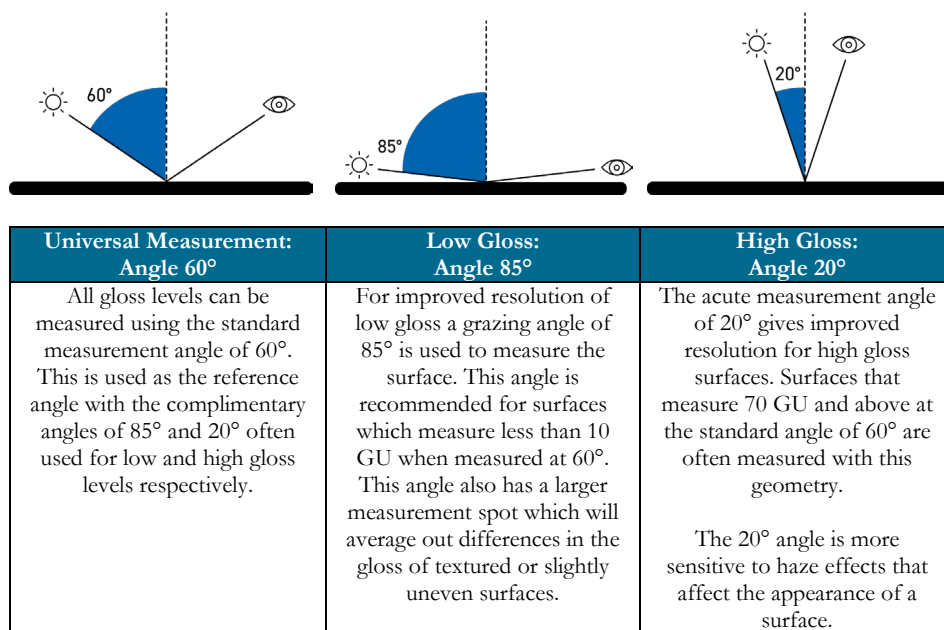


Figure 1: Gloss measurements
(Rhopoint Instruments, 2024).

2 Methods and Materials

Five different commercially available pearlescent pigments from Merck (gold, polar white, green, blue and lilac) with the same particle size were used in the study. The pigments were overprinted on black background color on printing material (Yupo) using the offset printing process. The print gloss was measured at three different angles (20°, 60°, 85°) using the QIP GlossMaster multi-angle gloss meter. The

measurements comply with the ASTM D523 standard measurement protocol for specular gloss measurements. Gloss is measured in gloss units (GU).

Table 1: Properties of printing material (Yupo).

Properties	Grammage	Thickness	Specific volume	ISO Whitness
Values	160 g/m ²	200 μ m	1.3 cm ³ /g	95 %

In this study we used a scanning electron microscope (JSM–5610)JOEL) to evaluate the pigment particles and the surface of the printing material. The synthetic paper Yupo was used as the printing material. It consists mainly of polypropylene film, to which inorganic fillers and small amounts of additives (CaCO₃) are added, and is also used for packaging (Yupo, 2024).

Table 2: Properties of pearlescent pigments.

Pigment name / Properties	Iriodin 325 Solar Gold Satin	Iriodin 119 Polar White	Iriodin 231 Rutile Fine Green	Iriodin 221 Rutile Fine Blue	Iriodin 223 Rutile Fine Lilac
Pigment color	gold	silver	green	blue	lilac
Foam	powder	powder	powder	powder	powder
Substrate	natural mica	natural mica	natural mica	natural mica	natural mica
Effects & properties	masstone, improved chroma, silky	interference, silky	interference, reference chroma, silky	interference, reference chroma, silky	interference, reference chroma, silky
TiO ₂ modification	rutile	rutile	rutile	rutile	rutile
Particle size	5-25 η m	5-25 η m	5-25 η m	5-25 η m	5-25 η m

With increasing TiO₂ layer thickness on the mica, an interference color develops, varying from silver to green (Figure 2).

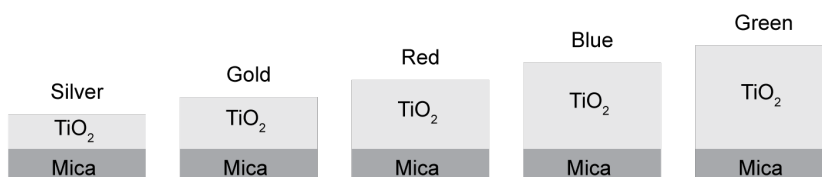


Figure 2: Interference colors

(Pfaff, 2008).

3 Results and Discussion

The SEM analysis was carried out in the first part of the study. All five pigments are based on natural mica, have the same particle size and, as can be seen in the figures, they all have a “cornflake” shape. In Figure 5 (right) we see the unprinted surface of the printing material (Yupo). The surface is very smooth.

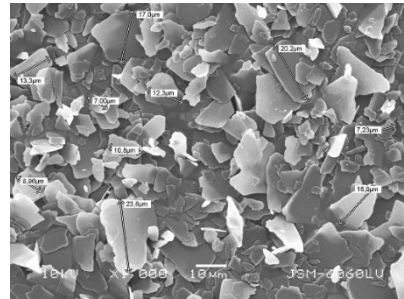
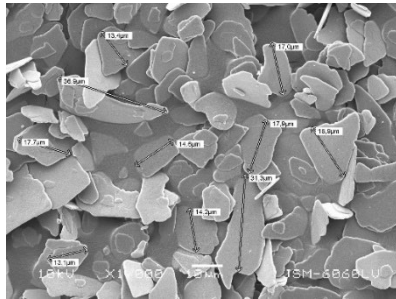


Figure 3: SEM micrograph: *gold pigments (left), silver pigments (right).*

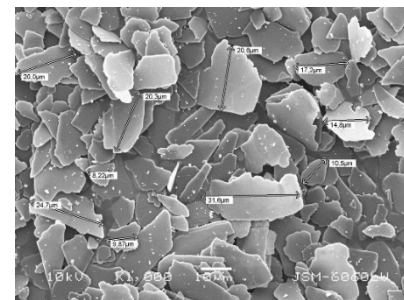
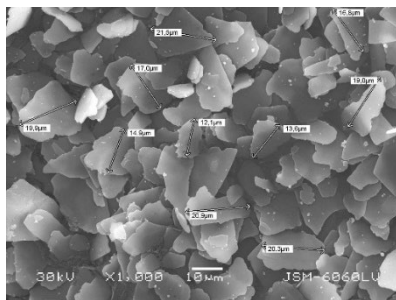


Figure 4: SEM micrograph: *green pigments (left), blue pigments (right).*

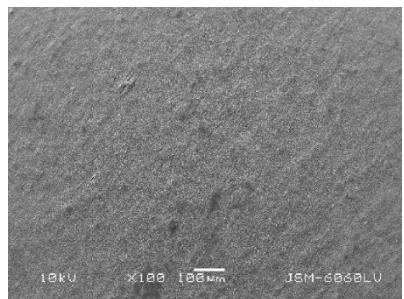
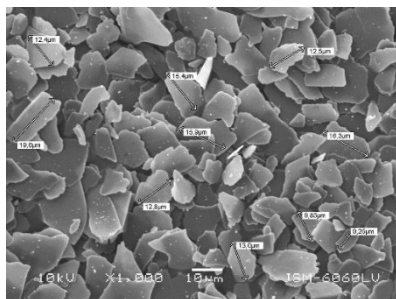


Figure 5: SEM micrograph of *lilac pigments (left) and printing material (right).*

The perception of the gloss is usually correlated to the way objects reflect light from their surfaces and is usually perceived independently from the color appearance; but the underlying color of the object can influence the perception of the gloss and vice versa. Most often the gloss appearance is excluded from the total visual stimulus as it is separated from the color appearance. To determine precisely the gloss values it is important to quantify them by an appropriate measurement device. The classical glossmeters are measuring the intensity of the specular reflection of the sample (I_{sample}) relative to some smooth reference standard ($I_{\text{reference}}$) for the appropriate measurement angle. The average value of the specular gloss G can be defined by the following equation:

$$G_s = 100 \times I_{\text{sample}} / I_{\text{reference}}$$

The total appearance of any object is the combination of its chromatic attributes (color defined through hue, saturation, lightness) and its geometrical attributes (gloss, translucency, texture, shape) inside an surrounding where is the object observed (Karlović, 2010).

Table 3 shows the print gloss of printed pigments on a white and black background.

As we can see from Table 3, all pigments printed on white background obtained lower print gloss compared to black background. The blue pigments printed on both background colors achieved the highest print gloss, where the gloss range from 55.33 for the white background to 66.33 for the black background. The standard deviation on white background was $\sigma=0.21$, while on black background was $\sigma=1.10$. On the other hand, the silver pigments printed on both background colors achieved the smallest print gloss, where the gloss range from 31.30 for the white background to 39.80 for the black background.

The incident light on the printed surface undergoes through several processes of scattering, absorption and reflection depending on the surface topography and structure of the material. The specular part of the surface reflection is commonly attributed as the geometric component of the reflection, and when measured is associated with specular gloss (Karlović, 2010).

Table 3: Print gloss of printed pigments on white and black background.

Gold pigments		
	White background	Black background
Print gloss	38.60	45.17
Std. Dev.	0.45	0.47
Silver pigments		
	White background	Black background
Print gloss	31.30	39.80
Std. Dev.	0.29	1.51
Green pigments		
	White background	Black background
Print gloss	50.40	66.20
Std. Dev.	0.57	0.29
Blue pigments		
	White background	Black background
Print gloss	55.33	66.33
Std. Dev.	0.21	1.10
Lilac pigments		
	White background	Black background
Print gloss	46.00	59.60
Std. Dev.	0.36	0.42

In Figure 6 the influence of background color is presented.

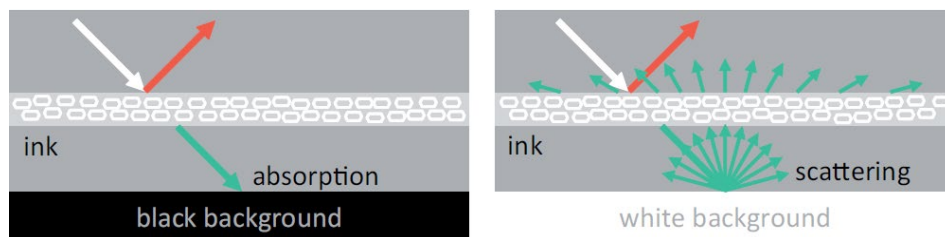


Figure 6: Influence of background color: *black background (left), white background (white).*

In the colored layer, the effect of thin-film interference amplifies and attenuates the incident light, which is symbolized by a white arrow at certain wavelengths. In the specular direction, the reflected light has a specific interference color, which is symbolized by a red arrow. The transmitted light is colored in the complementary color, which is symbolized by a green arrow. The complementary colored light that passes through the color layer hits the background. In the case of a black

background, as shown on the left in Figure 6, most of the transmitted light is absorbed. This means that the complementary color (green arrow) no longer has any influence on the resulting color impression. The perceived color corresponds to the interference effect color of the reflected light (red arrow). In contrast, a white background scatters the transmitted light, as shown in Figure 6 on the right. The intense interference effect color (red arrow) in the direction of reflection is overlaid by a pale complementary color (green arrows) in the entire half-space above the sample.

In the case of gloss and texture, the manipulation concerns the appearance of contrast. The gloss of any light surface is a locally bright reflection of light. The perceived gloss correlates with the difference in lightness of the bright reflection relative to the surroundings. The texture of a surface is based on a pattern of differently colored areas. The difference in color of the brightly shining pigments on the background of some kind determines the perceived texture. For example, gloss and texture are perceived more strongly on the black printed background (Kehren, 2013).

4 Conclusions

The study of printed pearlescent pigments and their effects on visual appearance, such as print gloss, emphasises the crucial role of surface texture in enhancing aesthetic appeal. Gloss, a measure of surface reflectivity, significantly influences how pearlescent pigments interact with light, affecting their perceived vibrancy, depth and shimmer. The print gloss measurements showed that all five pigments had a lower print gloss on a white background than on a black background. When comparing the print gloss of the individual pigments, we found that the highest print gloss was achieved with the blue pigment and the lowest gloss with the silver pigment. Finally, the relationship between printing material and pearlescent pigments influences the significance of the final appearance of the printed packaging. A strong visual appeal is particularly important for high-quality or luxury packaging.

Acknowledgments

The authors would like to acknowledge the financial support of Horizon Europe projects UPSTREAM (GA 101112877), REMEDIES (GA 101093964) and the financial support of the Slovenian Research Agency through the Program P2-0152.

References

- Buxbaum, G. in Pfaff, G. (2005). *Industrial Inorganic Pigments*. 3rd Revised Edition. WILEY-VCH Verlag GmbH & Co KGaA, Weinheim, p. 230.
- Debeljak, M., *et al.* (2012) 'Print gloss of screen printed effect pigments on rich mineral paper', *Celulozã și hãrtie*, 61(1), pp. 3-7.
- Chen, L. *et al.* (2019) 'Metal-dielectric pure red to gold special effect coatings for security and decorative applications', *Surface and Coatings Technology*, 363, pp. 18–24. Available at: <https://doi.org/10.1016/j.surfcoat.2019.01.098>. <https://www.sciencedirect.com/science/article/pii/S025789721930115X?via%3Dihub>
- Gajadhur, M. and Łuszczynska, A. (2017) 'Influence of pearlescent pigments on light-fastness of water-based flexographic inks', *Dyes and Pigments*, 138, pp. 119–128.
- Karlovic, I., Novakovic, D. and Novotny, E. (2010) 'The influence of surface topography of UV coated and printed cardboard on the print gloss', *Journal of Graphic Engineering and Design*, 1(1), pp. 23-31. Available at: <https://doi.org/10.24867/jged-2010-1-023/>.
- Kehren, K. (2013) 'Optical properties and Visual Appearance of Printed Special Effect Colors', *PH diss.*, Technischen Universität Darmstadt, pp. 23-50.
- Klein G. A. (2010) *Industrial Color Physics*. 1st ed. Springer Series in Optical Sciences, pp. 63-92.
- Lin Chen *et al.* (2019) 'Metal-dielectric pure red to gold special effect coatings for security and decorative applications', *Surface & Coatings Technology*, 363 (2019) pp. 18–24.
- Maile, F.J., Pfaff, G. and Reynders, P. (2005) 'Effect pigments—past, present and future', *Progress in Organic Coatings*, 54(3), pp. 150–163. Available at: <https://doi.org/10.1016/j.porgcoat.2005.07.003>.
- Maile, F.J., Pfaff, G. and Reynders, P. (2005) 'Effect pigments—past, present and future', *Progress in Organic Coatings*, 54(3), pp. 150-163.
- Pfaff, G. *et.* (2008) *Special Effect Pigments: Technical Basics and applications*, 2nd Revised Edition, Hannover: Vincentz Network, p. 44.
- Rhopoint Instruments (2024). Available at: <https://www.rhopointinstruments.com/product/rhopoint-iq-20-60-85-gloss-haze-doi-meter/> (Retrieved 20 October 2024).
- Rossi, S., Russo, F. and Bouchakour Rahmani, L. (2020) 'Study of the Durability and Aesthetical Properties of Powder Coatings Admixed with Pearlescent Pigments', *Coatings*, 10(3), p. 229. Available at: <https://doi.org/10.3390/coatings10030229>.
- Thompson, B. (2004). *Printing Materials: Science and Technology*, 2nded., Pira International, pp. 351-355.
- Yupo (2024). Available at: <https://www.yupo.eu/> (Retrieved 20 October 2024).

HIGH-TEMPERATURE RADICAL COPOLYMERIZATION OF DIBUTYL ITACONATE WITH N-BUTYL ACRYLATE, METHYL METHACRYLATE AND STYRENE

NINO KOKOL,¹ TOMAŽ PIRMAN,¹ MARTIN OCEPEK,¹
ROBIN A. HUTCHINSON²

¹ Helios Resins, KANSAI HELIOS Slovenija d.o.o., Domžale, Slovenia
nino.kokol@resinshelios.com, tomaz.pirman@resinshelios.com,
martin.ocepek@resinshelios.com

² Queen's University, Department of Chemical Engineering, Kingston, Canada
robin.hutchinson@queensu.ca

The homopolymerization of itaconates results in relatively short polymer chains and low monomer conversions. To study whether copolymerization provides a more favorable result, dibutyl itaconate was copolymerized with n-butyl acrylate, methyl methacrylate and styrene. In addition to representing the most commercially preferred monomer families, these co-monomers were also chosen due to the differences in the secondary reactions that occur during polymerization at elevated temperatures. Experiments were conducted under semi-batch operating conditions at 110 °C with equal molar ratios of the co-monomer to dibutyl itaconate to enable direct comparison of the results. The impact of varying monomer compositions on polymer molecular mass distributions and polymerization rates was studied, with samples analysed using size exclusion chromatography and high-performance liquid chromatography.

DOI
[https://doi.org/
10.18690/um.fkkt.1.2025.5](https://doi.org/10.18690/um.fkkt.1.2025.5)

ISBN
978-961-286-959-5

Keywords:
copolymerization,
dibutyl itaconate,
monomer composition,
polymer molecular mass
distribution,
semi-batch process



1 Introduction

Commercial acrylic resins are typically produced by solution radical polymerization of methacrylates, styrene and acrylates, with the monomer selection based on both - material costs and the superior chemical and mechanical properties that they impart to the product. Free radical polymerization is versatile because it can polymerize many different monomers under relatively simple conditions. Due to the pursuit of sustainable development, there is a growing desire to replace these petroleum-based monomers with bio-based alternatives. As well as being amenable to polymerization, the bio-derived monomer substitute should match or even improve resin performance to be commercially beneficial (Li et al., 2016; Preusser and Hutchinson, 2016; Pirman et al., 2023; Pirman et al., 2024). One promising bio-based candidate is dibutyl itaconate (DBI), which is obtained by esterification of itaconic acid with butyl alcohol (Yu et al., 2020).

Common practice in commercial resin production is to continuously feed the monomers and initiator into the reactor pre-charged with solvent, operating under isothermal conditions at a temperature > 100 °C. Relatively low feed rates are used with this semi-batch operating strategy to facilitate high instantaneous conversions, such that the copolymer composition matches the comonomer feed composition over the entire course of the reaction. This feeding strategy also allows for better control of the heat generation compared to other reactor systems (Li et al., 2016; Wang and Hutchinson, 2008).

Our previous study has shown that DBI homopolymerization conducted under these operating conditions results in low monomer conversions and very low polymer molar masses, with the system limited by the increased importance of depropagation (Pirman et al., 2024). To study whether copolymerization provides a more favorable result, DBI was copolymerized individually with a monomer from each of the families typically used to produce acrylic resins: n-butyl acrylate (BA), methyl methacrylate (MMA) and styrene (St).

2 Experimental part

2.1 Materials

For experiments the following monomers were used: dibutyl itaconate (DBI; 99.3% purity, Novasol Chemicals), n-butyl acrylate (BA; 99% purity, Sigma-Aldrich), methyl methacrylate (MMA; 99.9% purity, Sigma-Aldrich) and styrene (St; 99.0% purity, Sigma-Aldrich). The solvent was butyl acetate (BAC; 99.5% purity, Sigma-Aldrich) and the initiator was 2,2'-azobis(2-methylpropionitrile) (AIBN; 98.0% purity, Sigma-Aldrich). Acetonitrile (99.9% purity, Honeywell), formic acid (98% purity, Merck) and tetrahydrofuran (THF; 99% purity, Fisher Scientific) were used for characterization. All chemicals were used as received.

2.2 Laboratory Semi-batch Experiments.

Semi-batch copolymerizations of DBI with BA, MMA and St were conducted at a Helios Resins laboratory under reaction conditions intended to mimic standard industrial operations using a Mettler Toledo OptiMax 1001 setup with a 1 L reactor vessel. The mass fraction of DBI in the feed was adjusted to keep the molar composition of the feed identical in all three copolymerizations. AIBN as the initiator was premixed with the monomer at a level of 2 wt % in relation to the total monomer, with the mixture dosed for 5 h at a constant rate into the stirred reactor vessel precharged with BAC solvent and maintained at 110 °C. At the end of dosing, the solvent level was 50 wt % of the total 200 g of solution, with the reactor kept at 110 °C for another 1 h before cooling. Multiple 1 mL samples were taken during the reaction.

2.3 High-Performance Liquid Chromatography (HPLC)/UV Analysis

A Waters HPLC system with separation module e2695 and XBridge C18 5 μm , 4.6 mm \times 150 mm column was used for the determination of monomer conversions. The mobile phase was acetonitrile with 0.1% formic acid at different gradients throughout the 20 min run time at a 1 mL \cdot min⁻¹ flow rate and 40 °C. Three parallels of samples and standards were prepared and filtered through a 0.45 μm filter. A calibration curve was made for all monomers and conversion was calculated based on the obtained quantity of either monomer in relation to the amount of monomer

added up to the point of sampling. Gravimetry and gas chromatography were not used for the determination of conversion due to the high boiling point of DBI (284 °C).

2.4 Size-Exclusion Chromatography (SEC) Analysis

Samples were diluted in THF to achieve a polymer concentration of $\sim 5 \text{ mg}\cdot\text{mL}^{-1}$ and passed through $0.2 \text{ }\mu\text{m}$ nylon filters in preparation for measurement of the polymer molar mass distributions (MMDs) using an Agilent Technologies 1260 Infinity SEC instrument with an Agilent Technologies G1362A RI detector operating at $40 \text{ }^\circ\text{C}$ with a $0.3 \text{ mL}\cdot\text{min}^{-1}$ flow rate and using a single PLgel $5 \text{ }\mu\text{m}$ Mixed-C column. Calibration was established using polystyrene (Poly(St)) standards in the range $580\text{--}2750000 \text{ g}\cdot\text{mol}^{-1}$. Based on repeat injections, the reproducibility of the measurements was within 10 %. The obtained polymer MMDs were relative to polystyrene and were therefore transformed to absolute values using Mark–Houwink parameters taken from the literature (Table 1).

Table 1: Mark-Houwink parameters for poly-DBI, poly-BA, poly-MMA and polystyrene (PS) in THF within the molecular weight ranges suitable for this study.

Polymer	K ($10^{-3} \text{ ml g}^{-1}$)	α
Poly(-DBI)	24.9	0.58
Poly(-BA)	12.2	0.70
Poly(-MMA)	14.3	0.71
Poly(St)	11.4	0.72

source: (Szablan et al., 2007; Wang and Hutchinson, 2010; Menges and Schmidt-Naake, 1998).

3 Results and discussion

3.1 Polymerization rate

The free monomer levels in the reactor, as determined using HPLC, were used to calculate overall monomer conversion over the course of the semi-batch polymerizations. Figure 1 compares the conversion profiles for the three monomer pairings, with each copolymerization system investigated at three different molar levels of DBI in the feed mixture. It is seen that the overall rate of conversion as well as the final conversion achieved decreases as the fraction of DBI in the feed is

increased from 0.150 to 0.346 to 0.614. This result is explained by the influence of DBI depropagation on the system (Pirman et al., 2023).

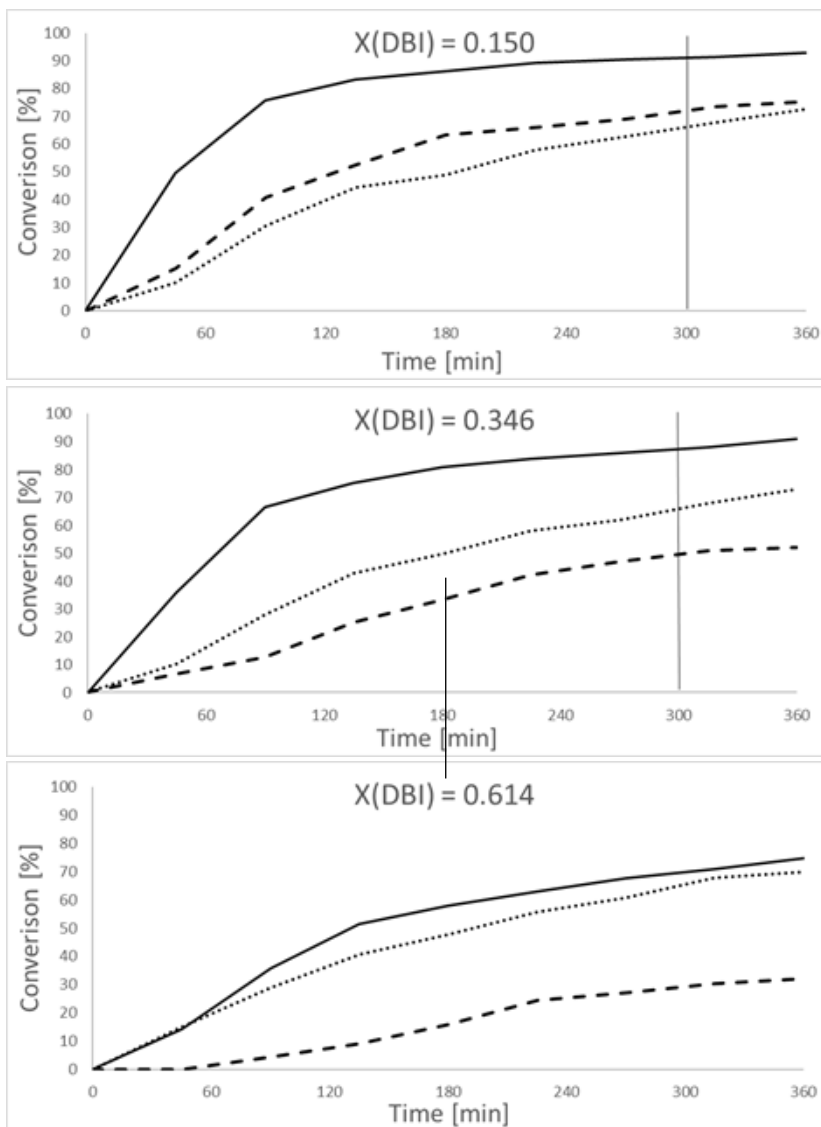


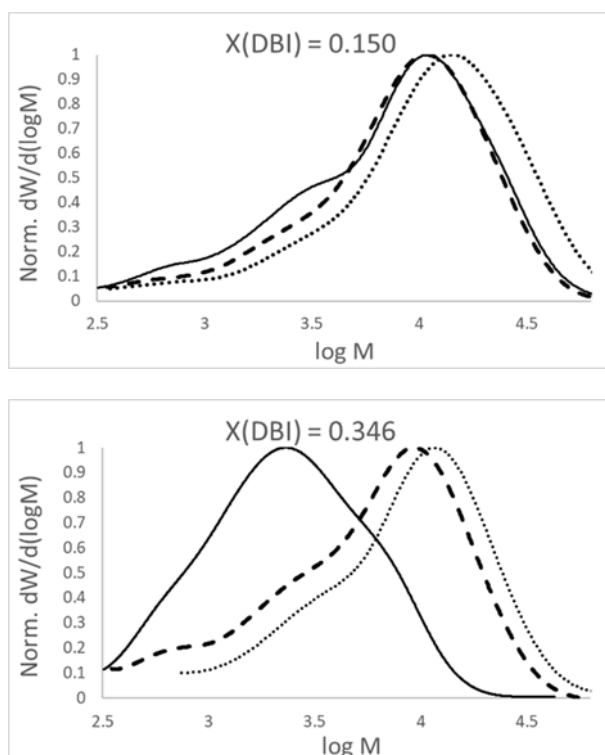
Figure 1: Experimentally obtained data for overall monomer conversion taken during the reactions. Copolymerization of DBI with BA (solid lines)/MMA (dashed lines)/St (dotted lines) for various amounts of DBI (mole fraction). The vertical line represents the end of dosing.

Source: own.

For all feed compositions, the highest monomer conversion is achieved with the acrylate (BA) as comonomer, with only the highest DBI level leading to an observable decrease in the final BA/DBI conversion due to the influence of depropagation. At the lowest DBI level (0.150), the rate of conversion is higher for DBI/MMA than DBI/St, a result consistent with the known higher homopolymerization rates of MMA compared to St. However, the DBI/St rates and final conversions are higher when DBI level is increased, indicating the increased importance of depropagation for the methacrylate-itaconate pairing. Another interesting finding is that copolymerization DBI/St at all three fractions of added DBI leads to similar final conversion ($\sim 70\%$).

3.2 Polymer MMDs

Figure 2 shows the MMDs measured for the final polymer samples at the end of the reaction, demonstrating how the comonomer choice and the DBI level affects the copolymer product.



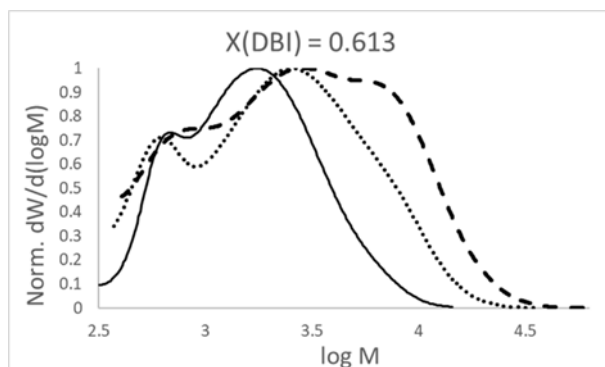


Figure 2: Experimentally obtained data for MMDs – final samples. Copolymerization of DBI with BA (solid lines)/MMA (dashed lines)/St (dotted lines) for various amounts of DBI (mole fraction).

Source: own.

According to Figure 2, it is evident that the greater the proportion of added DBI, the shorter the polymer chains on average. It is also easy to notice that at all three molar ratios, the polymer chains in the copolymerization of DBI/MMA and DBI/St are no longer compared to the copolymerization of DBI/BA, despite the higher rates of conversion observed for the DBI/BA system. This interesting result suggests that the influence of chain transfer mechanisms is higher for this copolymerization system, a result that must be studied further.

4 Conclusion

The comparison of the three DBI copolymerization systems provided some interesting findings and optimistic results showing the incorporation of bio-based monomers into copolymer formed under commercial operating conditions. However, it is necessary to limit the molar level of DBI, in order to produce polymers with sufficiently high molar masses at a reasonable rate. Although the copolymerization of DBI with BA had the highest rates, the polymer molar masses were lower than those measured for DBI/St and DBI/MMA. Based on these experiments, the optimal comonomer combination is dibutyl itaconate and styrene with 35 mol. % DBI, which is equivalent to slightly more than 55 wt. %. To more accurately determine the optimal proportion of DBI for copolymerization with St or other comonomers, additional experiments over a broader range of conditions

are required, along with an evaluation of economic, environmental, and other factors that must be considered for commercial application.

Acknowledgments

We sincerely thank all the organizers of TBMCE for the opportunity to participate in the international conference in Portorož.

References

- Li, X., Mastan, E., Wang, W.-J., Li, B.-G., & Zhu, S. (2016). Progress in reactor engineering of controlled radical polymerization: A comprehensive review. *Reaction chemistry & engineering*, 1, 23–59. <https://doi.org/10.1039/c5re00044k>
- Menges, M., & Schmidt-Naake, G. (1998). Correlation between molecular structure and copolymer composition and the Mark-Houwink constants of methyl methacrylate N-phenylmaleimide copolymers. *Angewandte makromolekulare chemie*, 258, 51–55.
- Preusser, C., & Hutchinson, R. A. (2016). Measuring and modelling the peculiarities of aqueous-phase radical polymerization. *Canadian journal of chemical engineering*, 94, 2045–2051. <https://doi.org/10.1002/cjce.22592>
- Pirman, T., Sanders, C. A., Grojzdek, E. J., Lazić, V., Očepek, M., Cunningham, M. F., Likozar, B., & Hutchinson, R. A. (2023). Free-Radical Homopolymerization Kinetics of Biobased Dibutyl Itaconate. *ACS applied polymer materials*, 5, 9213–9224. <https://doi.org/10.1021/acsapm.3c01708>
- Pirman, T., Sanders, C. A., Očepek, M., Cunningham, M. F., Likozar, B., & Hutchinson, R. A. (2024). Free radical copolymerization kinetics of bio-based dibutyl itaconate and n-butyl acrylate. *Chemical Engineering Journal*, 499, 156127. <https://doi.org/10.1016/j.cej.2024.156127>
- Szablan, Z., Huaming, M., Adler, M., Stenzel, M. H., Davis, T. P., & Barner-Kowollik, C. (2007). Depolymerization kinetics of di(4-tert-butyl cyclohexyl) itaconate and Mark-Houwink-Kuhn-Sakurada parameters of di(4-tert-butyl cyclohexyl) itaconate and di-n-butyl itaconate. *Journal of Polymer Science Part A: Polymer Chemistry*, 45, 1931–1943. <https://doi.org/10.1002/pola.21957>
- Yu, Y., Wang, S., Yang, Z., Wang, F., & Deng, L. (2020). A novel environment-friendly synthetic technology of dibutyl itaconate. *Journal of chemical technology and biotechnology*, 95, 2879–2885. <https://doi.org/10.1002/jctb.6447>
- Wang, W., & Hutchinson, R. A. (2008). Recent advances in the study of high-temperature free radical acrylic solution copolymerization. *Macromolecular reaction engineering*, 2, 199–214. <https://doi.org/10.1002/mren.200700051>
- Wang, W., & Hutchinson, R. A. (2010). High Temperature Semibatch Free Radical Copolymerization of Styrene and Butyl Acrylate. *Macromolecular Symposia*, 289, 33–42. <https://doi.org/10.1002/masy.200900005>

WASTE CONVERTING INTO PRODUCTS

ANITA KOVAČ KRALJ

University of Maribor, Faculty of Chemistry and Chemical Engineering, Maribor,
Slovenia
anita.kovac@um.si

The usage of the fossil must reduce because of a negative effect on the environment. Waste, such as municipal solid waste (MSW), which includes a lot of carbon hydrogen, is resource for chemical and energy productions. This applied study presents the methodology, which is reused the different MSW from unsorted to sorted, created by the mathematical model and the Aspen Plus® simulator for syngas synthesised into different products: methanol, ethanol, synthetic gasoline etc. The mathematical model based on the most real and something simulated parameters. MSW was gassed by using the gasification and the purified circulated flue gas from chimney can enter as raw materials into reforming for syngas production. After the reforming was synthesised the syngas, which is raw material for many products, such as methanol, ethanol and/or synthetic gasoline. During the processes are generated a lot of hydrogen, which can be cleaned and produced as co-product. An existing methanol process can be replaced natural gas with waste different for the methanol or ethanol or synthetic gasoline productions, which could reduce the garbage and CO₂ emission of $0.106 \cdot 10^6$ t/a and of $0.084 \cdot 10^6$ t/a.

DOI
[https://doi.org/
10.18690/um.fkkt.1.2025.6](https://doi.org/10.18690/um.fkkt.1.2025.6)

ISBN
978-961-286-959-5

Keywords:

waste,
syngas,
methanol,
ethanol,
synthetic gasoline



University of Maribor Press

1 Introduction

Non-renewable petroleum resources could be replaced with gasification of sustainable resources, such as waste, intermediate raw materials, bio-waste, for methanol, ethanol, gasoline or other product` productions, using different catalytic converters of Fischer-Tropsch (FT) synthesis, fixed-bed reactors, plasma etc.

Santos and Alencar (2020) upgraded the research of the syngas production from biomass gasification, which is converted into fuels through the Fischer-Tropsch synthesis. This study included many analyses of the catalysts, industrial process requirements, and chemical reaction kinetics and mechanisms of Fischer-Tropsch synthesis. Lignocellulosic material of biomass would be considered a low-cost raw material to the liquid biofuel production. Campanario and Ortiz (2017) presented the upgrade of the Fischer-Tropsch biofuels` production from syngas obtained by supercritical water reforming of the bio-oil aqueous phase. The highlights of this research contained the upgraded production of syngas by using water-gas-shift, dry reforming and Fischer-Tropsch (FT) reactors, and achieved the optimal conditions in the upgraded FT reactor. Gharibi et al. (2024) developed the study of the metaheuristic particle swarm optimization for enhancing energetic and exergetic performances of hydrogen energy production from plastic waste gasification. The improvements contained multi-objective particle swarm optimization for plastic gasification, using grey relational analysis, and achieving lower heating for the polypropylene gasification. Gharibi et al. (2024a) prepared a few novel research to predict polyethylene waste performance in gasification using multilayer perceptron (MLP) machine learning algorithms and interpreting them using multi-criteria decision-making methods, including MLP artificial neural networks and regression models for polyethylene gasification. Mojaver et al. (2018) researched the novel thermodynamic assessment of an integrated solid oxide fuel cell with a steam biomass gasification, including power production. The model of the system was performed using mass and energy conservation laws and equilibrium constants. Mojaver et al. (2019) developed the multi-objective optimization using response surface methodology and exergy analysis during integrated biomass gasification, including the electrical power and the exergy efficiency. Hasanzadeh and Azdast (2024) presented the novel machine learning utilisation on air gasification of polyethylene terephthalate waste, including the machine learning algorithms. Doniavi et al. (2024) defined the efficiency of polyethylene gasification. This study

was based on the energy, exergy, and environmental impact in relation to the material conditions, including the generation the optimal parameters. Hasanzadeh and Abdalrahman (2023) presented the improvements of the processing parameters for polyvinyl chloride waste gasification, including the validated thermodynamic model and different regression models. Khalilarya et al. (2021) presented stud, which combined a heat and power system which consisted of a gasifier, a micro gas turbine, an organic Rankine cycle, a heat exchanger and domestic heat recovery, including the generated power system. Mojaver et al.(2019a) presented the study of a fluidised bed gasifier system with steam as the gasifying agent. The results indicated that the amounts of hydrogen and carbon dioxide were increased, and the amount of carbon monoxide was reduced. Hasanzadeh et al. (2021) developed the gasification model of polyethylene waste, by using the Gibbs free energy minimisation and Lagrange method of undetermined multipliers. Hydrogen production was increased significantly by 48% during steam raising. Mojaver et al. (2022) compared the performances between biomass and plastic waste gasification. The improvement of this study was the analytical hierarchy process/technique for order performance by similarity to the ideal solution coupled method that was employed in gasification of conventional biomass and plastic waste. Mojaver et al. (2021) researched the steam gasification system of polyethylene, polypropylene, polycarbonate and polyethylene terephthalate waste, including the effect of plastic waste ratio, temperature and pressure. The findings revealed that the gasification of polypropylene waste led to the highest hydrogen production at all the processing conditions.

In this study, the waste raw material can be synthesised into syngas, such as raw material for further sustainable different products production. This applied technique based on the complete circular economy, the input unit was upgraded with combustion, gasification and reforming. The conventional natural gas can be replaced with the municipal solid waste (MSW) and flue gas and thereby can reduce the dependence on natural gas.

2 The Applied technique

The municipal solid waste (MSW) and the flue gas can be used as the sustainable raw materials. The usage of waste by using combustion, gasification can be reduced the waste on landfill. The applied technique was presented on the reuse of different MSW from unsorted to sorted and purified flue gas from chimney, based

on the mathematical model including real and simulated data, by using Aspen Plus® simulator. Syngas can be produced from waste by using combustion, gasification and reforming. Syngas was converted into different sustainable products: methanol, ethanol, synthetic gasoline etc. The mathematical model contains the most real and something simulated parameters, giving by Aspen Plus® simulator. The existing reforming system can be enlarged with combustion and gasification for MSW processing (Fig. 1). The purified fuel gas of combustion, including steam and carbon dioxide, such as additional raw materials, is entered into the gasification-reforming system. A comparison between natural gas and waste for syngas production was analysed. The wastes allow higher syngas productions.

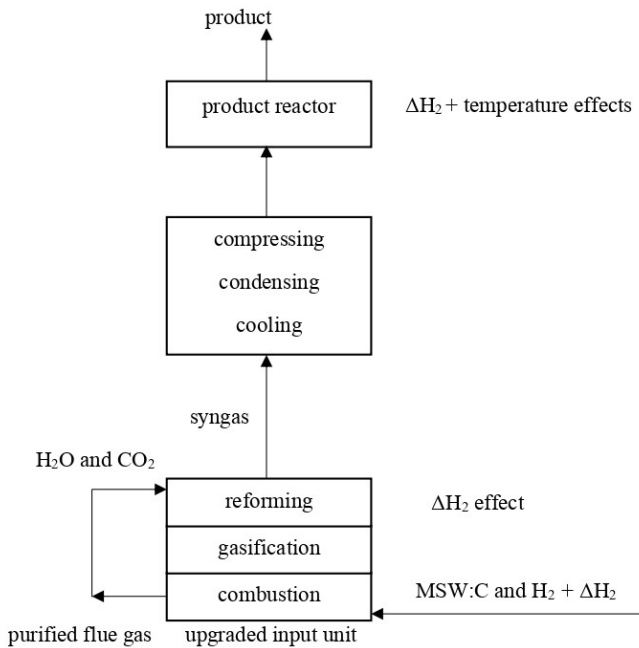


Figure 1: The upgraded system of the combustion, gasification and reforming.

From sustainable syngas can be synthesised the basic methanol product (process P1) during first level (Fig. 2), which can be produced for sales and further formaldehyde production (process P2) during the second level. Different products, such as ammonia (process P3), urea (process P4) and glycolic acid (process P5), can be synthesized from surplus components (hydrogen, nitrogen, carbon dioxide and carbon monoxide) after methanol cleaning during the second level. Products from

the second level (ammonia, urea, formaldehyde) can be synthesized for urea formaldehyde resin (process P6) and hexamine (process P7) productions during the third level. The third level contains products with the highest added value. Methanol production is dependent on the amount of carbon monoxide (CO). The processes of the second and fourth levels are dependent on the amounts of components, such as hydrogen, carbon dioxide, carbon monoxide (H₂, CO₂, CO).

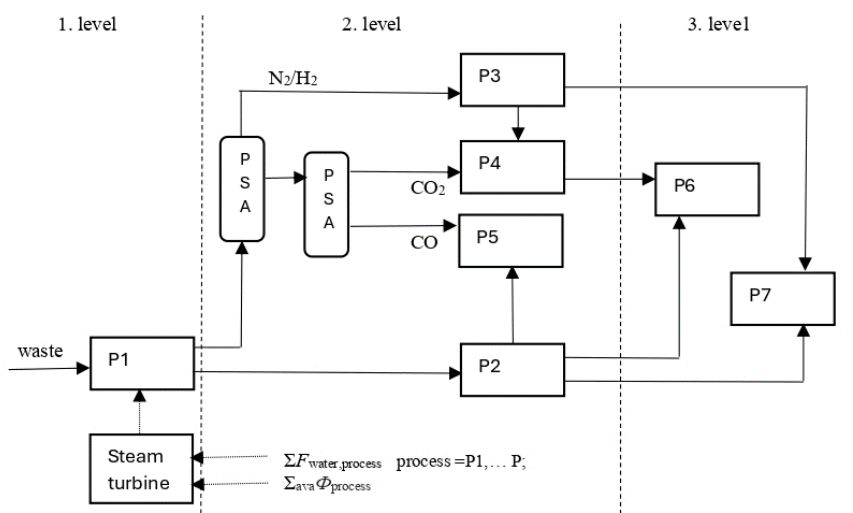


Figure 2: The different products productions from methanol process.

3 Case study

The research study was included the simulation of the methanol, ethanol or synthetic gasoline productions from waste gasification, by using the existing process units and real parameters (Fig. 3). The productions of all processes were profitable.

3.1 Methanol

The sustainable syngas was compressed by using the two-stage compressors. Methanol was synthesized by using the catalytic hydrogenation of carbon monoxide and/or carbon dioxide within reactor, during the following reactions:



From the crude methanol was separated the non-reacted syngas and the water.

3.2 Ethanol production

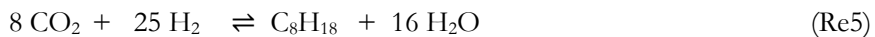
The syngas, from waste generating, was compressed during the two-stage compressors. Ethanol was synthesized by using the catalytic hydrogenation of carbon monoxide within reactor, during the main reaction:



From the crude ethanol was separated the non-reacted syngas and the water.

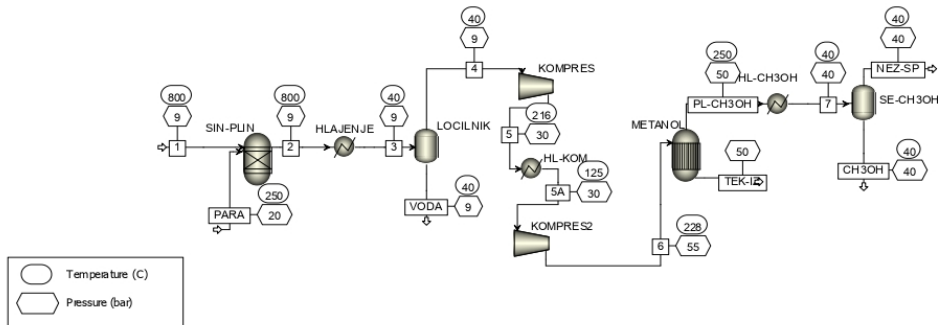
3.3 Synthetic gasoline production

The syngas converts to the synthetic gasoline (C₈H₁₈) into the reactor by using two basic exothermic reactions:

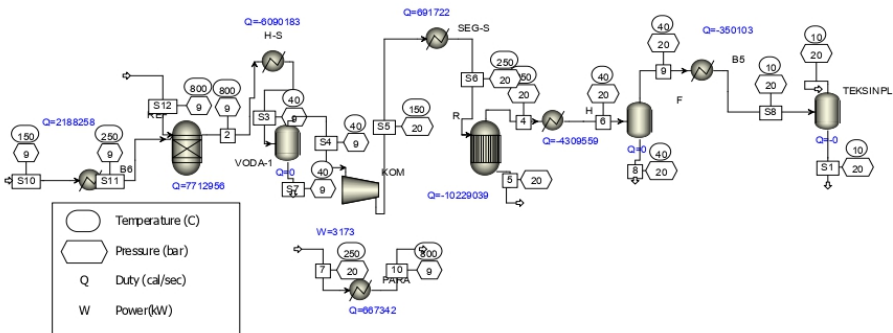


From the crude synthetic gasoline was separated the water and the non-reacted syngas.

Methanol:



Synthetic gasoline



Ethanol

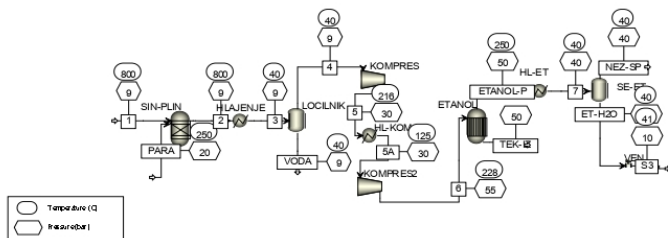


Figure 3: The different products productions from syngas.

4 Conclusions

Natural gas can be replaced with MSW and flue gas for syngas production. From syngas can be synthesized different useful sustainable products, such as methanol, ethanol and synthetic gasoline, by using the applied technique. This technique base on the upgraded input system with combustion, gasification and reforming for syngas production from wastes, and mathematical model, which is depending on the real and simulated parameters. Simulated parameters were obtained by using the Aspen Plus simulator. This technique allows the higher products` production. The MSW and flue gas as raw material can be synthesized sustainable products` production after the complete circular system. A comparison between natural gas and waste as raw material for different products` production were analysed. The wastes allow higher products` productions.

References

- Campanario F. J. and F. J. G. Ortiz. (2017). Fischer-Tropsch biofuels production from syngas obtained by supercritical water reforming of the bio-oil aqueous phase. *Energy Conversion & Management*, 150, 599–613. doi.org/10.1016/j.enconman.2017.08.053
- Doniavi E., R. Babazadeh, R. Hasanzadeh. (2024). Polyethylene gasification for sustainable plastic waste management with respect to energy, exergy, and environmental considerations: A non-linear programming optimization. *Process Safety & Environmental Protection*, 182, 86–97. doi.org/10.1016/j.psep.2023.11.068
- Gharibi A., E. Doniavi, R. Hasanzadeh. (2024). A metaheuristic particle swarm optimization for enhancing energetic and exergetic performances of hydrogen energy production from plastic waste gasification. *Energy Conversion & Management*, 308, 118392. doi.org/10.1016/j.enconman.2024. 118392
- Gharibi A., R. Babazadeh, R. Hasanzadeh. (2024a). Machine learning and multi-criteria decision analysis for polyethylene air-gasification considering energy and environmental aspects. *Process Safety & Environmental Protection*, 183, 46–58. doi.org/10.1016/j.psep.2023.12.069
- Hasanzadeh R. and T. Azdast. (2024). Machine learning utilization on air gasification of polyethylene terephthalate waste. *Waste Management Bulletin*, 2, 75–82. doi.org/10.1016/j.wmb.2023.12.011
- Hasanzadeh R. and R. Abdalrahman. (2023). A Regression Analysis on Steam Gasification of Polyvinyl Chloride Waste for an Efficient and Environmentally Sustainable Process. *Polymers*, 15, 2767. doi.org/10.3390/polym15132767
- Hasanzadeh R., M. Mojaver, T. Azdast, C. B. Park. (2021). Polyethylene waste gasification syngas analysis and multi-objective optimization using central composite design for simultaneous minimization of required heat and maximization of exergy efficiency. *Energy Conversion & Management*, 247, 114713. doi.org/10.1016/j.enconman.2021.114713
- Khalilarya S., A. Chitsaz, P. Mojaver. (2021). Optimization of a combined heat and power system based gasification of municipal solid waste of Urmia University student dormitories via ANOVA and taguchi approaches. *International Journal of Hydrogen Energy*, 46, 1815–1827. doi.org/10.1016/j.ijhydene.2020.10.020

- Mojaver P., S. Khalilarya, A. Chitsaz. (2018). Performance assessment of a combined heat and power system: A novel integrated biomass gasification, solid oxide fuel cell and high-temperature sodium heat pipe system part I: Thermodynamic analysis, *Energy Conversion & Management*, 171, 287–297. doi.org/10.1016/j.enconman.2018.05.096
- Mojaver P., S. Khalilarya, A. Chitsaz. (2019). Multi-objective optimization using response surface methodology and exergy analysis of a novel integrated biomass gasification, solid oxide fuel cell and high-temperature sodium heat pipe system. *Applied Thermal Engineering*, 156, 627–639. doi.org/10.1016/j.applthermaleng.2019.04.104
- Mojaver P., S. Jafarmadar, S. Khalilarya, A. Chitsaz. (2019a). Study of synthesis gas composition, exergy assessment, and multi-criteria decision-making analysis of fluidized bed gasifier. *International Journal of Hydrogen Energy*, 44, 27726–27740. doi.org/10.1016/j.ijhydene.2019.08.240
- Mojaver M, R. Hasanzadeh, T. Azdast, C. B. Park. (2022). Comparative study on air gasification of plastic waste and conventional biomass based on coupling of AHP/TOPSIS multi-criteria decision analysis. *Chemosphere*, 286, 131867. doi.org/10.1016/j.chemosphere.2021.131867
- Mojaver M., T. Azdast, R. Hasanzadeh (2021). Assessments of key features and Taguchi analysis on hydrogen rich syngas production via gasification of polyethylene, polypropylene, polycarbonate and polyethylene terephthalate wastes. *International Journal of Hydrogen Energy*, 46, 29846–29857. doi.org/10.1016/j.ijhydene.2021.06.161
- Santos R. G. and A. C. Alencar (2020). Biomass-derived syngas production via gasification process and its catalytic conversion into fuels by Fischer Tropsch synthesis: A review. *International Journal of Hydrogen Energy*, 45, 36, 18114–18132. doi.org/10.1016/j.ijhydene.2019.07.133

GEORIS PAVERS – A SMALL SCALE DEMONSTRATION WITHIN THE GEORIS PROJECT

MOJCA LONCENAR,¹ LUBICA KRISKOVA,²
CHRISTOS GEORGOPOULOS,³ DIMITRA SKENTZOU,⁴
ANŽE TESOVNIK,⁵ VILMA DUCMAN⁵

¹ SIJ Acroni, Jesenice, Slovenia
mojca.loncenar@acroni.si

² KU Leuven, Leuven, Belgium
lubica.kriskova@kuleuven.be

³ ENALOS Research and Development IKE, Chalandri, Greece
georgopoulos@enalos.com

⁴ SE&C IKE, Markopoulo, Greece
skentzou@senc.gr

⁵ Slovenian National Building and Civil Engineering Institute, Ljubljana, Slovenia
anze.tesovnik@zag.si, vilma.ducman@zag.si,

Technology of alkali activation is an alternative sustainable approach to producing paving paver, where reactive aluminosilicate precursor undergoes a reaction with an alkaline solution to form binded product. The case study presents the functional usability of a technology as part of the Georis project. The construction pavers are composed of over 75% industrial residues, with the majority of the materials sourced from steel slag industry. Laboratory testing of pavers confirmed the promising mechanical properties, demonstrating high compressive and flexural strength, as well as resistance to frost and abrasion. The results support the feasibility of scaling up from lab-scale to pilot manufacturing. The innovative approach in this project was the pilot production process itself, where more than 20 m² of pavers were manufactured and cured in a mobile unit. To assess their real-world performance, a demonstration case was implemented at the SIJ Acroni courtyard, where the pavers were installed to observe their application in a practical setting and to monitor their long-term durability. The valorisation of residues within GEORIS pavers highlights lower CO₂ emissions compared to conventional cement-based pavers and the potential of technology for industrial symbiosis and circular economy initiatives, making it an attractive solution for environmentally conscious industries.

DOI
[https://doi.org/
10.18690/um.fkkt.1.2025.7](https://doi.org/10.18690/um.fkkt.1.2025.7)

ISBN
978-961-286-959-5

Keywords:
geopolymers,
metallurgical residues,
pavers,
properties,
steel slag



University of Maribor Press

1 Introduction

Due to the rapid growth in both construction and population in many places around the world, large amounts of greenhouse gases are being emitted into the atmosphere, with a huge, negative environmental impact. The construction sector and its highly energy-intensive industry of material production contribute up to 40% of the greenhouse emissions. Concrete, the most used manmade material, requires binding by cement, which is responsible for 7% of greenhouse emissions on its own (United Nations Environment Programme, 2023). As a consequence, there is growing attentiveness to the development of sustainable materials in the construction sector, and among the most promising binders to replace Portland cement (OPC) are alkali-activated binders (AAB).

The technology behind AAB is based on the chemical reaction between a solid amorphous material rich in silicon and aluminium and an alkaline solution. This reaction leads to the formation of a solid-bound matrix composed of aluminosilicate gels, which serve as the primary binding phase. Various precursor materials can be used for AAB, with industrial residues and waste materials proving to be viable options for producing high-strength concrete with favourable mechanical properties (Shi et al., 2019). This technology with achievable comparable properties not only provides an alternative to OPC but also promotes sustainable construction by repurposing waste streams.

Although there are several types of alkaline activators, with also research on environmentally friendly alternative alkaline solutions (Mendes et al., 2021), the most commonly used activators are based on alkali hydroxide and silicate solutions (Provis, 2018), with sodium-based solutions dominating, mainly due to their availability and cheaper production. The function of alkaline solutions is to initiate the dissolution reaction of Si and Al species in a high pH environment, where free and reactive silicates undergo nucleation to form a solid interlinked aluminosilicate network.

Among metallurgical slags, ground granulated blast furnace slag (GGBFS) is one of the most widely used source materials for geopolymerisation. The abundance of SiO_2 and Al_2O_3 in GGBFS, its substantial production as a direct by-product of the iron industry, together with suitable physical and latent hydraulic properties, are the

main reasons for its extensive use in the development of AAB. The significant amount of CaO and MgO in GGBFS enhances the structural integrity of the AAB matrix while contributing to a reduction in the required curing temperature (Mishra et al., 2024), making it more sustainable. As a result of the high Ca content and the presence of Ca^{2+} ions in alkaline media due to GGBFS, it leads to the formation of mainly calcium aluminosilicate hydrate (C-A-S-H) gel, that form binding at ambient conditions (Rashid et al., 2024). The amount of C-A-S-H gel is directly related to the development of mechanical properties such as compressive strength. GGBFS-based geopolymers have a characteristic fast development of high strength (early age strength) and high durability performance even at low curing temperatures (Mishra et al., 2024). Excessively high Ca content in GGBFS, one of its main chemical constituents, can significantly affect the performance of the material. To control these issues, such as reduced setting time, higher shrinkage, microcrack development and occurrence of expansion (Lee et al., 2019), proper mix design is essential to ensure a balanced ratio of precursors, activators and additives. Compared to highly amorphous precursors such as GGBFS, fly ash and metakaolin, the main challenge in using steel slag is its high crystallinity, which limits its reactivity. While the amorphous phase of steel slag can participate in the binding reaction, the crystalline phase acts primarily as an inert filler, contributing minimally to alkali activation but potentially influencing the microstructure and mechanical properties of the final material.

The hydration sensitivity and even mechanical behaviour of the material with regard to activation depend on several factors, such as the phase compositions and fineness of the precursor, the curing conditions and alkaline conditions, including initial alkalinity, and the type and concentration of activator used (Liu et al., 2021). Sun et al. (2020) found that alkali activated steel slag has a faster reaction time, fewer hydration products, poorer crystallization of $\text{Ca}(\text{OH})_2$, a lower Ca/Si ratio, and a similar Al/Si ratio of gels compared to Portland cement.

The activation behaviour and mechanical performance of AAB are influenced by multiple factors, including the chemical composition and granulation of the precursor, as well as external conditions such as curing temperature, initial alkalinity, the type and concentration of the alkaline activator used (Liu et al., 2021). Research by Sun et al. (2020) indicates that alkali-activated steel slag reacts more rapidly than Portland cement but produces fewer hydration products. Additionally, it exhibits

poorer crystallization of portlandite (CH), a lower Ca/Si ratio, and a comparable Al/Si ratio in the resulting gel structure. However, Adesanya et al. (2017) showed that ladle slag has the potential to serve as a sole precursor for AAB. After alkali activation, the major product was a silicate hydrate, achieving high compressive strength, 65 MPa, at 28 days. When steel slag is combined with GGBFS, the resulting blended AAB material exhibits significant cementitious properties when activated with an alkaline solution. As shown by You et al. (2019), the inclusion of steel slag influences several key characteristics of the material, including reduced hydration heat, mitigated autogenous and drying shrinkage, prolonged setting time and enhanced workability.

The aim of this study was to develop a low-carbon AAB from metallurgical residues while maximizing the use of metallurgical residues as aggregates. The developed GEORIS pavers were tested in the laboratory, used in the pilot-scale optimized production of pavers and implemented in a test demonstration site. The performance of the pilot pavers was tested to the standard for concrete pavers (EN 1338), as no specific standards exist for AAB pavers.

2 Experimental

2.1 Materials

In this study, two distinct types of industrial residues were utilized: carbon slag (EAF C slag) and the mineral product of processed stainless slag and ladle slag (Ekominut S1, SIJ Acroni). To formulate the mixtures of blended precursors, Ekominut S1 was mixed with finely ground secondary copper slag (SCS) and ground granulated blast furnace slag (GGBFS), leveraging their combined reactivity to enhance the cementitious potential of the system. In contrast, EAF C slag was incorporated as an aggregate, contributing to the overall structural stability of the material and maximizing the valorisation of poorly reactive slags as aggregates. This approach aimed to explore the synergetic effects of these industrial by-products in AAB systems, assessing their suitability for sustainable pavers.

The chemical compositions of these materials are given in Table 1. Ekomin S1 was found to be highly crystalline, consisting mainly of γ -C2S, β -C2S, merwinite and periclase. Whereas SCS and GGBFS showed a predominantly amorphous structure (>90%), indicating high reactivity.

Table 1: The chemical compositions of the metallurgical residues presented in wt%.

Parameters	Ekomin S1	EAF C slag	GGBFS	SCS
LOI (950 °C)	4	0.1	-	-
SiO ₂	17	8	30	25
Al ₂ O ₃	9	5	12	8
CaO	36	30	43	3
MgO	13	10	7	1
K ₂ O	-	<1	1	-
Fe ₂ O ₃	10	32	-	56
MnO	2	5	-	-
TiO ₂	<1	<1	-	-
Na ₂ O	-	<1	-	-
SnO ₃	-	-	2	-
ZnO	<1	-	-	6
Cr ₂ O ₃	3	2	-	-

2.2. Development of recipe and pilot production of GEORIS pavers

The mix design for GEORIS pavers was first developed on a small scale in the laboratory (Kriskova et al., 2025). Different parameters were evaluated, including the OPC or GGBFS and different type of activating solutions (hydroxide-based NaOH, KOH, Na₂SiO₃), and tested. After the optimum laboratory mix design for the GEORIS pavers was defined, the scalability, pot life, and castability for pilot production were considered. Additionally, maximizing the valorisation of metallurgical residues was set as the primary goal. Consequently, the mix design was adjusted to meet these criteria.

For the pilot production of GEORIS pavers (dimensions: 40x40x4 cm³), the Na-based activator was used instead of the K-based alkaline solution, which required further modification of the l/s ratio. The shrinkage-reducing agent was also added to reduce the drying shrinkage of the pilot pavers. The mix design of the pilot pavers, incorporating 75 % metallurgical residues, of which 63% were SIJ Acroni metallurgical residues, is shown in Table 3.

Table 2: Mix-design of the large format tiles, in wt%.

Phase (wt.%)							
Elkominit S1	SCS	GGBFS	M800-fine quartz sand	EAF slag	1.65 NS 65	Shrinkage reducing agent	Binder/liq uid
11.5	11.5	4.1	8.0	51.6	13.0	0.4	2.08

More than 20 m² of GEORIS pavers (dimensions: 40x40x4 cm³) were produced in one of KU Leuven's mobile units (Figure 1). The production of GEORIS pavers is a very simple process, and not a lot of equipment is needed. The most demanding step with regard to utilizing metallurgical residues with geopolymerization technology is to obtain the proper mix design.

The GEORIS pavers demonstration site is located in the courtyard of SIJ Acroni in Slovenia, where the installed pavers will be continuously monitored under real-world conditions (Figure 2). A sufficiently large area exceeding 20 m² has been paved, ensuring exposure to regular foot traffic and operational loads, allowing for a comprehensive assessment of their long-term durability and performance in practical applications.

**Figure 1: KU Leuven mobile unit for the production of GEORIS pavers**

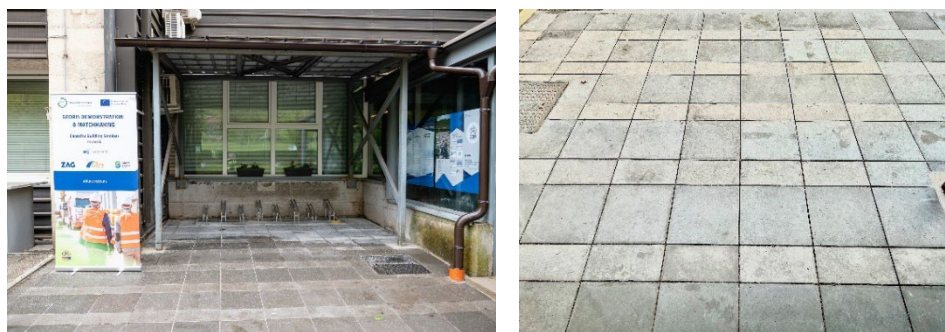


Figure 2: The area paved with GEORIS pavers at SIJ Acroni, Slovenia.

2.3. Methods

Based on current technical standards relevant for the GEORIS project and intended use of the GEORIS pavers, the properties listed in Table 3 have been tested.

Table 3: Test protocols

Testing method:	Standard:	Method type
Work dimensions (mm)	EN 1344	Non-destructive method
Flexural strength (MPa)	SIST ISO 10545 - 4	Destructive method
Freeze-thaw resistance in the presence of de-icing salts (g/m ²)	SIST 1026	Destructive method
Freeze-thaw resistance (visual)	ASTM 666	Destructive method
Hg porosity	-	Destructive method
Leaching (mg/kg)	EN 12457-2	Destructive method
Abrasion resistance (mm)	EN 1338	Destructive method

The environmental impact of the newly developed GEORIS pavers was compared to that of an alternative scenario, by using the standardized Life Cycle Assessment (LCA) method, conducted to evaluate the environmental impact of GEORIS pavers. The LCA analysis was performed using SimaPro 11.0 (v. 9.5) in combination with the Ecoinvent 3 LCI database, ensuring a realistic and consistent representation of the pavers' environmental performance. The focus of LCA was on assessing the environmental impact arising from the production of GEORIS pavers, rather than the development of the End-of-Life (EoL) scenarios, in order to have an idea of what causes this impact and how best to reduce it. This study was conducted for one functional units: the production of GEORIS pavers to cover an area of 1 m², which

equals 97 kg of GEORIS pavers. The system boundaries of the GEORIS product that will be examined are as described in the EN 15804:2012+ A2:20199 standard.

3 Results and discussion

The GEORIS pavers produced in this study were tested according to standard procedures for concrete pavers. In order to compare the GEORIS pavers, they were compared with tests of commercially available concrete pavers tested in a previous study (Frankovič et al., 2020).

Table 4: Properties of GEORIS pavers from pilot production compared to the reference commercial product.

Testing parameter/samples	Freeze-thaw resistance in the presence of de-icing salts	Freeze-thaw resistance	Bending strength (MPa)	Skid resistance	Abrasion resistance
GEORIS pavers	0.01 - 0.03 mg/ mm ²	No visual change after 150 cycles	5.4	64	15.6 mm
Reference concrete product (Frankovič et al.)	Non-resistant	Non-resistant	4	69	22.1 mm



Figure 3: Evaluating freeze-thaw resistance through resonant frequency measurements with a GrindoSonic after n-cycles (left); samples after abrasion resistance testing (right).

The frost resistance evaluation revealed no visible changes or surface damage after 30, 90, and 150 freeze-thaw cycles, demonstrating the pavers’ durability and resistance to freeze-thaw conditions, maintaining their structural integrity and surface quality throughout the testing period. The optimized GEORIS paver mixture exhibited satisfactory frost durability when exposed to a de-icing salt solution (3% NaCl), with surface scaling remaining well below the permitted values (0.038 mg/mm² after 20 cycles). These results confirm the material's suitability for applications in environments where de-icing salts are used, ensuring a non-slip surface in cold conditions while maintaining structural integrity.

The average skid resistance measured under wet conditions across all three directions was 64 (Pendulum Test Value), indicating a surface texture that meets safety standards for walkable applications, such as pavers. If required, the surface skid resistance can be further reduced through additional mechanical or chemical surface treatments.

Table 5: Values of leaching parameters of GEORIS pavers, compared to the permissible values in Slovenian waste regulations.

Parameter	Permissible levels of pollutants in leachate	GEORIS pavers
Cd	0.025	<0.0025
Cu	0.5	<0.05
Ni	0.4	<0.08
Pb	0.5	<0.035
Zn	2	<0.35
Cr	0.5	0.5
Hg	0.005	<0.001
Co	0.03	<0.003
Mo	0.5	0.9
Sb	0.3	<0.03
Se	0.06	<0.06
Ba	20	<0.5
As	0.1	0.02
F ⁻	10	<5
Cl ⁻	800	<50
SO ₄ ²⁻	2500	220

Long-term loss of mass due to wear and tear (traffic, walking, etc.) is an important parameter in assessing how the material will perform in the future. The GEORIS paver was subjected to a wear machine to test the wear resistance of the surface

layer. The high abrasion resistance (15 mm) can be attributed to the compressive strength of the surface (Gencil et al., 2011). In addition to the geopolymerisation of the amorphous precursors, the remaining crystalline slag filler can increase the abrasion resistance, as reported for steel slag aggregates in road construction tests (Díaz-Piloneta et al., 2021).

While incorporating steel slag into AAB offers benefits like waste valorisation and enhanced material properties, it is also crucial to address the potential leaching of heavy metals. The leaching results for elements from crushed GEORIS pavers, tested in accordance with SIST EN 1744-3, revealed slightly elevated molybdenum levels (0.9 mg/kg), exceeding the threshold limit of 0.5 mg/kg. Additionally, chromium concentrations reached the threshold limit of 0.5 mg/kg as specified by the Slovenian directive on permissible pollutant content in products.

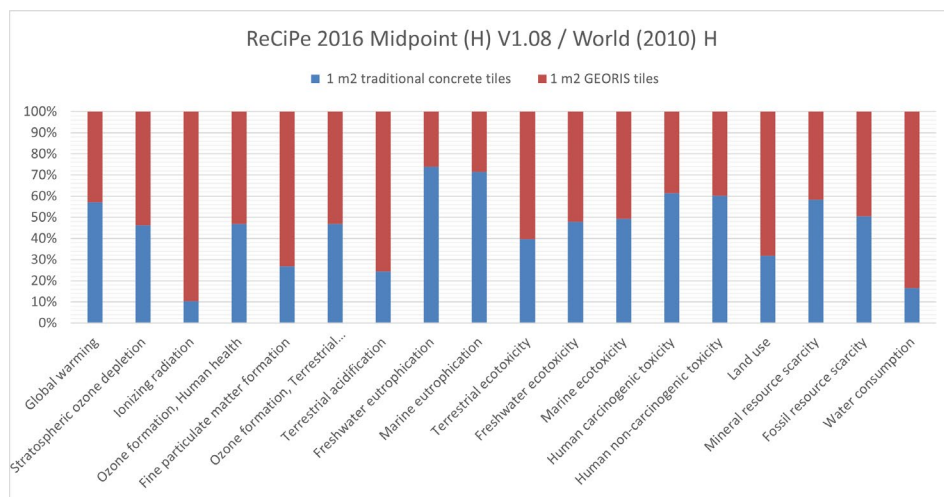


Figure 4: Comparison of impact factors of 1 m² GEORIS paving block vs 1 m² traditional paving block in the scenario of a larger-scale industrial production process.

Several strategies can be employed to mitigate leaching in AAB, focusing on both material design and process optimization. Binder composition can be optimized with secondary precursors, and another strategy is to optimize type and concentration of activator used (Łach et al., 2020). Matrix densification with micro- and nano-silica has been shown to limit the transport pathways available for leachable elements in cement-based materials (Kong et al., 2012; Fu et al., 2022), and this can also be

achieved with post-treatment methods like carbonation curing (Greve-Dierfeld et al., 2008).

The LCA results for the manufacturing of GEORIS pavers are promising, beside the waste valorisation the impact on the environment was reduced compared to concrete pavers. The pavers demonstrated a significantly lower CO₂ footprint compared to conventional concrete tiles, achieving an approximately 26% reduction in carbon emissions per m². Additionally, the LCA results indicate a notable decrease in eutrophication potential, with GEORIS pavers showing a 60% lower impact than traditional concrete tiles. This reduction contributes to minimizing water pollution and mitigating ecosystem degradation, making them a more environmentally friendly alternative.

4 Conclusion

It has been shown that metallurgical residues can be used to a significant extent as reactive precursors or aggregate fillers for the production of pavers using AAB technology. By adjusting the mix through the process of laboratory testing and up-scaling to pilot production, the final product has comparable properties to OPC-based concrete pavers. The GEORIS pavers have high compressive strength and optimum durability prospects. They are resistant to frost (no visible damage after 150 cycles) and maintain their frost resistance even in the presence of de-icing salts following optimization. Additionally, they demonstrate exceptional abrasion resistance. From an environmental standpoint, the leaching parameters of GEORIS pavers generally meet regulatory standards, with the exception of molybdenum (Mo) and, in certain conditions, chromium (Cr). To ensure compliance before scaling up to industrial production, adjustments to the material composition may be necessary. Alternatively, mitigation strategies, such as the application of protective coatings, could be explored to minimize leaching and enhance environmental performance. In terms of environmental footprint, it has been confirmed that metallurgical residues (Ekominut S1, EAF C, SCS, GGBS) can be used instead of raw material, helping to reduce the carbon footprint and save natural resources. The GEORIS pavers demonstrated a lower CO₂ equivalent compared to conventional concrete pavers, highlighting their potential as a more sustainable alternative in the construction sector. As global policies continue to shift towards net-zero targets and stricter carbon emission regulations, the demand for low-carbon construction

materials is expected to rise. In this context, the GEORIS technology may become even more economically viable, as industries seek cost-effective solutions that align with climate action goals.

By advancing to a higher Technology Readiness Level (TRL) through pilot production, key technological parameters of steel slag residues AAB have been identified, providing a solid foundation for further upscaling. These findings will facilitate the transition from pilot-scale to industrial production, ensuring optimized processing conditions and improved material performance, ultimately contributing to the market adoption of sustainable construction products.

Acknowledgments

This research was funded by the European Union under the KIC GEORIS project - Innovative technologies for waste processing in ESEE region (grant number 21107).

References

- Adesanya, E., Ohenoja, K., Kinnunen, P., Illikainen, M. (2017). Alkali Activation of Ladle Slag from Steel-Making Process. *J. Sustain. Metall.*, 3, 300–310. doi.org/10.1007/s40831-016-0089-x
- Díaz-Piloneta, M., Terrados-Cristos, M., Álvarez-Cabal, J.V., Vergara-González, V. (2021). Comprehensive Analysis of Steel Slag as Aggregate for Road Construction: Experimental Testing and Environmental Impact Assessment. *Materials*, 14(13), doi.org/10.3390/ma14133587
- Frankovič, A., Ducman, A., Kriskova, L., Tatsis, E., Petrica, P., Pontikes, Y. (2020). The development and assessment of alkali activated paving blocks. Proceedings in 3rd International Conference on Technologies & Business Models for Circular Economy, Portorož, Slovenia.
- Gaitero, J.J., Campillo, I., A. Guerrero, A. (2008) Reduction of the calcium leaching rate of cement paste by addition of silica nanoparticles. (2008). *Cem. Concr. Res.* 38, 1112-1118. doi.org/10.1016/j.cemconres.2008.03.021
- Gencel, O., Sabri Gok, M., Brostow, W. (2011). Effect of metallic aggregate and cement content on abrasion resistance behaviour of concrete. *Mater. Res. Innov.*, 15(2), 116–123. doi.org/10.1179/143307511X12998222918877
- Kong, D., Du, X., Wei, S., Zhang, H., Yang, Y., P. Shah, S. (2012). Influence of nano-silica agglomeration on microstructure and properties of the hardened cement-based materials. *Constr. Build. Mater.* 37, 707-715. doi.org/10.1016/j.conbuildmat.2012.08.006
- Kriskova, L., Ducman, V., Loncnar, M., Tesovnik, A., Žibret, G., Skentzou, D., Georgopoulos, C. Alkali-activated mineral residues in construction : case studies on bauxite residue and steel slag pavement tiles. *Materials*. 2025, 18,(2), 257, pp. 1-18, doi.org/10.3390/ma18020257.
- Łach, M., Korniejenko, K., Walter, J., Stefańska, A., Mikula, J. (2020) Decreasing of Leaching and Improvement of Geopolymer Properties by Addition of Aluminum Calcium Cements and Titanium Oxide. *Materials*, 13(3), doi.org/10.3390/ma13030495

- Lee, W.-H., Wang, J.-H., Ding, Y.-C., Cheng, T.-W. (2019). A study on the characteristics and microstructures of GGBS/FA based geopolymer paste and concrete. *Constr. Build. Mater.*, 211, 807-813. doi.org/10.1016/j.conbuildmat.2019.03.291
- Mendes, B. C., Pedroti, L. G., Vieira, C. M. F., Marvila, M., Azevedo, A. R. G., De Carvalho, J. M. F., Ribeiro, J. C. L. (2021). Application of eco-friendly alternative activators in alkali-activated materials: A review. *Journal of Building Engineering*, 35, 102010, doi.org/10.1016/j.jobe.2020.102010
- Mishra, J., Nanda, B., Kumar Patro, S., Krishna, R.S. (2024). A comprehensive review on compressive strength and microstructure properties of GGBS-based geopolymer binder systems. *Constr. Build. Mater.*, 417, doi.org/10.1016/j.conbuildmat.2024.135242
- Qiang Fu, O., Zhao, X., Zhang, Z., Xu, W., Niu, D. (2022). Effects of nanosilica on microstructure and durability of cement-based materials. *Powder Technol.*, 404, doi.org/10.1016/j.powtec.2022.117447
- Provis, J.L. (2018). Alkali-activated materials. *Cem. Concr. Res.*, 114, 40–48. doi.org/10.1016/j.cemconres.2017.02.009
- Rashid, K., Naeem Raouf, M., Maheen Daud, A., Wang, Y., Ju, M. (2024). One-part alkali activated binder activated by sodium metasilicate and ternary-factored sustainability of structural block. *Structures*, 68, doi.org/10.1016/j.istruc.2024.107108
- Shi, C., Qu, B. and Provis, J.L. (2019). Recent progress in low-carbon binders. *Cem. Concr. Res.*, 122, 227-250. doi.org/10.1016/j.cemconres.2019.05.009
- Sun, J., Zhang, Z., Zhuang, S., He, W. (2020). Hydration properties and microstructure characteristics of alkali activated steel slag, *Constr. Build. Mater.*, 241, doi.org/10.1016/j.conbuildmat.2020.118141
- United Nations Environment Programme (2023). Building Materials and the Climate: Constructing a New Future. Nairobi
- You, N., Li, B., Cao, R., Shi, J., Chen, C., Zhang, Y. (2019). The influence of steel slag and ferronickel slag on the properties of alkali-activated slag mortar, *Constr. Build. Mater.*, 227, doi.org/10.1016/j.conbuildmat.2019.07.340

UNLOCKING VALUE FROM BY-PRODUCTS IN SLOVENIA'S BIOECONOMY

KATJA MAKOVŠEK, BLAŽ LIKOZAR, UROŠ NOVAK

National Institute of Chemistry, Ljubljana, Slovenia

katja.makovsek@ki.si, blaz.likozar@ki.si, uros.novak@ki.si

Slovenia has significant raw material potential for the development of the bioeconomy. The Interreg Central Europe project TeBiCE focuses on Territorial Biorefineries for a Circular Economy and explores the utilization of biomass, by-products, and residues from primary production and the agri-food processing industry as new sources for producing high-value products. In Slovenia's contribution to the TeBiCE project, three key sectors were evaluated: fruit production and processing, oil production and processing, and the wood processing industry (timber). The potential for developing value chains in Slovenia was assessed using the Value Chain Generator® artificial intelligence tool (VCG.AI). Three value chains were outlined, where polyphenols, biochar, and pectin can be produced through the application of supercritical fluid extraction (SFE), pyrolysis, and enzymatic extraction. Biochar and polyphenols show high potential for exploiting by-product biomass in Slovenia. The VCG.AI tool was demonstrated to be an applicable resource for the fast and effective evaluation of by-products' potential for developing value chains.

DOI
[https://doi.org/
10.18690/um.fkkt.1.2025.8](https://doi.org/10.18690/um.fkkt.1.2025.8)

ISBN
978-961-286-959-5

Keywords:
bioeconomy,
project TeBiCE,
value chain evaluation,
grape pomace,
apple pomace,
olive pomace,
pumpkin seed cake,
wood bark,
Value Chain Generator ®



University of Maribor Press

1 Introduction

Slovenia has a significant raw material potential for development of the bioeconomy, but it has similar as other Central and Eastern European countries sub optimally exploited potential. There is a great need to increase the growth potential of the bioeconomy, which will bring Slovenia not only new jobs, but also environmentally friendly technologies and better prospects for the future (Juvančič, 2021). By-products from primary production and the agri-food processing industry are potential source for production not only energy but also high value products produced by cascade concept of biorefineries (Juvančič, 2021).

Territorial Biorefineries for Circular Economy or shorter TeBiCE is the Interreg Central European project focused on removal the barriers in bio- and circular economies in the Central Europe area, in order to pave the way for the establishment of sustainable market for high-value bio-products. Project TeBiCE promotes the starting of new value chains, based on cutting-edge technologies and new business models, generating a more efficient and competitive economy. Project works on removing of legislative barriers and encourage more harmonized regulation to ensure a more efficient market for by-products and residues of primary production and agri-food processing in the Central Europe area. In project collaborate 8 project partners from 8 regions of Central Europe and 6 countries, Italy, Germany, Poland, Austria, Slovakia and Slovenia. The project started on April 2023 and will finished by the end of March 2026. ¹

In the present contribution the development of value chains (VC) in three sectors in Slovenia, fruit production and processing, oil production and wood processing, is presented and was performed by TeBiCE project. For evaluation the potential of by-products and residue of the selected sectors and for the development of high added value chain, the Value Chain Generator® artificial intelligence tool (VCG.AI) was used. In the contribution, the first the TeBiCE project is introduced, followed by introduction and application of VCG.AI in the context of the project.

¹ Project TeBiCE documentation: CE0100433_TeBiCE_en_en_20220224_083412

2 Introduction of TeBiCE project and by-products potential in Slovenia

Territorial Biorefineries for Circular Economy or shorter TeBiCE is the Interreg Central European project focused on the utilization of biomass, by-products, and residues from primary production and the agri-food processing industry as a new source for producing high-value products. In project is collaborate 8 project partners form 6 countries: Venetian Agency for Innovation in the Primary Sector – Veneto Agricoltura (Italy) – coordinator of TeBiCE project, National Institute of Chemistry (Slovenia), Fraunhofer Italia Research scarl-Innovation Engineering Center (Italy), Chemie-Cluster Bayern GmbH (Germany), University of Warmia and Mazury in Olsztyn (Poland), Kujawsko-Pomorskie Voivodeship (Poland), Carinthia UAS - non-profit limited liability company (Austria) and Slovak University of Agriculture in Nitra (Slovakia). The project started on April 2023 and will finished by the end of March 2026.

Project is divided in three work package (WP) where different aspects of project implementation are evaluated. Figure 1 schematically represents activities of separate WP of TeBiCE project. The potentialities for by-products and waste of the primary and agri-food sectors in Central Europe regions were evaluated in WP1. There was carried out an assessment of the situation and potential application of by-products and residues in Central Europe, including Slovenia. As part of project activities, the application Value Chain Generator® artificial intelligence tool (VCG.AI) was evaluated and applied by project. WP2, Pilot actions to define, by an "on-the-field" approach, constraints and potentialities for value chains, allow the establishment of value chains for the valorization of by-products and waste from residual biomass from the primary production and agri-food processing sectors and the adoption of business model oriented to circular economy. In the WP3, supporting a more harmonized policy scenario and regulatory framework for value chains in Central Europe area, the aim is to remove the institutional barriers and promote a more harmonized regulatory framework in the Central Europe to consolidate the establishment of market of by-products and waste from the primary and agri-food processing sectors.²

² Project TeBiCE documentation: CE0100433_TeBiCE_en_en_20220224_083412

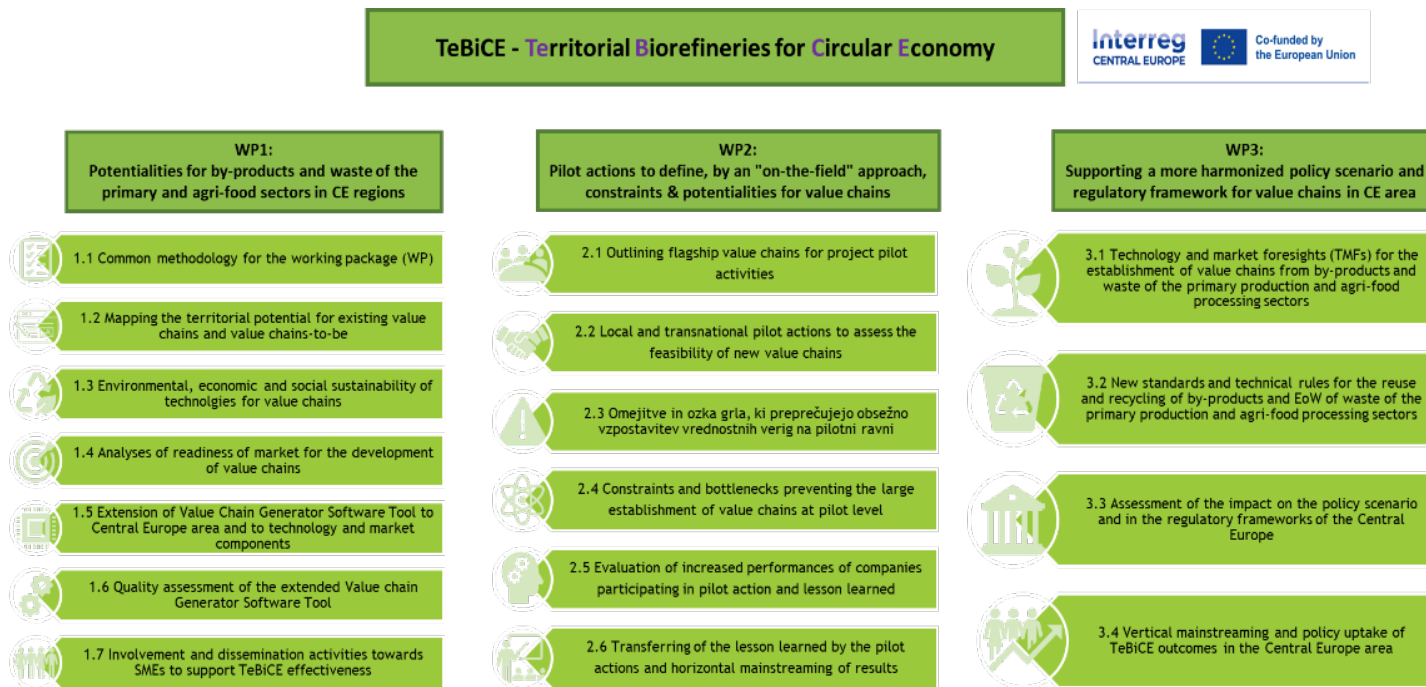








Figure 1: The implementation of TeBiCE project.³

Source: own.

³ Project TeBiCE documentation: CE0100433_TeBiCE_en_en_20220224_083412

Table 1: The potential of by-products evaluated in Slovenian VCs in TeBiCe project.

Evaluated by-product	High added value products	Middle added value products	Low added value products	References
Grape pomace 	<ul style="list-style-type: none"> • Polyphenolic compounds for natural antioxidants (extraction) • Industrial enzymes for citrus acid production; (fermentation) • Pectin for dietary fibers (extraction) • Bio-ethanol, bio-butanol, bio-gas (fermentation) • Poly-hydroxy-butirate (PHB) biopolymer (fermentation) • Grape seeds oil (mill) 	<ul style="list-style-type: none"> • Bio-char (anaerobic pyrolysis) • Bio-fertilizer (fermentation) • Mushroom cultivation • Functional food additives (mill) 	<ul style="list-style-type: none"> • Animal feed • Fertilizer • Energy (combustion) 	Beres, 2017 Sirohi, 2020 Spinei, 2021
Red grape pomace 	<ul style="list-style-type: none"> • Anthocyanins for natural colorants (extraction) • Polyphenolic compounds for natural antioxidants (extraction) • Proanthocyanins (tannins) for natural additives (extraction) 	<ul style="list-style-type: none"> • Bio-char (anaerobic pyrolysis) • Pyrolysis oil (fast pyrolysis) • Bio-fertilizer (fermentation) 	<ul style="list-style-type: none"> • Animal feed • Fertilizer • Energy (combustion) 	Giacosa, 2023 Sirohi, 2020
Apple pomace 	<ul style="list-style-type: none"> • Polyphenolic compounds for natural antioxidants (extraction) • Pectin for dietary fibers (extraction) • Bio-ethanol (fermentation) 	<ul style="list-style-type: none"> • Fruit leather, paper • Bio-char (anaerobic pyrolysis) • Apple flour for food additive 	<ul style="list-style-type: none"> • Animal feed • Energy (combustion) 	Costa, 2022
Olive pomace 	<ul style="list-style-type: none"> • Polyphenols for natural antioxidants (extraction) • Pectin for dietary fibers (extraction) • Bio-fuels (fermentation) 	<ul style="list-style-type: none"> • Bio-char (anaerobic pyrolysis) • Bio-fertilizer (fermentation) 	<ul style="list-style-type: none"> • Animal feed • Energy (combustion) 	Millan-Linares, 2021 Podgornik, 2019 Riberio, 2020
Pumpkin seed cake 	<ul style="list-style-type: none"> • Polyphenols, tocopherols, sterols as natural antioxidants (extraction) • Amino acids for dietary supplement (extraction) 	<ul style="list-style-type: none"> • Protein flours for functional nutrition (mill) • Pumpkin seed flour for food production additive (mill) 	<ul style="list-style-type: none"> • Animal feed 	Singh, 2024
Wood bark 	<ul style="list-style-type: none"> • Lignin for chemical production (extraction) • Phenolic components for adhesives (extraction) • Condensed tannins for polymer resins (extraction) 	<ul style="list-style-type: none"> • Cellulose production (extraction) • Bio-char (anaerobic pyrolysis) • Pyrolysis oil (fast pyrolysis) 	<ul style="list-style-type: none"> • Energy (combustion) 	Das, 2020 Jablonsky, 2017 Juvančič, 2021

Source of pictures: red grape pomace: <https://www.academicwino.com/wp-content/uploads/2012/11/grape-pomace-The-Academic-Wino.jpg>, olive pomace: https://www.zrs-kp.si/wp-content/uploads/2023/11/Moznosti_uporabe_ostankov_SPLETNA-IZDAJA.pdf, pumpkin seed cake: https://www.carphunterco.com/images/thumbnail/produkte/large/AR_25274_0.jpg; grape pomace and wood bark: free accessed on web; apple pomace: own.

The possibilities of application of by-products and residues from primary production and the agri-food processing industry as a potential source for new products were evaluated by development of value chains regarding the region potential of project partners. Slovenia have long and reach tradition of grooving fruits such as grape and apple and oily plants such as olive and oily pumpkin and processing them to wine and oil. Slovenia is also very reach in forest and therefore the wood processing industry had good background for it developed. By-products and residue of presented industries, grape and apple pomace, oil cake and pomace, wood bark and residue are not properly used jet in context of circularity and bioeconomy and there exist the potential for development of value chains with high

added value products, which were evaluated by TeBiCE project. Three key sectors were identified for evaluation by project TeBiCE:

- Fruit production and processing (grape and apple);
- Oil production and processing (olive and pumpkin seed);
- Wood processing industry, particularly timber (wood bark).

Within this framework, six value chains (VC) were developed and assessed: grape pomace VC, red grape pomace VC, apple pomace VC, olive pomace VC, pumpkin seed cake VC, and wood bark VC. Table 1 represents the potential of grape pomace (white and red), apple pomace, olive pomace, pumpkin seed cake and wood bark evaluated in TeBiCE project VCs.

By products such as grape pomace, apple pomace and olive pomace are reach source of various phenolic components and also of polysaccharides like pectin (Sirohi, 2020, Costa, 2022, Millan-Linares, 2021). Red grape pomace is rich in natural colorants, anthocyanins, those could be applied as natural colorants (Giacosa, 2023). Since grape pomace contain high amount of free accessed sugars is good source of nutrients for fermentation process for production of industrial enzymes, bio-ethanol, bio-gases, chemicals produced by fermentation process such as citric acid or bio-biased polymers such as poly-hydroxy-butyrate (Sirohi, 2020). Apple pomace is also good source for fermentation processes, especially for bio-ethanol production (Costa, 2022). All presented by-products, especially, grape pomace, apple pomace and olive pomace, are mostly used for feed production or are deposited in nature as fertilizer (Sirohi, 2020, Costa, 2022, Podgornik, 2019). By investing in application of processes such as pyrolysis and fermentation, the by-products could be processed in middle added value products such as bio-chair or bio-fertilizer were additional benefits are given by energy or bio-gas production (Sirohi, 2020, Costa, 2022). Pumpkins seed cake is residue of pumpkin oil production and contain high amount of fibers and proteins and is usually used for animal feed. Because they high nutritional value is interested also as functional food ingredient (Singh, 2024). The main by-product from timber industry (sawmills) is wood bark that contain wide range of natural component. Tannins are one of high interest because wide range of applications (Das, 2020). Wood bark is also important source of lignin and phenolic components those could be applied in production of chemicals and adhesives

(Jablonsky, 2017). Common application of wood bark is production of energy by combustion. By processing wood bark by pyrolysis bio-char and pyrolysis oil can be produced together with energy (Juvančič, 2021).

In the follow the potential of selected by products and they producers, biomass providers, in Slovenia was evaluated by Value Chain Generator® artificial intelligence tool.

3 Application of Value Chain Generator® - an artificial intelligence tool

The Value Chain Generator® - an artificial intelligence tool (VCG.AI) is a smart data platform for the development of the circular industry. VCG.AI uses a modelling system to develop circular value chains that incorporate clean technologies and processes (vcg.ai, 2024). The application of VCG.AI tool in TeBiCE project was part of WP1 activities, where preliminary evaluation of bioeconomic potential of by-products and residues from primary production and the agri-food processing industry of project partners was evaluated. The evaluation was performed based on the data of small and medium-sized enterprises (SMEs) from the partner regions.

For preliminary evaluation of bioeconomic potential in Slovenia, data of SMEs from the following sectors were collected:

- Fruit production and processing (Fruit and vegetables preserving and processing),
- Wine production (Vineyard and wine production),
- Oil production (Pumpkin seed and olive oil production),
- Wood industry (Sawing, planning and impregnation of wood) and
- Production of natural extracts (production of condiments, spices, fragrances and other additives; production of essential oils; production of other chemical products).

The collected data included basic information on companies (name, location, activity, NACE code) and was collected from a free access webpage Poslovni Asistent Bizi⁴ (eng. Business Assistant Bizi). Collated data was analyzed by VCG.AI, the results are presented in the following paragraph.

⁴ <https://www.bizi.si/>

Figure 2 represents results of evaluation of collated data. Figure 2 A represents an overview of collected information of 308 SMEs from Slovenia that were included in the VCG.AI evaluation. The largest percentage of biomass providers (by-product producers) comes from the wood processing sector (sawmill and wood planning, 108), which accounts for 35.6%. This is followed by the wine production sector at 21.5% (62) and the oil and fat production sector at 21.1% (61). Figure 2 B illustrates the primary mass flows within these evaluated sectors: wood processing (sawmills), wine production (manufacturing), and oil production (oil mills). The main by-products from sawmills – woodchips (26%), bark (19%), and sawdust (8%) – constitute over half (53%) of the wood mass flows. These by-products are typically used as a significant biomass source, often for thermal energy. It could be applied also for new high-added value products. In wine production (wine manufacturing) the main by-product represents grape pomace (10 %), grape seeds (5 %), stalks (3 %) and other residue (5 %) that represents more than 23 % of all mass flows. In oil production depending on applied technologies different by-products are produced such as oil-cake or pomace. They represent around 55 % of mass flows.

Figure 2 C – E represents distribution of SMEs, by-product producers in Slovenia for evaluated sectors: wood processing, sawmills (C), wine production (D) and oil production, oil mill (E). The distribution of by-product producers shows as distribution, density of location where separate by-products is available in Slovenia. By-product producers are potential biomass providers, therefore locations with a high concentration of by-products provide a strong foundation for further evaluation and the development of value chains. Most concentrated regions of the wood processing industry (sawmills) and its by-products were in the surrounding area of cities Ljubljana, Kranj and Celje, whereas others were evenly distributed throughout Slovenia (figure 2 C). Wine production mostly concentrated around regions in the South-Western part of Slovenia surrounding the cities Koper and Nova Gorica and in the Eastern part of Slovenia (figure 2 D). The oil producers were concentrated mostly in two regions: the coastal part of Slovenia where olives are grown and processed to olive oil and in Eastern Slovenia where pumpkin seed oil is produced (figure 2 E).

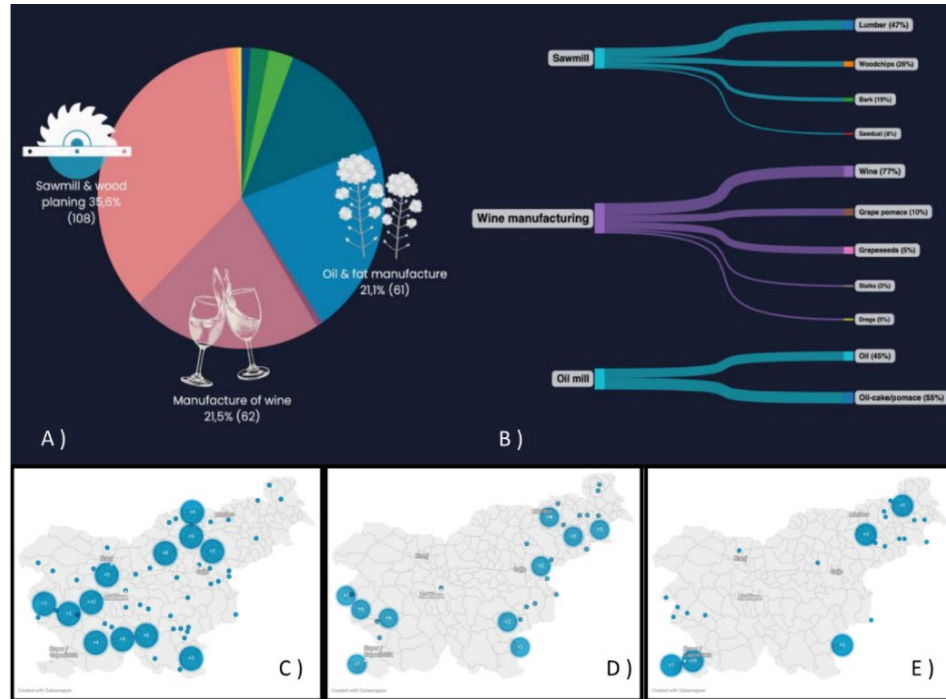


Figure 2: Results of evaluation of collated data of SME-s in selected sectors in Slovenia: A) statistical overview of collected data; B) Mass flow overview in sawmill, wine manufacturing and oil mill; C–E) Distribution of by-product producers in Slovenia for sawmills (C), wine manufacturing (D) and oil mill (E).⁵

⁵ Internal TeBiCE project report: VCG.AI_TeBiCE_Slovenia (1)

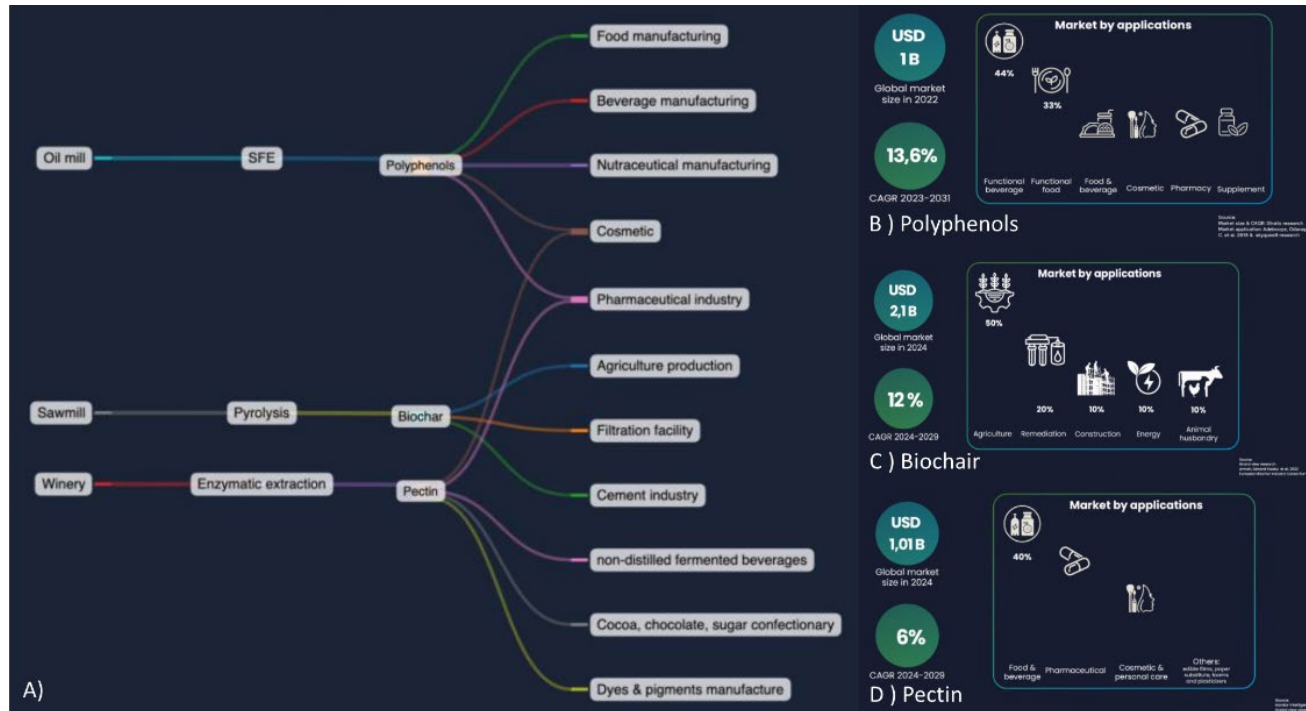


Figure 3: High potential value chains in Slovenia generated by VCG.AI: A) Mass flow of sawmill by-product VC, wine producing by-product VC and oil production residue VC; B–D) Economical potential of VC products, polyphenols (B), biochar (C) and pectin (D).⁶

⁶ Internal TeBiCE project report: VCG.AI_TeBiCE_Slovenia (1)

By following evaluation of collected data and regarding priority stated, three value chains were outlined, where tree products polyphenols, biochar and pectin can be produced by three proper valorization technologies SFE, pyrolysis and enzymatic extraction. Figure 3 represents final VCG.AI generated VCs (A), together with economical potential of products (B – polyphenols, C – biochar and D – pectin). In the follow detailed evaluation of each product was performed.

Polyphenols in Slovenia could be produced from all tree biomass providers using SFE technology and can be applied as natural food preservatives or as active ingredients of functional beverage, nutraceuticals, cosmetics, pharmaceuticals. In Slovenia pectin could be produced from wine and oil production residue by enzymatic extraction and applied as gelling agent in food industry, stabilizer in some beverage and cosmetics and as drug delivery in pharmaceuticals. Biochar can be produced from wood and oil production residue by pyrolysis. Its main application is as soil amendment in agriculture, as pollutant adsorbent and as additive in cement industry.

For all three product the market insight was prepared to light out the global market possibilities (Figure 3 B – D). The bigger Global Market size in 2024, with 2,1 B USA, was evaluated for biochar, followed by pectin with 1,01 B USD and polyphenols with 1 B USD in 2022. The bigger market growth in years 2024 – 2029 was predicted for polyphenols with more than 13 %, following by biochar (12 %) and pectin (6 %). Biochar and polyphenols have a better economical prediction and a broad spectrum of potential uses in comparison to pectin those is mostly applied in food application. Therefor biochar and polyphenols have high potential for exploiting by-products of evaluated sectors in Slovenia.

3 Conclusions

The potential of by-products and residue from three sectors in Slovenia, fruit production and processing, oil production, and wood processing industry, were evaluated in the framework of TeBiCE project by application of Value Chain Generator® artificial intelligence tool. Three value chains were outlined, where three products polyphenols, biochar and pectin can be produced by three valorization technologies SFE, pyrolysis and enzymatic extraction. For all three products the market overview was performed. Biochar and polyphenols have a better economical

prediction and a broad spectrum of potential application regarding to pectin and therefore are products with high potential for exploiting by-products biomass in Slovenia. VCG.AI tool was shown as applicable tool for fast and good evaluation of by-products potential for development of value chains in the context of circular bioeconomy.

Acknowledgments

The authors would like to thank Interreg Central Europe and the European Union for their financial support in the implementation of the TeBiCE project and VCG.AI for their data processing and technical support.

References

- Beres, C., Costa, G. N. S., Cabezudo, I., da Silva-James, N. K., Teles, A. S. C., Cruz, A. P. G., Mellinger-Silva, C., Tonon, R. V., Cabral, L. M. C., Freitas, S. P. (2017). Towards integral utilization of grape pomace from winemaking process: A review. *Waste Management*, 68. doi.org/10.1016/j.wasman.2017.07.017
- Costa, J. M., Ampese L. C., Ziero H. D., Sganzerla W. G., Forster-Carneiro, T. (2022). Apple pomace biorefinery: Integrated approaches for the production of bioenergy, biochemicals, and value-added products – An updated review. *Journal of Environmental Chemical Engineering, Volume 10, Issue 5*, 108358. doi.org/10.1016/j.jece.2022.108358.
- Das A. K., Islam Md. N., Faruk Md. O., Ashaduzzaman Md., Dungani R. (2020). Review on tannins: Extraction processes, applications and possibilities. *South African Journal of Botany*, 135, 58-70. doi.org/10.1016/j.sajb.2020.08.008 .
- Giacosa, S., Ferrero, L., Paissoni, M. A., Río Segade, S., Gerbi, V., Rolle, L. (2023). Grape skin anthocyanin extraction from red varieties during simulated maceration: Influence of grape seeds and pigments adsorption on their surface. *Food Chemistry*, 424. doi.org/10.1016/j.foodchem.2023.136463.
- Jablonsky, M., Nosalova, J., Sladkova, A., Haz, A., Kreps, F., Valka, J., Miertus S., Frecer, V., Ondrejovic, M., Sima, J., Surina, I. (2017). Valorisation of softwood bark through extraction of utilizable chemicals. A review. *Biotechnology Advances, Volume 35, Issue 6*. doi.org/10.1016/j.biotechadv.2017.07.007.
- Juvančič, L., Arnič, D., Berne, S., Grilc, M., Hočevcar, B., Humar, M., Javornik, S., Kocjan, D., Kocjančič, T., Krajnc, N., Križnik, N. B., Likožar, B., Lovec, M., Mavsar, S., Mešl, M., Mihelič, R., Novak, A., Osojnik Črnivec, I. G., Oven, P., Poklar Ulrih, N., Prislan, P., Rac, I., Ščap, Š. (2021) Bridging gaps in Bioeconomy: from Forestry and Agriculture, *Final report CRP V4-1824*.
- Millan-Linares, M.C., Montserrat-de la Paz, S., Martin, M.E. (2021). Pectins and Olive Pectins: From Biotechnology to Human Health, *Biology*, 10, 860. doi.org/10.3390/biology10090860.
- Podgornik, M., Bučar-Miklavčič, M., Levart A., Salobir, J., Rezar, V., Poklar Ulrih, N., Skrt, M., Butinar, B. (2019). Možnosti uporabe ostankov proizvodnje v oljkarstvu. *Poročilo o ciljnoražiskovalnem projektu »CRP V4-1621«*.
- Ribeiro, T. B., Oliveira, A. L., Costa, C., Nunes, J., Vicente, A. A., Pintado, M. (2020). Total and Sustainable Valorisation of Olive Pomace Using a Fractionation Approach. *Applied Sciences*, 10 (19), 6785. doi.org/10.3390/app10196785.

- Singh, A., Kumar, V. (2024). Pumpkin seeds as nutraceutical and functional food ingredient for future: A review. *Grain & Oil Science and Technology*, 7, 12–29. doi.org/10.1016/j.gaost.2023.12.002.
- Sirohi, R., Tarafdar, A., Singha, S., Negic, T., Guard, V. K., Gnansounouf, E., Bharathirajag, B. (2020). Green processing and biotechnological potential of grape pomace: Current trends and opportunities for sustainable biorefinery. *Bioresource Technology*, 314, 123771. doi.org/10.1016/j.biortech.2020.123771.
- Spinei, M., Oroian, M. (2021). The Potential of Grape Pomace Varieties as a Dietary Source of Pectic Substances. *Foods*, 2021, 10, 867. doi.org/10.3390/foods10040867.
- vcg.ai. (2024). Value Chain Generator®. www.vcg.ai.

ECO-FRIENDLY BIOLEACHING: INNOVATIVE TECHNOLOGY FOR EXTRACTING CRITICAL RAW MATERIALS FROM WEEE

DRAGICA MARINIČ, MIHA ŠTRUC, PRIMOŽ OPRČKAL

Slovenian National Building and Civil Engineering Institute, Ljubljana, Slovenia
dragica.marinic@zag.si, miha.struc@zag.si, primoz.oprckal@zag.si

The rapid growth of the quantity of generated electronic waste (e-waste), driven by the increasing demand for electrical and electronic equipment (EEE), has raised urgent concerns regarding its environmental and health impacts. E-waste is the fastest-growing global waste stream, with only a small fraction recycled sustainably. Printed circuit boards (PCBs), a major component of e-waste, contain valuable metals and hazardous substances, complicating recycling efforts. This study explores bioleaching as an environmentally friendly alternative to traditional recycling methods. Bioleaching, utilising microorganisms such as *Acidithiobacillus ferrooxidans* and *A. thiooxidans*, which can effectively extract metals like copper, nickel, and zinc from e-waste, reducing environmental contamination. Our research, conducted under the EIT RawMaterials WEEE-NET9 project, focuses on bioleaching's potential for sustainable recovery of critical raw materials (CRMs) from e-waste. Results demonstrate the effectiveness of bioleaching in metal extraction, supporting the EU's goals of increasing CRM recycling and reducing reliance on primary sources for critical materials, which we have to import into the EU.

DOI
[https://doi.org/
10.18690/um.fkkt.1.2025.9](https://doi.org/10.18690/um.fkkt.1.2025.9)

ISBN
978-961-286-959-5

Keywords:

WEEE,
E-waste,
circular economy,
critical raw materials,
bioleaching



University of Maribor Press

1 Introduction

The growing demand for innovative technologies and electrical and electronic equipment (EEE) has led to a rapid increase in waste electrical and electronic equipment (WEEE or e-waste). E-waste is the fastest-growing waste stream globally, expanding at an annual rate of 3–5% (Ji et al., 2022). According to the *Global E-waste Monitor 2024* (Baldé et al., 2024), e-waste production reached 62 million metric tons in 2022 (Figure 1), an 82% increase since 2010, with only a small fraction recycled in an environmentally sound manner. In 2022, just 22.3% of e-waste was formally collected and recycled (Figure 2). In Europe, 13.5 million tonnes of EEE are placed on the market annually, generating 4.9 million tonnes of e-waste, with less than 40% recycled and an average of 11 kg collected per person (EC ENV, 2024). E-waste contains hazardous and valuable materials, including critical raw materials (CRMs) and rare earth elements (REE), making recycling complex. The OECD projects global material demand will rise from 79 billion tonnes today to 167 billion tonnes by 2060 (Blengini et al., 2020).

It is estimated that 82 million metric tons of electronic waste will be generated in 2030, a significant increase from the 62 million tonnes generated in 2022 (Statista 2025). This situation underlines the urgent need for effective e-waste management strategies and the development of innovative technologies for extracting critical raw materials from e-waste. One of these technologies is also bioleaching, where we use microorganisms for CRM extraction from e-waste, for example PCBs.

The 2022 report on e-waste in the European Union (EU) and EFTA countries, based on data collected under Directive 2012/19/EU, outlines trends in the collection and processing of e-waste. In 2022, the collection rate in the EU reached 40.1%, measured as the weight of e-waste collected relative to the average weight of electronic equipment put on the market in 2019-2021. From 2012 to 2022, the amount of electrical and electronic equipment (EEE) on the EU market grew by 89.3%, from 7.6 million tonnes to 14.4 million tonnes. Over the same period, the total collected e-waste increased by 67.9%, from 3.0 million tonnes to 5.0 million tonnes, while treated e-waste grew by 56.8%, from 3.1 to 4.9 million tonnes. Recovered e-waste rose by 72.1%, from 2.6 million tonnes to 4.5 million tonnes, and e-waste recycled and prepared for reuse grew by 66.6%, from 2.4 to 4.0 million tonnes (Figure 3).

(in million metric tons)

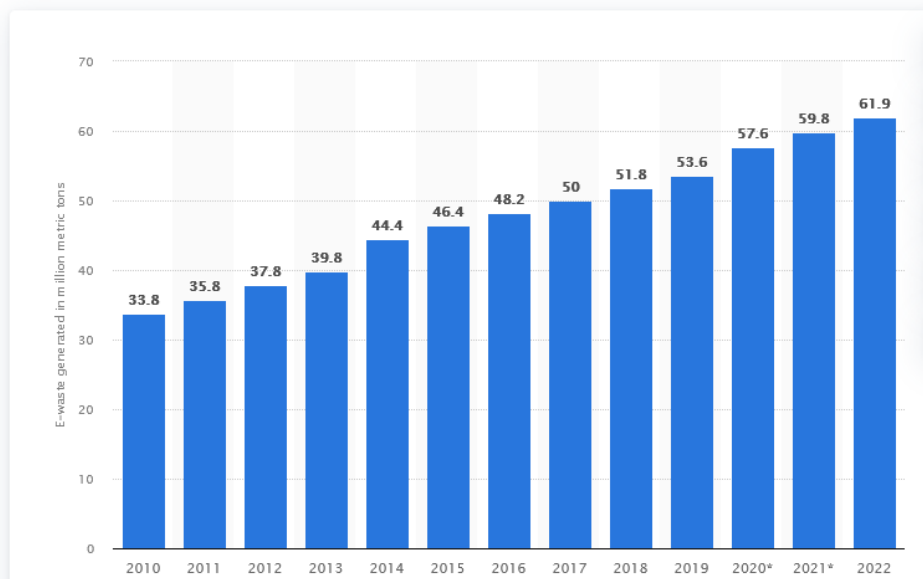


Figure 1: Electronic waste generated worldwide from 2010 to 2022.

Source: Statista 2025

Amount of e-waste generated and collected globally

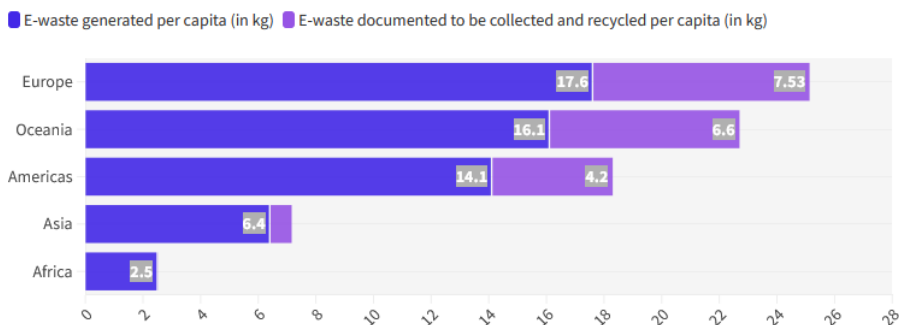


Figure 2: Amount of e-waste generated and collected globally

Source: Unitar 2024

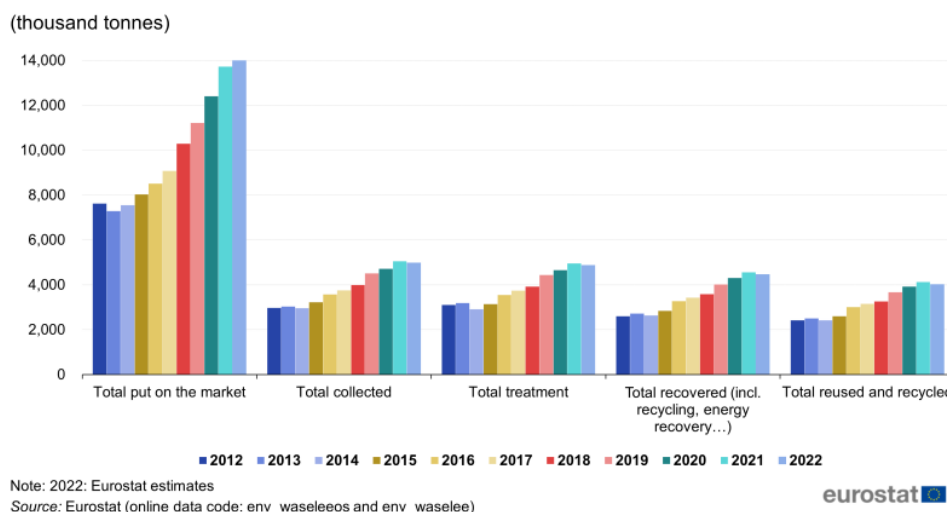


Figure 3: E-waste put on the market and waste EEE collected, treated, recovered, recycled and prepared for reuse, EU, 2012–2022.

Source: Eurostat, 2025

2 Definition and classification of e-waste

E-waste has a highly heterogeneous composition, consisting of both hazardous and non-hazardous materials. It contains polymers, glass fiber, flame retardants, and various ferrous and non-ferrous metals. Additionally, e-waste includes precious metals (e.g., Au, Ag, Pt-group metals), base metals (Al, Co, Cu, Ni, Zn, Fe), rare earth elements (e.g., In, Nd, Ta), and other elements (e.g., Be, Cd, Cr, Hg, Pb, Sb, Sn, Ti). Due to the high metal content, often exceeding that of some natural ores, e-waste is considered a valuable secondary resource (Fu et al., 2021; Rautela et al., 2021).

On the other hand, e-wastes also contain hazardous, making recycling and extraction of and valuable materials, such as critical raw materials (CRMs) and rare earth elements (REE) very complex task. Properly managing and recycling e-waste is not just a necessity, but a crucial step towards EU's 2050 climate neutrality targets under the EU Green Deal (2019), contributes to the EU policy in the field of critical and strategic raw materials, and supports the transition to a circular economy and decarbonisation. The most essential parts of e-wastes are PCBs (printed circuit

boards). Today, a significant portion of e-waste and PCBs end up being incinerated or landfilled, where they are covered up, which can lead to environmental contamination (Yaashikaa et al., 2022). The urgent need for effective and sustainable e-waste management is underscored by its severe risks to human health and the environment (Jain et al., 2023; N. Perkins et al., 2014).

Innovative strategies are needed to improve awareness, collection, pre-treatment, recycling, and reuse of electronic products. Both society and researchers are encouraged to develop new technologies for recovering critical raw materials (CRMs) from e-waste. Sustainable PCB processing methods, such as bioleaching, can tackle environmental and economic challenges while strengthening the value chain and creating jobs in the EU's recycling and raw materials sectors.

2.1.1 Environmental and Health Effects of E-Waste

The improper management of e-waste poses a serious threat to both the environment and human health. E-wastes is made up of a number of toxic organic and inorganic compounds such as polybrominated diphenyl ethers – polychlorinated biphenyls, brominated flame retardants, dioxins and a whole range of heavy metals which are harmful to any ecosystem and living organisms. Most of these toxins find their way into the environment in various forms (Yaashikaa et al., 2022; Rautela et al., 2021; Li & Achal, 2020).

There are several different ways through which a person might be exposed to e-waste. Fine and coarse particles from disintegrated wastes can be inhaled, or leached skin contaminants from the e-waste can be ingested directly, as well as hazardous dust. The high toxicity of pollutants such as e-waste increases concentration as an individual moves up the food chain. This heightened concentration can lead to serious health consequences including heart failure, skin dermatitis, various types of cancer, DNA damage and even birth defects (Adetunji et al., 2023; Anaya-Garzon et al., 2021). Improper disposal also releases dust particles and toxins such as dioxins into the environment, contributing to air pollution and respiratory problems (Rautela et al., 2021).

3 What is bioleaching?

Bioleaching, also known as biomining, is a biotechnological process that utilizes microorganisms to extract valuable metals from e-waste. It has gained attention as an environmentally friendly alternative to traditional methods like pyrometallurgy and hydrometallurgy (Pathak et al., 2017). Printed circuit boards (PCBs) are particularly suitable for bioleaching (Figure 4). Microorganisms such as *Acidithiobacillus ferrooxidans* and *Acidithiobacillus thiooxidans* play a key role due to their ability to oxidize iron and sulfur compounds, leading to sulfuric acid formation and iron mineral oxidation (Mostafavi et al., 2018). During bioleaching, microorganisms interact with metal-bearing particles, facilitating oxidation, reduction, and acidolysis reactions that dissolve solid metals into the leaching solution. Several factors influence the process, including pH, temperature, pulp density, bacterial growth, and particle size (Arshadi et al., 2019).

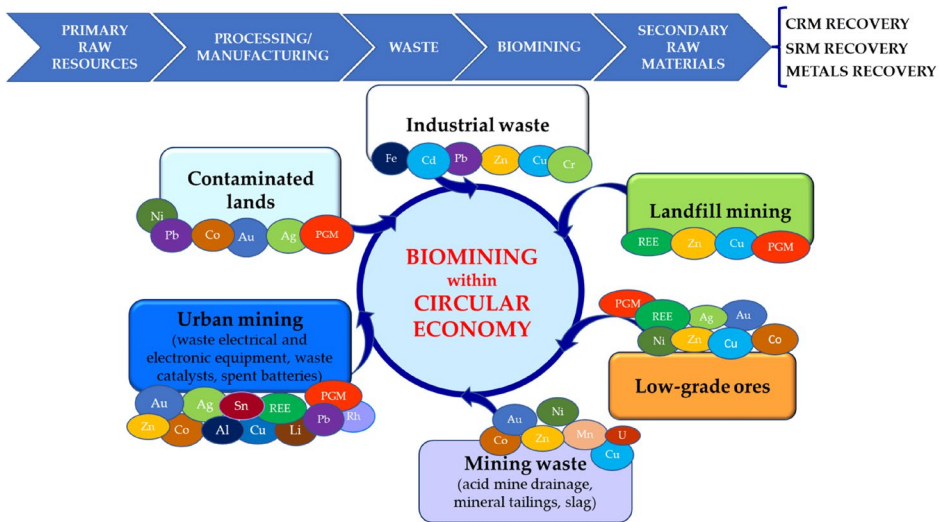


Figure 4: Bioleaching within circular economy

Source: Cozma et al., 2024

Like any other technique, bioleaching has some advantages and some disadvantages, which are presented in Table 1.

Table 1: Advantages and disadvantages of bioleaching.

Advantages	Disadvantages
Environmentally sustainable	Slow process kinetics
Low cost of operation and energy requirement	Long processing time
Minimal use of strong chemical reagents	Not feasible in highly toxic environments
High metal recovery efficiency	Low efficiency at high pulp density
No toxic fume release	Hard process control measures

4 Materials and methods

The study included PCB and mobile phoned samples codes SP-1, PG-2, and PM-2, each with distinct origins and processing characteristics (Table 2). SP-1 consisted of mobile phone materials from the MSH (Metal Shredder Hungary) new batch, which were processed using a hammermill to an intermediate stage with particles smaller than 1 mm. PG-2 represented PCB samples from the Gorenje batch, categorised as communication intermediate products with particle sizes below 1 mm. Similarly, PM-2 comprised PCB materials from the MSH, also processed with a hammermill to achieve an intermediate stage with particle sizes under 1 mm (Figure 5). At first, samples had to be grinded up to a size below 100 μm. Composition of samples: copper (Cu), zinc (Zn), nickel (Ni) and barium (Ba) are the dominant elements in all the samples.

Table 2: E-waste samples used in our research

Sample	Batch	Description
SP-1	Mobile phones - MSH new	hammermill intermediate II <1 mm
PG-2	PCB Gorenje	< 1 mm, communication intermediate product
PM-2	PCB MSH new	hammermill <1mm, intermediate



Figure 5: Codes of e-waste samples used in the bioleaching process.

Before initiating the bioleaching process, the e-waste samples were autoclaved at 121 °C for 15 minutes to ensure sterility. The process began with SP1 smartphone samples, PM2 printed circuit boards, and PG2 printed circuit board samples. The next step involved preparing the MIX media for culturing *Acidithiobacillus ferrooxidans* and *Acidithiobacillus thiooxidans* in a 50:50 ratio (Table 3).

Table 3: Chemicals needed for MIX medium preparation

Growth media	MIX medium
Bacteria	<i>Acidithiobacillus ferrooxidans</i> and <i>Acidithiobacillus thiooxidans</i> (50:50)
Media composition (g)	
(NH ₄) ₂ SO ₄	4.00
KCl	0.10
K ₂ HPO ₄	0.50
MgSO ₄ × 7H ₂ O	0.50
Ca(NO ₃) ₂	0.01
FeSO ₄ × 7H ₂ O	22.10
S	5.00

Once the MIX was ready, 200 mL of the medium was dispensed into 250 mL Erlenmeyer flasks, each containing 3 grams of electronic waste. A 10% inoculum of the bacteria (50% *Acidithiobacillus ferrooxidans* and 50% *Acidithiobacillus thiooxidans*) was added to the medium. The flasks were placed in a shaking incubator set to 30 °C for 25 days (Figure 6). Samples were collected and analysed after 2, 6, 8, 11, 14, 18, 21, and 25 days.

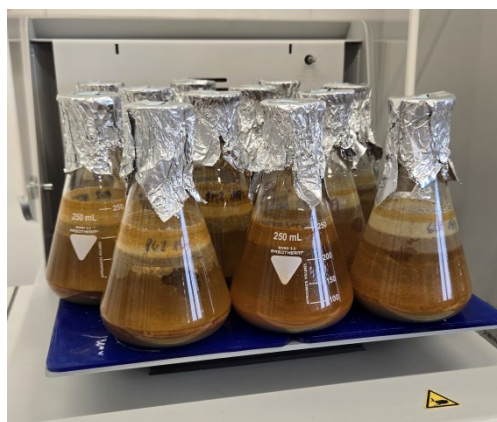


Figure 6: Bioleaching setup

The entire process was conducted in a sterile environment. Each sample was first centrifuged at 9,000 rpm for 10 minutes, then filtered through a 0.22 μm filter. The filtrate was analysed using ICP-MS (7900x, Agilent Technologies, Tokyo, Japan). To ensure reliable results, every experimental condition was run in parallel.

5 Results

The results for the MIX medium showed differences in pH and elemental concentrations over 25 days for SP1, PM2, and PG2 samples (Figure 7).

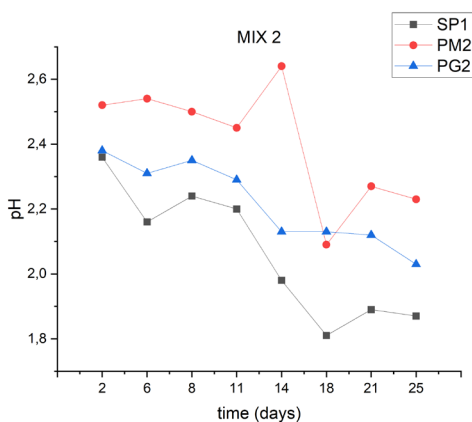


Figure 7: pH results for SP1, PM2 and PG2 samples.

For SP1, the pH steadily dropped from 2.3 to below 1.9 by day 25. Copper (Cu) peaked early on day 6, while zinc (Zn) reached its maximum on day 18. Nickel (Ni), cobalt (Co), and chromium (Cr) didn't reach their highest concentrations during the experiment (Figure 8).

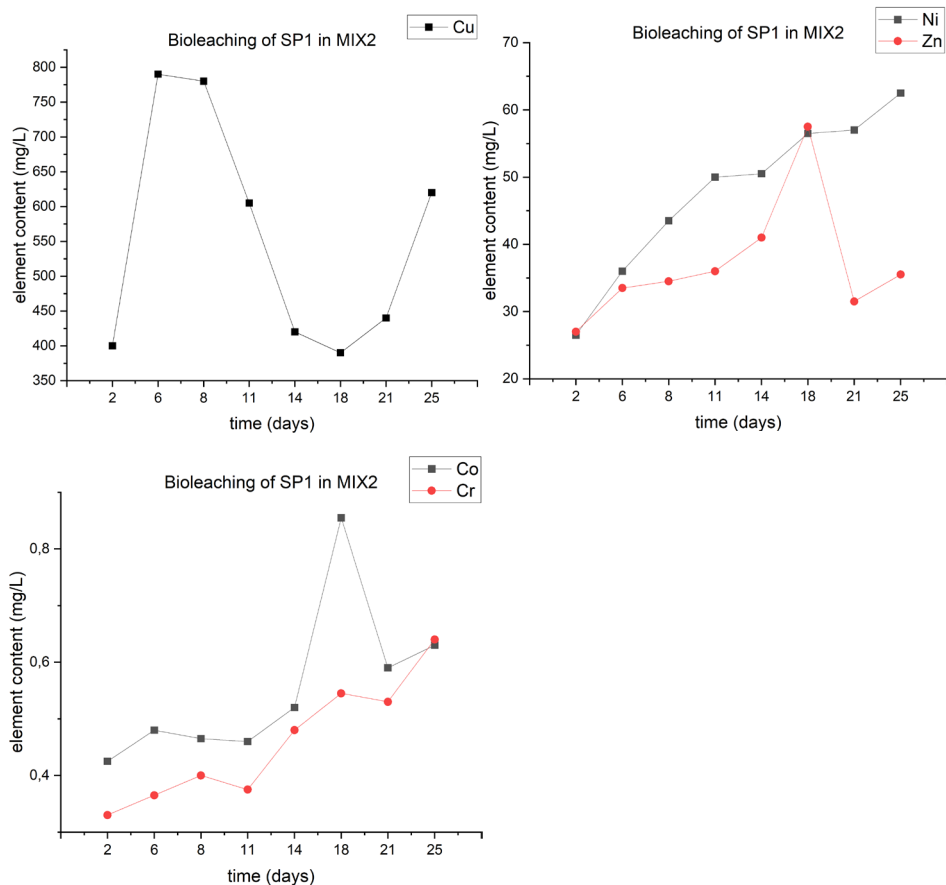


Figure 8: Results for SP1 – mobile phone samples

PM2 had a more stable pH, staying between 2.4 and 2.6 with a spike around day 14. Copper (Cu) peaked on day 21, and nickel (Ni) on day 18. Zinc (Zn), cobalt (Co), and chromium (Cr) showed lower activity and didn't reach maximum levels (Figure 9). Some of the data in the graphs is missing, due to unreliable results.

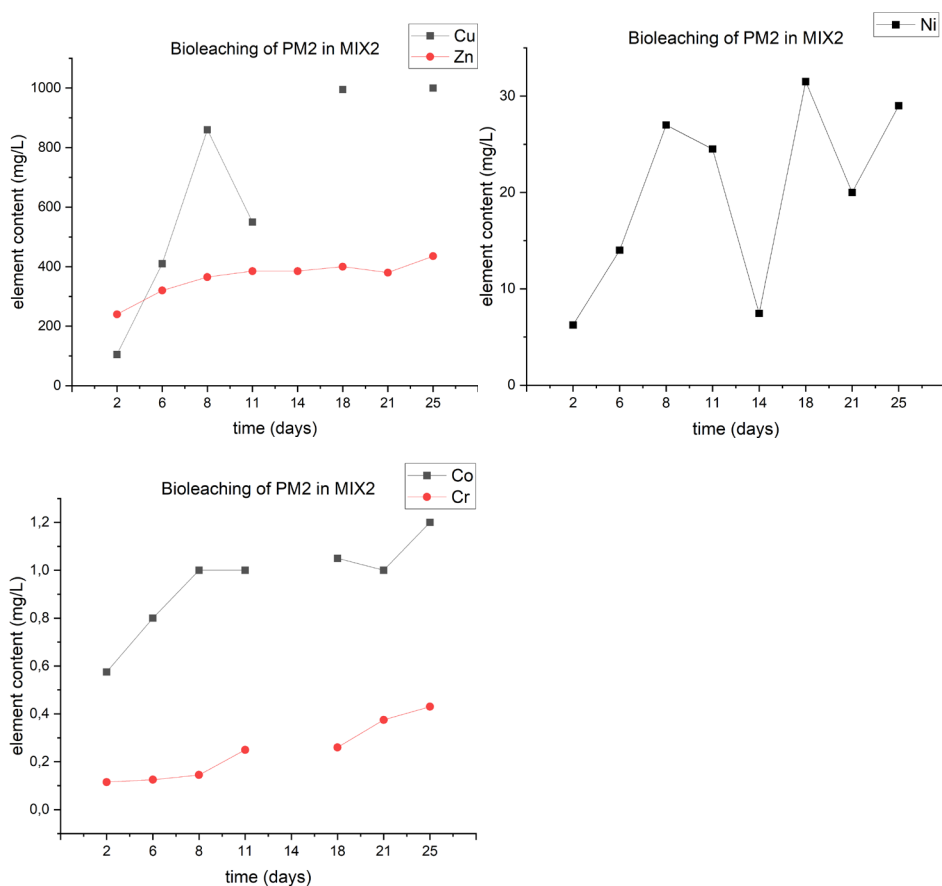


Figure 9: Results for PM2 – printed circuit boards.

For PG2, the pH decreased gradually, staying between 2.1 and 2.4. None of the elements, including Cu, Ni, Zn, Co, or Cr, reached their peak concentrations, suggesting slower bioleaching progress (Figure 10).

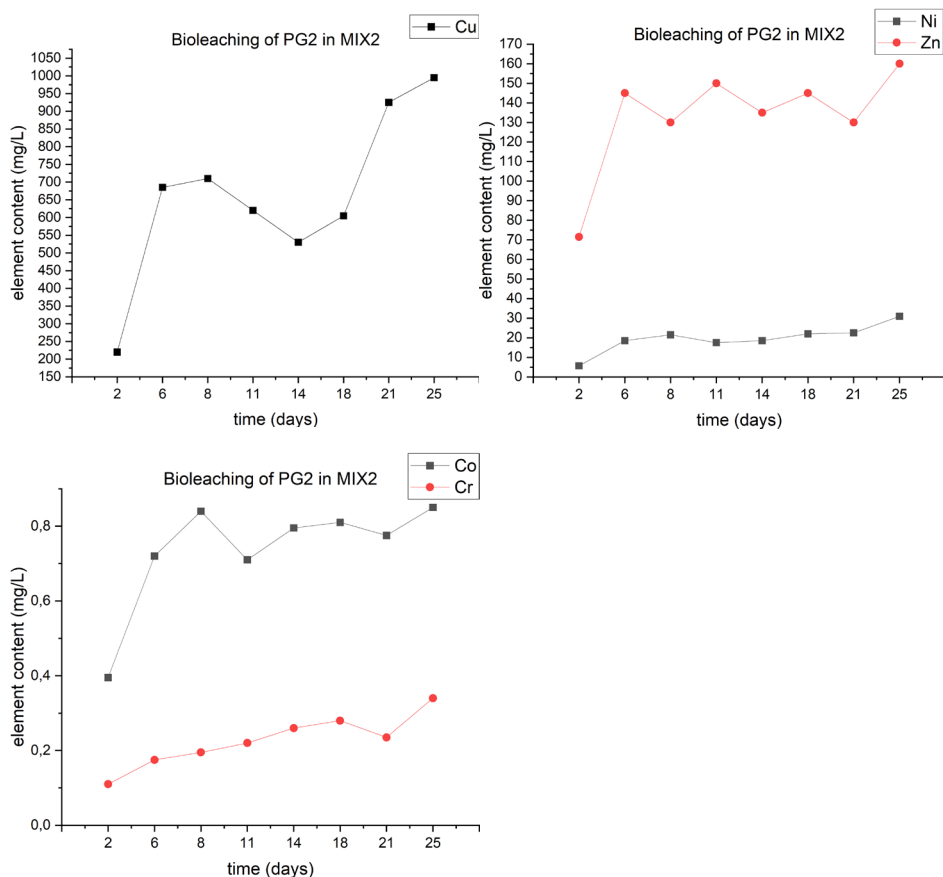


Figure 10: Results for PG2 – printed circuit boards

6 Conclusion

E-waste presents a growing threat to both the environment and human health due to the improper handling of its potentially toxic components. As the electronics and electrical industries expand globally, the challenges associated with e-waste management become increasingly urgent. Innovative strategies, such as recycling and bioleaching, are gaining attraction as sustainable solutions. Recycling plays a crucial role in mitigating environmental harm, while bioleaching offers a modern, environmentally friendly approach to recovering valuable metals from waste.

Bioleaching stands out as a promising method for e-waste management, using microorganisms to extract precious metals and reduce reliance on traditional mining. This process not only supports resource sustainability but also minimises the quantity of hazardous waste. Microorganisms such as *Acidithiobacillus ferrooxidans* and *Acidithiobacillus thiooxidans* are commonly used in bioleaching. To fully harness its potential, further advancements are needed, including the optimisation of bioprocesses, the development of novel catalysts, genetic enhancements of microorganisms, and the exploration of hybrid technologies and innovative microbial substrates. If these enhancements are made, it may be possible to optimise bioleaching for efficient waste management.

Acknowledgements

The article was created for the WEEE-NET9 project (Project no. 21115, co-financed by EIT RawMaterials and the European Union).

References

- Adetunji, A. I., Oberholster, P. J., & Erasmus, M. (2023). Bioleaching of Metals from E-Waste Using Microorganisms: A Review. *Minerals*, 13(6), 828. <https://doi.org/10.3390/min13060828>
- Anaya-Garzon, J., Hubau, A., Joulhan, C., & Guezennec, A.-G. (2021). Bioleaching of E-Waste: Influence of Printed Circuit Boards on the Activity of Acidophilic Iron-Oxidizing Bacteria. *Frontiers in Microbiology*, 12, 669738. <https://doi.org/10.3389/fmicb.2021.669738>
- Arshadi, M., Yaghmaei, S., & Mousavi, S. M. (2019). Optimal electronic waste combination for maximal recovery of Cu-Ni-Fe by *Acidithiobacillus ferrooxidans*. *Journal of Cleaner Production*, 240, 118077. <https://doi.org/10.1016/j.jclepro.2019.118077>
- Baldé, C. P., Kuehr, R., Yamamoto, T., McDonald, R., D'Angelo, E., Althaf, S., Bel, G., Deubzer, O., Fernandez-Cubillo, E., Forti, V., Gray, V., Herat, S., Honda, S., Iattoni, G., di Cortemiglia, V. L., Lobuntsova, Y., Nnorom, I., Pralat, N., & Wagner, M. (2024). *THE GLOBAL E WASTE MONITOR 2024*.
- Blengini, G. A., Horváth, B., Navarro, J., Sonnemann, G., & Manfredi, S. (2020). *Study on the EU's list of Critical Raw Materials – Final Report*. Publications Office of the European Union, Luxembourg.
- Cozma, P., Bețianu, C., Hlihor, R.-M., Simion, I. M., & Gavrilăscu, M. (2024). Bio-Recovery of Metals through Biomining within Circularity-Based Solutions. *Processes*, 12(9), 1793. <https://doi.org/10.3390/pr12091793>
- European Commission. (2019). *The European Green Deal: Communication from the Commission to the European Parliament, the European Council, the Council, the European Economic and Social Committee, and the Committee of the Regions (COM 640 final)*. European Commission.
- Eurostat. (2024). *Waste electrical and electronic equipment (WEEE) by waste management operations*. Eurostat. Retrieved January 24, 2025, from https://ec.europa.eu/eurostat/web/products-datasets/-/env_waselec
- Fu, K., Tian, L., Hou, P., Long, M., Chen, S., & Lin, H. (2021). Stirred-tank leaching of coarse-grained waste, printed circuit boards with *Acidithiobacillus ferrooxidans*. *Physicochemical Problems of Mineral Processing*. <https://doi.org/10.37190/ppmp/141558>

- Jain, M., Kumar, D., Chaudhary, J., Kumar, S., Sharma, S., & Singh Verma, A. (2023). Review on E-waste management and its impact on the environment and society. *Waste Management Bulletin*, 1(3), 34–44. <https://doi.org/10.1016/j.wmb.2023.06.004>
- Ji, X., Yang, M., Wan, A., Yu, S., & Yao, Z. (2022). Bioleaching of Typical Electronic Waste—Printed Circuit Boards (WPCBs): A Short Review. *International Journal of Environmental Research and Public Health*, 19(12), 7508. <https://doi.org/10.3390/ijerph19127508>
- Li, W., & Achal, V. (2020). Environmental and health impacts due to e-waste disposal in China – A review. *Science of The Total Environment*, 737, 139745. <https://doi.org/10.1016/j.scitotenv.2020.139745>
- Mostafavi, M., Mirazimi, S. M. J., Rashchi, F., Faraji, F., & Mostoufi, N. (2018). Bioleaching and Kinetic Investigation of WPCBs by A. Ferrooxidans, A. Thiooxidans and their Mixtures. *Journal of Chemical and Petroleum Engineering*, 52(1). <https://doi.org/10.22059/jchpe.2018.255842.1227>
- N. Perkins, D., Brune Drisse, M.-N., Nxele, T., & D. Sly, P. (2014). E-Waste: A Global Hazard. *Annals of Global Health*, 80(4), 286. <https://doi.org/10.1016/j.aogh.2014.10.001>
- Pathak, A., Morrison, L., & Healy, M. G. (2017). Catalytic potential of selected metal ions for bioleaching, and potential techno-economic and environmental issues: A critical review. *Bioresource Technology*, 229, 211–221. <https://doi.org/10.1016/j.biortech.2017.01.001>
- Rautela, R., Arya, S., Vishwakarma, S., Lee, J., Kim, K.-H., & Kumar, S. (2021). E-waste management and its effects on the environment and human health. *Science of The Total Environment*, 773, 145623. <https://doi.org/10.1016/j.scitotenv.2021.145623>
- Statista. (2024). Global e-waste generation 2010-2022. Statista. Retrieved January 24, 2025, from <https://www.statista.com/statistics/499891/projection-ewaste-generation-worldwide/>
- United Nations Institute for Training and Research. (2024). Global e-Waste Monitor 2024: Electronic Waste Rising Five Times Faster than Documented E-waste Recycling. UNITAR. Retrieved January 24, 2025, from <https://unitar.org/about/news-stories/press/global-e-waste-monitor-2024-electronic-waste-rising-five-times-faster-documented-e-waste-recycling>
- Yaashikaa, P. R., Priyanka, B., Senthil Kumar, P., Karishma, S., Jeevanantham, S., & Indraganti, S. (2022). A review on recent advancements in recovery of valuable and toxic metals from e-waste using bioleaching approach. *Chemosphere*, 287, 132230. <https://doi.org/10.1016/j.chemosphere.2021.132230>

OVERVIEW OF THE IMPACTS OF ADDITIVE PRODUCTION TECHNIQUES ON THE ENVIRONMENT: PRODUCTION OF CONTINUOUS FIBERS, DIRECT LASER SINTERING OF METALS AND SELECTIVE LASER SINTERING TECHNIQUES

BRANKA MUŠIČ,¹ BARBARA HORVAT²

¹ Slovenian National Building and Civil Engineering Institute, Ljubljana, Slovenia
branka.music@zag.si

² Milan Vidmar Electric Power Research Institute, Ljubljana, Slovenia
barbara.horvat@eimv.si

Additive manufacturing (AM) has experienced significant growth in recent years, emerging as a transformative technology with broad applications across various industries. This review explores the advantages, disadvantages, and environmental impacts of AM, an important area of consideration as this technology continues to gain popularity. By analyzing existing literature, we assess the challenges associated with AM processes, particularly in comparison to traditional manufacturing methods. AM has the greatest potential to contribute to sustainable development by the production of lightweight components and complex industrial products with intricate designs. These products are made with minimal material usage. Consequently, also waste and emissions are reduced, which are significant environmental advantages. Overall, this review highlights the importance of AM as a tool for advancing sustainability in manufacturing and offers valuable insights for Continuous Fiber Fabrication, Direct Metal Laser Sintering, and Selective Laser Sintering techniques to enhance their competitive advantage while reducing their environmental impact.

DOI
[https://doi.org/
10.18690/um.fkkr.1.2025.10](https://doi.org/10.18690/um.fkkr.1.2025.10)

ISBN
978-961-286-959-5

Keywords:
additive manufacturing,
3D print,
continuous fiber fabrication,
direct,
metal laser sintering,
selective laser sintering,
AddCircles



University of Maribor Press

1 Introduction

Additive manufacturing (AM) has emerged as a promising alternative to traditional manufacturing methods, offering potential benefits in terms of sustainability and environmental impact (Zhou et al, 2024, Rasiya et al, 2021). This review focuses on three key AM techniques: Continuous Fiber Fabrication (CFF), Direct Metal Laser Sintering (DMLS), and Selective Laser Sintering (SLS). By examining these methods through the lens of environmental considerations and life cycle assessment (LCA), we aim to provide an overview of their respective impacts, supported by relevant statistics.

CFF technique uses continuous fibers made from fiberglass, carbon fiber or even Kevlar. Fibers are integrated into thermoplastic matrices (e.g. polyamide), which improves the mechanical properties of printed parts, and makes those parts stronger and more durable (Kuschmitz et al, 2021). CFF is a dual-extrusion process, where the first extruder lays down the base material (matrix) and forms the shape of the printed product. The second extruder embeds continuous fiber within the printed layers of the matrix focusing on hot spots where mechanical wear out is expected. Working temperature in the nozzle (up to ~ 300 °C) depends on the matrix material and not on the continuous fiber, because fiber should not melt to contribute its physical properties to the melted matrix material. While targeting for the maximum performance of the layer-by-layer printed product, the use of the fiber is minimized, and the creation of waste is reduced with complete control of the process with the software. After printing, the thermoplastic with a reinforced internal structure cools and solidifies. It becomes a composite material that combines the strength of the fiber with the flexibility of the polymer. Because the addition of fiber is a selectively targeted process, printed products with enhanced mechanical properties remain lightweight and can be used for prosthetic limbs, frames for bicycles, brackets and fixtures for cars, parts for drones and even satellites.

While CFF is cited as particularly advantageous for producing lightweight, strong components, DMLS, an AM process that uses a high-powered laser to melt metal powders (titanium, stainless steel, aluminum, cobalt-chrome etc.), is often used for complex geometries (Anand et al, 2021). Computer-aided design (CAD) of the to-be-printed metal part is sliced into thin layers to guide the laser (working at

the power from 100 to 500 W) layer-by-layer in the machine's build chamber which is filled with a fine metal powder. Layer bed temperature is often heated to reduce thermal stress (temperatures are from 100 to 200 °C). The laser selectively scans the chamber in the predefined path and melts (and not sinters) the "beamed" metallic powder particles together. After finishing each layer, the build platform lowers, a new layer of metal powder is spread over the previous and the sintering process continues until the part is built. Because the process demands high temperatures, the solidified printed part is cooled down in the chamber along with the machine to avoid thermal stress and crack formation. While the non-fused powder is removed for reuse purpose, the printed part requires additional post-processing like surface finishing, polishing etc. Like CFF, also DMLS is used for aerospace, automotive, and medical device manufacturing.

Like DMLS, also SLS is a powder bed fusion (PBF) layer-by-layer technique that fuses powdered materials using a high-powered (CO₂) laser (working at the power from 30 to 200 W). The entire build chamber is usually heated just below the melting point of the powdered material to gain uniform melting and prevent warping (temperatures depend on the material used; usually from 170 to 190 °C). While DMLS is used for metals only, SLS is used for polymers (thermoplastics: polyamide, polypropylene, polyether ketone) and elastomers (flexible polymers: thermoplastic polyurethane, thermoplastic elastomer), where both can be mixed with metals (like aluminum powder), ceramics, carbon-fiber, and glass beads or glass fibers to enhance desired properties of the final (composite) product. SLS uses mostly polyamide, while composites and elastomers increase the variety of materials, making SLS suitable for prototyping, low-volume production, and production of parts that require high performance making it suitable for the aerospace, automotive, and healthcare industry.

The environmental impact of additive manufacturing techniques presents opportunities and challenges (Zhou et al, 2024). While these methods offer significant potential for reducing material waste and increasing design flexibility, they also face challenges related to high energy requirements (some printing technologies), emissions from material production, and challenges in recycling or disposing of materials. This review addresses the challenges and opportunities for AM techniques selected in the AddCircles project.

2 Environmental benefits and challenges

The answer to how much impact a certain technology has on the environment requires a comprehensive overview of its entire life cycle (Figure 1), i.e. LCA, and not just the technological capabilities of the technology itself. For the AddCircles project used AM technologies, SLS, DLMS and CFF, focus was on the most in-literature-exposed characteristics.

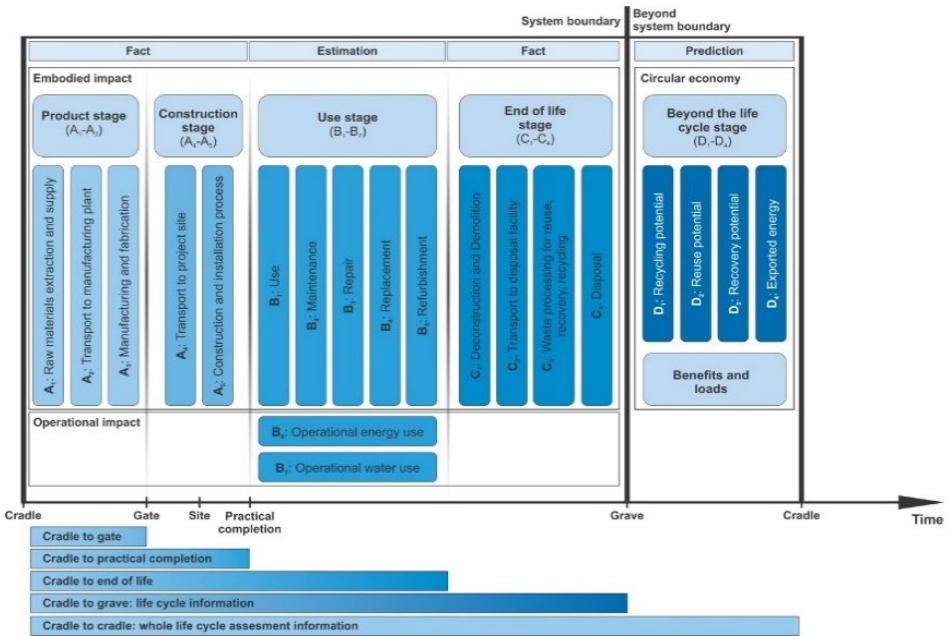


Figure 1: The main stages of LCA

The CFF technique has been found to be more material efficient, as continuous fiber manufacturing can reduce material consumption by 30-50% compared to traditional manufacturing methods due to its ability to optimize material placement and reduce waste. Studies have shown that this technique can lead to a solids-to-envelope ratio of less than 1:7, which is beneficial for reducing environmental impacts (Jung et al, 2023). However, it is also important to note that the production of synthetic fibers (e.g. carbon fibers), which is energy intensive and can emit up to 20 kg of CO₂ per kilogram produced, also has a large impact on the environment. This emphasizes the

need for sustainable sourcing of materials for CFF technology as well (Faludi et al, 2015). So, an important part of the impact on the environment is also the possibility of using recycled materials and the ability to recycle a newly designed product, as this contributes to the circular economy, reduces the demand for raw materials and reduces the amount of waste (Sanchez et al, 2020). Many of the thermoplastics used in the CFF process can be recycled (Sola et al, 2023). Often the environmental challenge is the energy consumption of CFF. The energy required for CFF ranges from 0.5 to 2 kWh per kilogram of material produced. If sourced from non-renewable energy, this can significantly impact the overall carbon footprint of the process (Gopal et al, 2023).

We have also high energy demand in DMLS additive manufacturing techniques. The energy consumption for DMLS ranges from 5 to 10 kWh per kilogram of metal powder processed (Gopal et al, 2023). The carbon footprint associated with this energy use can be significant if derived from fossil fuels (Macheter et al, 2023). There is certainly room for manoeuvre here to reduce the impact on the environment, as well as in the handling of metal dust. Effective management strategies can mitigate the safety and environmental risks in AM posed by the production and challenging handling of metal dust (Modupeola et al, 2024, Chen et al, 2020). A positive characteristic of DMLS technique is the huge ability to reduce material waste. DMLS can achieve a material waste reduction of up to 90% compared to traditional machining processes (Mecheter et al, 2023). This is due to its additive nature, where only the required amount of material is used. Also, DMLS has Life cycle benefits. Parts manufactured with DMLS often have superior mechanical properties, leading to longer life and reduced resource consumption over time. For example, DMLS components can be designed to be lighter, which in turn reduces energy consumption during product use – which is especially critical in industries such as the aerospace industry (Markforged and Metalcraft solutions, assessed on 19.9.2024).

As with DMLS, the source of energy required for SLS has a strong impact on the overall sustainability of the process, as the energy consumption rate for SLS is approximately 3-6 kWh per kilogram of processed material (Hegab et al, 2023). However, SLS technology also has advantages such as design flexibility and a good ability to recycle the material. SLS enables the production of complex geometries that would be difficult or impossible with conventional techniques. This flexibility

can lead to more efficient designs that use less material overall while improving performance. At the same time, SLS enables the recycling of unused powder, with studies showing that up to 70% of unused material can be recovered and reused in subsequent builds (Peng et al, 2018). This significantly improves the sustainability profile of SLS compared to traditional production methods. However, we must also pay attention to the fact that some powders can release harmful particles or volatile organic compounds (VOCs) during processing, which requires adequate ventilation and filtration systems to mitigate the impact on air quality.

Table 1: Energy consumption and material waste reduction for CFF, DMLS and SLS.

A type of additive manufacturing technique	Energy Consumption [kWh/kg]	Material Waste Reduction [up to %]
CFF	0.5-2	50
DMLS	5-10	90
SLS	3-6	70

LCA is a method supported by international standards (ISO 14040 and ISO 14044). LCA provides a comprehensive framework for assessing the environmental impacts associated with all stages of a product's life cycle – from raw material extraction to production, use and disposal. Some comparative LCA results are available in open access and provide conclusions regarding AM technologies. In line with LCA findings, AM processes generally exhibit lower greenhouse gas (GHG) emissions than traditional manufacturing when production volumes are small (under approximately 1,000 parts per year). For example, AM can reduce emissions by approximately 35-80%, depending on part geometry and production volume. AM also has the advantage of lower production volumes (below ~1000 units per year) due to cost efficiency and environmental benefits. In contrast, traditional methods become more favorable due to economies of scale when production exceeds approximately 42,000–87,000 units annually (Jung et al, 2023).

In Figure 2, we present a schematic illustration that highlights the relationship between production volume and production costs in additive manufacturing, juxtaposed with traditional manufacturing methods.

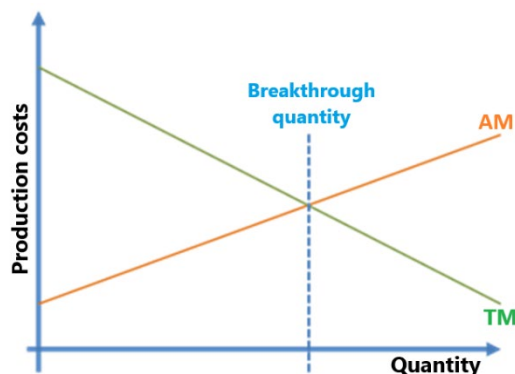


Figure 2: Relationship between production volume and production costs in additive manufacturing vs. traditional manufacturing.

The net environmental benefit of AM therefore depends on various factors. LCA has indicated that AM can reduce transportation distances with smarter logistic (Pilz et al, 2020, Kayikci, et al, 2018), as well as the associated transportation emissions. Traditional manufacturing (TM) often requires transporting goods over long distances, which can account for approximately 30% of a product's total carbon footprint (Nagabandi, 2023). AM and TM may also involve high energy consumption during production phases, where the important parameters are production scale and energy sources used during manufacturing.

The review identifies that AM has a big potential to contribute to sustainable development. Also, for small and medium-sized enterprises (SMEs), adopting AM can lead to substantial improvements in productivity, product quality, and environmental performance (Forth et al, 2018, Surya et al, 2021, and OECD 2019). However, successful implementation requires careful consideration of best practices to maximize the technology's benefits while mitigating its potential environmental drawbacks.

3 Conclusions

While AM can be seen as a sustainable alternative to TM, the degree to which the AM technique is environmentally friendly in the production of a certain product is specific for each individual case. If LCA output of AM can be lowered depends on

its ability to accept environmentally friendly inputs from all LCA phases and the consistency of following the recommendations. Certainly, a case-by-case LCA analysis is recommended.

To increase the sustainability potential of AM, future research should focus mainly on improving the energy efficiency of printing processes, on the development of more sustainable AM input materials, on choosing the energy sources with the smallest environmental impact, and on further minimizing the environmental impact coming from the energy production of the selected energy source. By addressing challenging areas with innovative approaches, like by using renewable energy sources, digitalization of supply chains, and improving recycling capabilities, AM can play a key role in advancing sustainable manufacturing practices worldwide while meeting increasing demands in various technology industries.

Acknowledgements

We appreciate to the EU Interreg program SLO-AUT for co-financing AddCirles project, which is a Cross Border Initiative for a Resilient and Circular Economy aiming for a More Resilient and Sustainable Region, and the Slovenian Research Agency program group no. P2-0273.



ADDCIRCLES

References

- Anand M., Alok K. D., 2021. "Issues in fabrication of 3D components through DMLS Technique: A review." *Optics & Laser Technology* 139: 106914.
- Chen, R., Yin, H., Cole, I. S., Shen, S., Zhou, X., Wang, Y., & Tang, S., 2020. Exposure, assessment and health hazards of particulate matter in metal additive manufacturing: A review. *Chemosphere*, 259, 127452.
- Faludi, J., Bayley, C., Bhogal, S. and Iribarne, M., 2015. "Comparing environmental impacts of additive manufacturing vs traditional machining via life-cycle assessment", *Rapid Prototyping Journal*, 21 No. 1, 14-33. <https://doi.org/10.1108/RPJ-07-2013-0067>
- Forth, John; Bryson, Alex, 2018. *The Impact of Management Practices on SME Performance*, IZA Discussion Papers, No. 11399, Institute of Labor Economics (IZA), Bonn. <https://hdl.handle.net/10419/180417>

- Gopal M., Hirpa G. L., and Endalkachew M. G., 2023. "Sustainable Additive Manufacturing and Environmental Implications: Literature Review" *Sustainability* 15, no. 1, 504. <https://doi.org/10.3390/su15010504>
- Hegab H. et al, 2023. Design for sustainable additive manufacturing: A review. *Sustainable Materials and Technologies*, 35: e00576. <https://markforged.com/resources/blog/3d-printing-and-the-environmental-impact-of-manufacturing> (assessed on 19.9.2024)
- <https://www.metalcraftsolutions.com/materials-and-capabilities/additive-manufacturing-dmls> (assessed on 19.9.2024)
- ISO 14040:2006. (2006). Environmental management — Life cycle assessment — Principles and framework. Geneva, Switzerland: International Organization for Standardization.
- ISO 14044:2006. (2006). Environmental management — Life cycle assessment — Requirements and guidelines. Geneva, Switzerland: International Organization for Standardization.
- Jung S., Kara L.B., Nie Z., Simpson T.W., 2023. Whitefoot KS. Is Additive Manufacturing an Environmentally and Economically Preferred Alternative for Mass Production? *Environ Sci Technol.* 25;57(16):6373-6386. doi: 10.1021/acs.est.2c04927.
- Kayikci, Y. (2018). Sustainability impact of digitization in logistics. *Procedia Manufacturing*, 21, 782-789. <http://dx.doi.org/10.1016/j.promfg.2018.02.184> » <http://dx.doi.org/10.1016/j.promfg.2018.02.184>
- Kuschmitz Sebastian A. S., Johannes B., Hagen W., Claudia S., Thomas V., 2021. "Development and Processing of Continuous Flax and Carbon Fiber-Reinforced Thermoplastic Composites by a Modified Material Extrusion Process" *Materials* 14, no. 9: 2332. <https://doi.org/10.3390/ma14092332>
- Mecheter A., Faris T., Murat K., 2023. "A Review of Conventional versus Additive Manufacturing for Metals: Life-Cycle Environmental and Economic Analysis" *Sustainability* 15, no. 16, 12299. <https://doi.org/10.3390/su151612299>
- Modupeola, D., Popoola, P., 2024. Safety practices and occupational hazards of the additive manufacturing of high entropy alloys. *Saf. Extreme Environ.* 6, 139–146. <https://doi.org/10.1007/s42797-023-00097-1>
- Nagabandi, N., Vice President of Materials and Process Engineering, How 3D printing can dramatically reduce carbon emissions in the manufacturing industry, 2023. [Essentiumhttps://uk-manufacturing-online.co.uk/how-3d-printing-can-dramatically-reduce-carbon-emissions-in-the-manufacturing-industry/](https://uk-manufacturing-online.co.uk/how-3d-printing-can-dramatically-reduce-carbon-emissions-in-the-manufacturing-industry/) (assessed on 23.9.2024)
- OECD (2019), Strengthening SMEs and Entrepreneurship for Productivity and Inclusive Growth: OECD 2018 Ministerial Conference on SMEs, OECD Studies on SMEs and Entrepreneurship, OECD Publishing, Paris, <https://doi.org/10.1787/c19b6f97-en>.
- Peng T.ao et al, 2018. Sustainability of additive manufacturing: An overview on its energy demand and environmental impact. *Additive manufacturing*, 21: 694-704.
- Pilz TL, Nunes B, Maceno MMC, Cleto MG, Seleme R. Systematic analysis of comparative studies between additive and conventional manufacturing focusing on the environmental performance of logistics operations. *Gest Prod [Internet]*. 2020;27(3):e5289. Available from: <https://doi.org/10.1590/0104-530X5289-20>
- Rasiya G., Shukla A., Saran K., 2021. Additive manufacturing-a review. *Materials Today: Proceedings* 47: 6896-6901.
- Sanchez, F. A. C., Boudaoud, H., Camargo, M., & Pearce, J. M., 2020. Plastic recycling in additive manufacturing: A systematic literature review and opportunities for the circular economy. *Journal of Cleaner Production*, 264, 121602.
- Sola A, Trinchi A, 2023. Recycling as a Key Enabler for Sustainable Additive Manufacturing of Polymer Composites: A Critical Perspective on Fused Filament Fabrication. *Polymers*, 15(21):4219. <https://doi.org/10.3390/polym15214219>

- Surya, B., Menne, F., Sabhan, H., Suriani, S., Abubakar, H., & Idris, M. (2021). Economic growth, increasing productivity of SMEs, and open innovation. *Journal of Open Innovation: Technology, Market, and Complexity*, 7(1), 20.
- Zhou L., Jenna M., Jeremiah V., Maksim M., Muhammad R., Quentin J., Zainab Al T., Gavyn H., Lavanya D. S., Jessica B., 2024. "Additive Manufacturing: A Comprehensive Review" *Sensors* 24, no. 9: 2668. <https://doi.org/10.3390/s24092668>

MINERAL WASTE INTO ALKALI-ACTIVATED PAVEMENTS

MAJDA PAVLIN,¹ KAJA ZUPANČIČ,² ALENKA PAVLIN³

¹ Slovenian National Building and Civil Engineering Institute, Ljubljana, Slovenia
majda.pavlin@zag.si

² University of Ljubljana, Faculty of Chemistry and Chemical Technology, Ljubljana, Slovenia

kaja.zupancic@siol.net

³ TERMIT, Moravče, Slovenia

alenka.pavlin@termit.si

The study highlights the pressing need to recycle mineral waste to mitigate resource depletion and environmental damage. It focuses on creating sustainable pavement slabs through alkali activation, using a variety of waste materials such as bio-ash, local slags and mineral wool. Through extensive testing of different mix designs, the optimal mixture was identified: bio-ash, ladle slag, and metakaolin, activated with sodium silicate. This combination demonstrated good mechanical properties and showed low concentrations of toxic elements in leaching tests, confirming environmental safety. The research also prioritized energy efficiency, with the curing process conducted at room temperature and demolding after just one day. A test field at Termit d.d. was established to assess the practical application and potential for commercial use of these innovative paving materials, aiming to support a circular economy by extending the lifecycle of resources.

DOI
[https://doi.org/
10.18690/um.fkkt.1.2025.11](https://doi.org/10.18690/um.fkkt.1.2025.11)

ISBN
978-961-286-959-5

Keywords:
mineral waste,
recycling,
waste ashes,
alkali activation,
pavement slabs



University of Maribor Press

1 Introduction

Alkali-activated materials (AAMs) are sustainable binders produced by activating industrial by-products such as slag and various ashes with alkaline solutions. They offer an environmentally friendly alternative to conventional cement, reducing carbon emissions while ensuring high strength and durability. Alkali-activated pavements must have high compressive and bending strength to withstand heavy loads and traffic. Durability is essential, with resistance to abrasion, chemical attack and freeze-thaw cycles ensuring long-term performance. They should have low permeability to prevent water ingress and avoid moisture damage. Appropriate surface texture and slip resistance are critical for safety, while thermal stability and minimal shrinkage help maintain structural integrity. In addition, these coverings should align with sustainability goals by containing industrial by-products and reducing environmental impact.

The durability of concrete is largely influenced by the properties of its pore structure and the extent of cracking. The ability of water, chloride ions, carbon dioxide, acids (including chlorides) and sulfates to penetrate the pavement directly affects its long-term performance and resistance to degradation (Mohd Tahir et al., 2022). When it comes to alkali-activated pavements, research studies mainly use ground granulated blast furnace slag (GGBFS) and fly ash (FA) as base materials and activate them with sodium silicate/sodium hydroxide (Girish et al., 2018; Girish et al., 2017; Badkul et al., 2022; Marathe et al., 2021; Phummiphan et al., 2018). Pavement construction promotes the development of special concretes with reduced cement content, which are produced from inexpensive raw materials and exhibit high early strength and improved durability, fatigue strength and shrinkage resistance. However, there is a lack of knowledge about the long-term performance of AAM, especially in terms of durability and AAM produced with unconventional raw materials (Rambabu et al., 2022).

Some studies have already described the production of alkali-activated paving slabs, but not all studies focus on the durability aspects. The study by Frankovič et al. used copper slag mixed with GGBFS and activated with a K-based alkali silicate solution. The results of splitting tensile strength, abrasion resistance, slip and skid resistance, freeze-thaw resistance and freeze-thaw resistance in the presence of de-icing salts show comparable results to those of commercially available concrete pavers. In

addition, certain properties (e.g. abrasion resistance, freeze-thaw resistance and freeze-thaw resistance in the presence of de-icing salts) were significantly better (Frankovič et al., 2020). Another study shows that a significant increase in pavement quality can be achieved by increasing the activator concentration and the GGBFS/FA content. However, an increase in the activator concentration above 12 M and a GGBFS content of over 28% did not show any significant effects (Badkul et al., 2022). By using GGBFS and FA in a weight ratio of 75:25 and recycled concrete aggregates, the desired mechanical strength and durability of the pavements were achieved, but only when up to 50% recycled aggregates were used (Marathe et al., 2021). The comparison of metakaolin (MK)-based concrete and Portland cement concrete shows comparable performance with higher stiffness and resistance to surface abrasion in the fuel resistance test (Eisa et al., 2022). In the study by Hossiney et al. alkali-activated pavers were produced using FA, GGBFS, NaOH, sodium silicate, natural aggregates and recycled asphalt aggregate (RAP), with 0, 25, 50 and 75% replacement of natural aggregates by weight. The tests showed that RAP reduced the compressive strength and abrasion resistance, but still met the standards for pedestrians and non-motorised road users. In addition, the use of RAP aggregates reduced production costs by up to 25.8% (Hossiney et al., 2020). Rambabu et al. investigated alkali-activated concrete for road pavements using low calcium FA partially replaced by 30% GGBFS, using an 8 M NaOH solution and curing at room temperature. Key tests included mechanical properties, abrasion resistance, shrinkage strain and microstructural analysis, as well as fatigue life comparison with Pavement Quality Concrete (PQC). The mixture of 70% FA and 30% GGBFS achieved optimum results after 28 days with a compressive strength of 45.7 MPa, a splitting tensile strength of 3.8 MPa and a bending strength of 4.6 MPa, while the shrinkage strains after 90 days were 31% lower than with PQC (Rambabu et al., 2024).

In the present work, various local mineral wastes (bio-ash, slag, waste stone wool) were used to develop and optimize a mix design for alkali-activated pavers. Through trial and error approach, many different mixes (pastes and mortars) were produced and the most suitable mix was selected based on mechanical properties, visual appearance and durability (freeze-thaw test, leaching test). Testing field was made to evaluate the long-term stability of the prepared pavements.

2 Materials and methods

Sample preparation

Various precursors (three bio-ashes labelled as B5, B6 and B7, ladle slag labelled as LS, waste stone wool labelled as SW and metakaolin labelled as MK) were selected as testing precursors for alkali-activated paving stones. The SW used for alkali-activation was first ground in a vibrating disc mill (Siebtechnik) and then sieved to below 63 μm . LS and three bio-ashes were sieved below 250 μm to remove larger particles such as pebbles, wood, etc. MK was used as received.

The alkali-activated paste was prepared by manually mixing different precursors and adding sodium silicate stepwise for 10 minutes. Sodium silicate Silvez (mining company Termit, 11.9% Na_2O and 28.5% SiO_2 , $M_{\text{SiO}_2/\text{Na}_2\text{O}} = 2.5$) was used for alkali activation. After mixing, the slurry was poured into silicone or urethane rubber moulds. All samples were cured at room temperature in closed PVC bags to prevent dehydration.

Analysis of the precursors and AAMs

All precursors were characterised based on their chemical and mineralogical composition using X-ray fluorescence (XRF) and X-ray powder diffraction (XRD). All samples used for XRF and XRD analysis were ground using the disc vibrating mill (Siebtechnik) and sieved below 125 μm .

The loss on ignition (LOI) was determined at 950 $^\circ\text{C}$. XRF analysis (XRF; Thermo Scientific ARL Perform'X Sequential XRF) was performed on melt beads prepared with Fluxana(s) (FX-X50-2, lithium tetraborate 50% / lithium metaborate 50%) to a lower melting point and with the addition of LiBr(l) (prepared from 50 ml H_2O and 7.5 g LiBr(s) from Acros Organics) to prevent the melt from sticking to the platinum vessel. The measured data were characterised using UniQuant 5 software. The chemical analyses of the measured samples are listed in Table 1.

Table 1: Chemical composition determined by XRF analysis.

	LS (wt%)	SW (wt%)	MK (wt%)	B5	B6	B7
Na ₂ O	-	2,14		1,02	0,41	0,79
MgO	8,11	11,5	0,17	4,56	0,64	5,58
Al ₂ O ₃	21,8	18,5	44,4	7,28	32,1	10,6
SiO ₂	17,2	38,6	52,2	39,0	10,9	37,8
SO ₃	1,57	0,02	-	0,76	4,09	0,14
K ₂ O	-	0,80	1,30	3,01	2,21	6,34
CaO	47,5	15,8	0,07	29,4	17,7	23,6
Other oxides	1,22	2,14	1,41	2,20	2,20	4,48
LOI	-	3,28	0,63	9,38	23,4	5,39

The mineralogical analysis (XRD analysis, Empyrean PANalytical X-ray diffractometer, Cu X-ray source) was performed using the X'Pert Highscore plus 4.1 software. Rietveld refinement was performed using the external standard corundum NIST SRM 676a to determine the amount of amorphous phase and minerals in the waste materials. The amount of amorphous phase is listed in Table 2.

Table 2: The amount of amorphous phase in the precursors used for alkali activation.

Sample	Amount of amorphous phase (wt%)
Ladle slag (LS)	31.9
Stone wool (SW)	99.7
Metakaolin (MK)	57.0
Bioash 5 (B5)	63.0
Bioash 6 (B6)	59.5
Bioash 7 (B7)	74.7

Measurements of the bending and compressive strength of AAMs were carried out using a compressive and bending strength testing machine (ToniTechnik ToniNORM) after 28 days of curing at room temperature.

The presence of toxic elements in the leachate was assessed after 28 days in accordance with the European standard SIST EN 12457-2 (SIST, 2002). The AAM was crushed to a particle size of less than 4 mm and placed in a glass bottle with deionized water, using a mass ratio of solid to liquid of 1:10. The suspensions were rotated around the vertical axis for 24 hours at room temperature and then filtered to a particle size below 0.45 μm . The filtered solution was acidified to a pH value below 2. All prepared solutions were used to determine the amount of released metals using an inductively coupled plasma mass spectrometer (ICP-MS, Agilent

7900). The results were compared with the total amount of toxic trace and trace elements measured in the preliminary stage and with the figures from the legislation (Decree on the landfill of waste (Official Gazette of Republic Slovenia, 2014) and Decree on waste (Official Gazette of Republic Slovenia, 2022)).

The durability of the prepared mortars under cold weather conditions was tested using the freeze–thaw test (the test was modified from the standard for roof tiles SIST EN 539-2/2013 and for concrete pavers ETAG 004). The samples were dried at 110 °C, weighed and examined for defects. They were then gradually immersed in water over a period of 5 days. After the coverings were fully immersed, they were soaked for a further 72 hours, then removed and weighed. They were then subjected to 150 freeze–thaw cycles, with the temperature operated in a range of (-16 ± 1) °C to $(+ 17 \pm 1)$ °C and the humidity in a range of 10% to 95% according to the standard procedure. In each cycle, the temperature of the samples is decreased from + 17 °C to 1 °C in 20 minutes, then from + 1 °C to -3 °C in 40 minutes, then from -3 °C to -16 °C in 1 hour and the temperature is maintained, then increased to 5 °C in 20 minutes, and then to + 17 °C in 30 minutes. The samples were tested at 30, 90 and 150 cycles. The samples were examined for cracks and other surface damage (spalling, flaking, peeling), delamination, fractures, structural damage etc. After 150 cycles, the samples were evaluated by visual observations for any change in surface properties and any deformation at the edges of the samples is also reported.

Pilot production

At Termit d.d., a separate area was set up for the machines and materials needed for the pilot production of paving stones. The main equipment included a machine for preparing the solid parts (a mixer for dry components), a dissolver mixer (R60, 1999, 2 kW) for batches of up to 50 kg, molds for shaping, a mobile frame for curing and a vibrating table (0.40 x 0.35 m, 0.18 kW) for compacting the mixture. The laboratory equipment included an electronic balance (EOB 35K10) for precise measurements and a slump test setup to assess the consistency of the slurry. Bending and compressive strength measurements were taken for each batch after 28 days of curing at room temperature.



Figure 1: Mixer for the production of mixes selected for the production of pavements slabs (wet mix).

3 Results and discussion

Mix design development

Many different mix designs were prepared (mixes with different mechanical properties, all cured at room temperature). Further selection was based on the workability of the mixture, the mechanical properties, the visual appearance of the cured samples (e.g. efflorescence, curvature, disintegration in water, etc.) and the concentrations of toxic elements (determined by the leaching tests). The prepared mixtures (pastes and mortars) are listed in Tables 3 and 4.

The mechanical properties of all the mixtures produced (pastes and mortars) were measured and the results are shown in Figures 2 and 3. The combination of different bio-ashes and a small amount of LS resulted in compressive strengths below 20 MPa and bending strengths around 10 MPa or below (Figure 2). The mechanical properties increase with the increase in LS and the addition of MK. Mixture Z (B7 with a combination of MK) shows the highest compressive strength (50.8 MPa), while the highest bending strength is exhibited by mixture AC (21.1 MPa).

Table 3: Various pastes prepared using three different bio-ashes (B5, B6 and B7), SW, LS, MK and sodium silicate as alkali activator.

Mass (g)	B5	B6	B7	SW	LS	MK	Alkali activator
Mixture A	100	25	25	/	/	/	80
Mixture A	100	25	/	/	25	/	80
Mixture C	100	/	25	/	25	/	80
Mixture D	/	50	50	/	50	/	80
Mixture E	25	100	25	/	/	/	80
Mixture F	/	100	25	/	25	/	80
Mixture G	25	100	/	/	25	/	80
Mixture H	25	25	100	/	/	/	80
Mixture I	/	25	100	/	25	/	80
Mixture I	25	/	100	/	25	/	80
Mixture K	25	25	/	/	100	/	80
Mixture L	/	25	25	/	100	/	80
Mixture M	25	/	25	/	100	/	80
Mixture N	50	/	/	/	50	50	80
Mixture O	/	50	/	/	50	50	80
Mixture P	/	/	50	/	50	50	80
Mixture R	25	25	25	/	25	50	80
Mixture S	25	25	/	/	50	50	80
Mixture Š	/	25	25	/	50	50	80
Mixture T	25	/	25	/	50	50	80
Mixture U	50	/	/	/	/	100	80
Mixture V	/	50	/	/	/	100	80
Mixture Z	/	/	50	/	/	100	80
Mixture Ž	25	25	25	/	/	75	80
Mixture X	50	/	50	/	/	50	80
Mixture Y	75	/	/	25	/	50	80
Mixture	50	/	25	25	/	50	80
Mixture	25	/	50	25	/	50	80

Table 4: Various mortars prepared using bioash B5, MK, LS, cement, aggregate (0-2 mm) and sodium silicate as alkali activator.

Masa (g)	B5	MK	Agreg	Cement	LS	Alkali
Mixture AD	30	30	80	10	/	80
Mixture AE	30	50	60	10	/	80
Mixture AF	30	30	70	20	/	80
Mixture AG	30	30	60	30	/	80
Mixture AH	30	30	50	40	/	80
Mixture AI	50	40	50	10	/	80
Mixture AJ	50	40	40	20	/	80
Mixture AL	50	30	50	20	/	80
Mixture AM	50	20	50	30	/	80
Mixture AO	30	50	60	/	10	80
Mixture AP	30	50	50	10	10	80
Mixture AR	30	50	50	/	20	80
Mixture AS	30	50	40	/	30	80
Mixture AŠ	30	60	50	5	5	80
Mixture AT	30	60	40	10	10	80
Mixture AU	30	80	30	/	10	80
Mixture AV	30	40	30	10	40	80

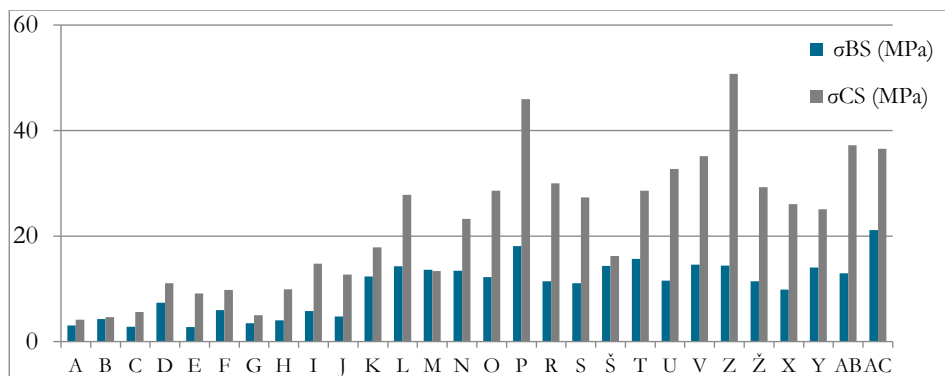


Figure 2: Mechanical properties of prepared pastes.

Compressive strengths of around 20 MPa and bending strengths in the range of 4.7-8.6 MPa were measured with the AD-AO mortar mixtures (Figure 3). Cement was added in all cases, except in mix AO, where LS was added instead of cement. In the AP-AV mixes, LS was added in addition to B5, MK and aggregate. In some cases, however, a small amount of cement was also added (AP, AŠ, AT and AV). The compressive strength increased to around 30 or even over 40 MPa (mixture AS), while bending strength was around 10 MPa (Figure 3).

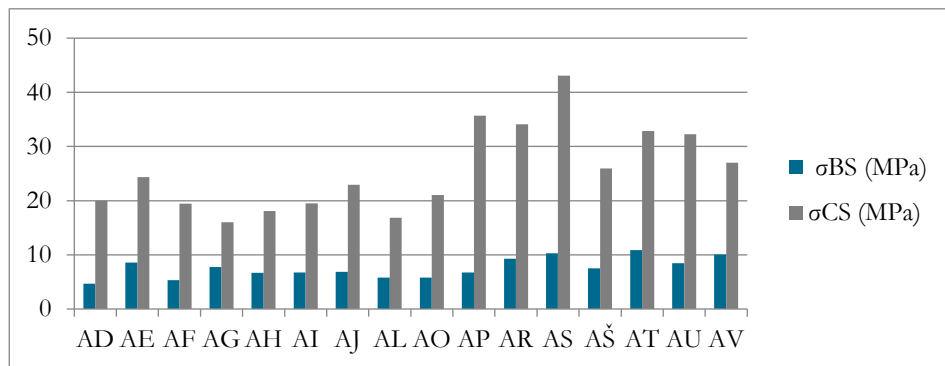


Figure 3: Mechanical properties of prepared mortars.

After measuring the compressive and bending strength, all samples were placed in water to see if they were stable or degraded under water conditions (Figure 4). If the samples showed signs of degradation, efflorescence or strong leaching of alkalis, indicated by the formation of a gel-like solution, these samples were excluded from

further testing. Some samples showed a coloured solution, probably due to the presence of organic compounds in the mixture.



Figure 4: Various samples were placed in water to test the initial water resistance of the prepared samples.

Based on the consistency of the mixture and curing time, mechanical properties and water resistance test (visual appearance of the sample after exposure to water), samples with good mechanical properties, no degradation in water, no efflorescence and no curvature were selected for leaching experiments to evaluate environmental acceptability.

Leaching tests

Leaching tests were first carried out to assess the environmental acceptability of the raw materials used. Table 5 shows the concentrations of toxic elements in the leachates of the starting materials. The concentrations for Cr, Mo, Ba, As and Pb in some samples were above the permissible limits for inert waste (taking into account the Directive on the landfill of waste with the establishment of criteria for the acceptance of waste in landfills) and/or the Slovenian Decree on Waste. However, the leaching potential of AAMs may differ from the leaching of elements from precursors.

Table 5: Concentrations of toxic elements in the leachates of various precursors. Red numbers indicate that the concentrations of the elements have exceeded the limits specified in the legislation (values in grey).

mg/kg	Cr	Co	Ni	Cu	Zn	As	Se	Mo	Cd	Sb	Ba	Hg	Pb
B5	0.826	0.006	0.011	0.043	0.110	0.000	0.027	0.669	<0.002	<0.001	8.091	<0.001	0.768
B6	0.308	0.011	0.006	0.022	0.002	0.525	0.480	6.546	0.007	0.004	1.379	<0.001	0.006
B7	0.416	0.006	0.008	0.076	0.390	0.001	0.006	0.294	<0.002	<0.001	57.11	<0.001	0.213
MK	0.001	<0.002	<0.002	0.006	<0.002	0.008	<lod	0.063	<0.002	<0.001	<0.002	<0.001	0.002
C42.5	17.04	0.028	0.007	0.084	0.048	<0.001	0.059	0.911	<0.002	<0.001	7.166	<0.001	0.106
SW	0.013	<0.002	0.008	0.025	0.002	0.015	0.003	0.024	<0.002	0.002	0.015	<0.001	0.001
LS	<0.002	<0.002	<0.002	<0.001	0.007	0.001	0.203	<0.002	<0.002	<0.001	14.24	<0.001	<0.005
Decree on waste	0.5	0.03	0.4	0.5	2.0	0.1	0.6	0.5	0.025	0.3	5.0	0.005	0.5
Inert waste	0.5	/	0.4	2.0	4.0	0.5	0.1	0.5	0.04	0.06	20.0	0.01	0.5
Non-hazardous waste	10.0	/	10.0	50.0	50.0	2.0	0.5	10.0	3	0.7	100.0	0.20	10.0

Table 6: Concentrations of toxic elements in the leachates of various pastes. Red numbers indicate that the concentrations of the elements have exceeded the limits specified in the legislation (values in grey).

mg/kg	Cr	Co	Ni	Cu	Zn	As	Se	Mo	Cd	Sb	Ba	Hg	Pb
Mixture K	0.506	0.008	0.008	0.112	0.021	5.225	0.719	6.242	0.006	0.102	0.019	<0.002	0.002
Mixture N	0.304	0.002	0.005	0.021	<0.002	0.422	0.112	1.650	0.001	0.062	0.037	<0.002	0.003
Mixture S	0.316	0.005	0.027	0.028	0.010	12.63	0.262	3.380	0.003	0.177	0.045	<0.002	0.009
Mixture L	0.503	0.010	0.013	0.090	0.009	5.567	0.424	5.956	0.005	0.104	0.020	<0.002	0.001
Mixture R	0.343	0.004	0.026	0.041	0.005	15.05	0.959	2.679	0.002	0.249	0.110	<0.002	0.058
Mixture T	0.332	0.003	0.020	0.032	<0.005	0.490	0.084	2.045	0.001	0.066	0.048	<0.002	0.004
Decree on waste	0.5	0.03	0.4	0.5	2.0	0.1	0.6	0.5	0.025	0.3	5.0	0.005	0.5
Inert waste	0.5	/	0.4	2.0	4.0	0.5	0.1	0.5	0.04	0.06	20.0	0.01	0.5
Non-hazardous waste	10.0	/	10.0	50.0	50.0	2.0	0.5	10.0	3	0.7	100.0	0.20	10.0

When testing the leaching concentrations of toxic elements produced from selected AAMs (pastes), some elements exceeded the limit values (e.g. Cr, As, Se and Mo) (Table 6). As and Se in the case of mixture R are even above the limit values for non-hazardous waste. Based on these results, additional mixtures were produced to reduce these concentrations.

The addition of a small amount of cement significantly reduced the leaching of Se and Mo, as well as that of As, but on the other hand an increase in Cr was observed (Table 7). Toxic metals can be immobilised by sorption in C-S-H (including physical and chemical adsorption (Chen et al., 2009)) or by ion substitution in ettringite (Glasser, 1997). In cement, however, Mo could also be immobilised in the form of powellite (CaMoO_4) (Diaz Caselles et al., 2021; Minocha and Goyal, 2013). Although we were able to significantly reduce the high As concentrations in some samples, the addition of cement still resulted in a slight increase in As in all samples analysed (Table 7). The study by Wang et al. suggests that the addition of $\text{Ca}(\text{OH})_2$ to calcined clay enables the hydration of clay minerals with efficient immobilisation of As and Pb by physical encapsulation (Wang et al., 2019). Bothe and Brown also suggested the addition of lime to reduce the mobility of As through the formation of poorly soluble Ca–As precipitates (Bothe and Brown, 1999). However, a high amount of lime is required, which affects the acceleration of hydration and thus shortens the setting time and increases the rate of early strength development. Based on our previous experiments (Pavlin et al., 2022), the presence of lime has a strong influence on workability and due to the fast setting time, it is sometimes almost impossible to mould the mixture.

A modification of the mixture was necessary to reduce the concentrations of Cr and As. Therefore, some additional mixtures were prepared in which we reduced the amount of cement or even removed it from the mixture. Six samples (AP, AR, AS, AŠ, AT and AU) were selected for leaching tests on the basis of their mechanical properties and appearance (no curvature, no efflorescence, no decomposition on contact with water). Due to the Mo concentrations in the leachates of the mixtures AP, AR, AS and AT, which were above the limits specified in the Slovenian Decree on waste, we selected the mixtures AŠ and AU for further testing (yellow colour in the Table 8). The mixture AŠ contains a small amount of cement, the mixture AU does not. As can be seen in Table 8, we have significantly reduced the amount of Cr, while the concentration of As is still slightly above the limit values of the Slovenian Decree on waste.

Table 7: Concentrations of toxic elements in the leachates of various mortars. Red numbers indicate that the concentrations of the elements have exceeded the limits specified in the legislation (values in grey).

mg/kg	Cr	Co	Ni	Cu	Zn	As	Se	Mo	Cd	Sb	Ba	Hg	Pb
Mixture AE	3.579	0.004	0.051	0.122	0.114	0.465	0.021	0.292	0.001	0.126	0.207	0.003	0.197
Mixture AD	3.325	0.003	0.039	0.111	0.078	0.463	0.022	0.301	0.001	0.155	0.136	0.003	0.108
Mixture AI	3.436	0.003	0.025	0.094	0.092	0.487	0.023	0.350	0.001	0.179	0.172	0.002	0.115
Mixture AL	6.903	0.002	0.008	0.054	0.024	0.574	0.031	0.502	0.001	0.255	0.081	0.002	0.025
Mixture AJ	6.791	0.002	0.008	0.046	0.053	0.568	0.029	0.491	0.001	0.230	0.092	0.002	0.024
Mixture AF	6.779	0.003	0.017	0.056	0.016	0.558	0.032	0.445	0.001	0.221	0.090	0.002	0.038
Decree on waste	0.5	0.03	0.4	0.5	2.0	0.1	0.6	0.5	0.025	0.3	5.0	0.005	0.5
Inert waste	0.5	/	0.4	2.0	4.0	0.5	0.1	0.5	0.04	0.06	20.0	0.01	0.5
Non-hazardous waste	10.0	/	10.0	50.0	50.0	2.0	0.5	10.0	3	0.7	100.0	0.20	10.0

Table 8: Concentrations of toxic elements in the leachates of selected mortars. Red numbers indicate that the concentrations of the elements have exceeded the limits specified in the legislation (values in grey).

mg/kg	Cr	Co	Ni	Cu	Zn	As	Se	Mo	Cd	Sb	Ba	Hg	Pb
Mixture AP	0.503	0.002	0.023	0.175	<0.002	0.582	0.068	0.686	<0.001	0.155	0.109	0.003	0.115
Mixture AR	0.201	0.002	0.029	0.059	<0.002	0.553	0.032	0.887	<0.001	0.099	0.134	0.003	0.106
Mixture AS	0.248	0.001	0.025	0.064	<0.002	0.583	0.038	1.242	<0.001	0.093	0.072	0.003	0.058
Mixture AŠ	0.268	0.002	0.051	0.110	<0.002	0.496	0.046	0.353	<0.001	0.114	0.247	0.003	0.328
Mixture AU	0.204	0.003	0.030	0.127	0.112	0.471	0.055	0.433	<0.001	0.101	0.567	0.002	0.642
Mixture AT	0.581	0.002	0.039	0.057	<0.002	0.598	0.063	0.697	<0.001	0.146	0.120	0.005	0.109
Decree on waste	0.5	0.03	0.4	0.5	2.0	0.1	0.6	0.5	0.025	0.3	5.0	0.005	0.5
Inert waste	0.5	/	0.4	2.0	4.0	0.5	0.1	0.5	0.04	0.06	20.0	0.01	0.5
Non-hazardous waste	10.0	/	10.0	50.0	50.0	2.0	0.5	10.0	3	0.7	100.0	0.20	10.0

Freeze-thaw test of selected samples AŠ and AU

Before we started pilot production, freezing and thawing tests were carried out to test the pavers' resistance to outdoor environmental conditions. The first step was to test water absorption. Less water was absorbed in the AU mix (Table 9). However, no damage occurred during freezing and thawing in either mixture or the loss of mass was lower in the AŠ mixture. It follows that both tested samples (Figure 5, mixtures AŠ-left and AU-right) pass the test of 150 freeze-thaw cycles. As we want to produce a low-carbon product, the AU mixture was chosen for the pilot production as it does not contain cement.

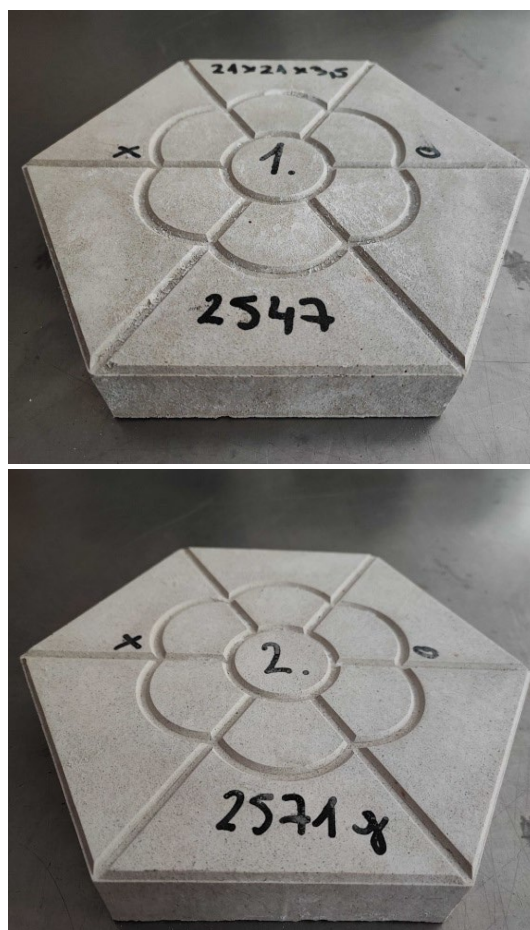


Figure 5: Pavements of mixtures AŠ (left) and AU (right) after freeze-thaw testing.

Table 9: Freeze-thaw test.

Sample	Water absorption			Mass loss during freeze-thaw test (g)	Description of damage
	m_0 (g)	m_1 (g)	w_a (%)		
1_AS	2547	2618	2,8	139	No damage
2_AU	2571	2629	2,2	164	No damage

Pilot production

The process began with the mixing of the dry components (quartz aggregate, MK, bio-ash and local slag), which were gradually added to a mixer with a glass of water and mixed for 10 minutes. The mixture is then poured into moulds, placed on a vibrating table for 5 minutes and left to harden for a day at room temperature and covered with the plastic bag. The next day, the pavers are demolded, placed on a rack and cured further at room temperature. Once 250 pavers had been produced, the test surface was prepared by levelling the ground, applying a crushed stone base layer compacted with a vibrating plate, spreading sand and laying the pavers. This area is used to test the performance and durability of the paving stones under real conditions.

Testing of mechanical properties (quality control of pilot production):

Mechanical properties were measured after 28 days for each batch of prepared pavements. Figure 6 shows the compressive and bending strength of the mixtures produced in the pilot production. Although the same formulation was used each time, slight variations in the mechanical properties were observed during the production of the pavements.

Another quality control parameter for the pilot production was slump test. By performing the slump test, we assessed the consistency (workability) of the fresh alkali-activated concrete. Table 10 shows the measured diameters of the spread, which vary slightly between the different batches.

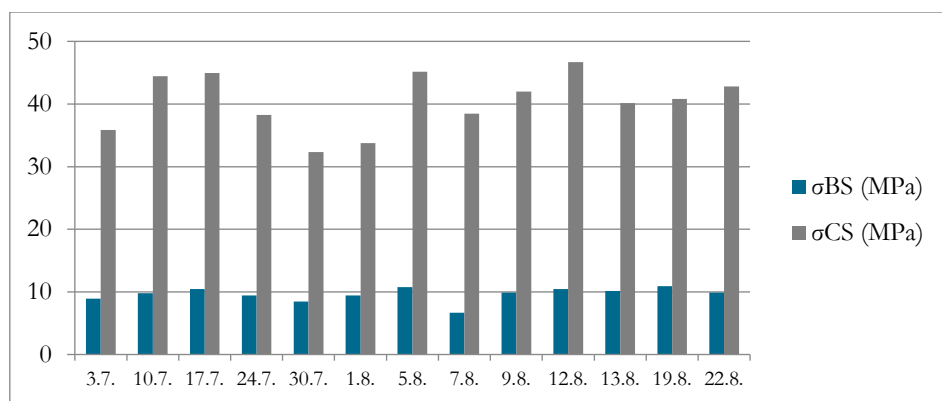


Figure 6: Quality control of the mechanical properties of prepared paving stones. Although the same material was used and the same sample preparation was carried out, there are some deviations due to the slight variations between the waste materials used in the alkali activation.

Table 10: Spread of the prepared mixture.

Sample (batch)	Slump test (mm/mm)
3. 7.	/
10. 7.	140/140
17. 7.	135/140
24. 7.	146/150
30. 7.	145/145
1. 8.	145/145
5. 8.	145/145
7. 8.	145/145
9. 8.	151/151
12. 8.	/
19. 8.	145/145
22. 8.	/

As can be seen in Figure 7 (left), the mixture was not so liquid that it could simply be poured into the molds, but we used our hands to pour the mixture into each mold. It should be emphasized that the mixture was not too dense and was easy to work with.

The final step was to create a test field in Termit d.d., as shown in Figure 7 (right). It provides a controlled environment to evaluate the performance of alkali-activated pavers under real-life conditions.



Figure 7: Filling the molds with the mixture AU (left) and testing field in the company Termit d.d. (right).

4 Conclusions

In this study a mix design for alkali-activated pavements slabs was successfully developed, taking into account critical parameters such as mechanical strength, durability and environmental acceptability. By using waste materials such as bio-ash, slag and mineral wool and testing different mix designs, the optimum formulation was determined. The selected mixture based on bio-ash, LS and MK activated with sodium silicate showed the desired mechanical properties, freeze-thaw resistance and low environmental impact. However, the mix design still needs to be optimised in the future to reduce two toxic elements (As and Pb) whose concentrations are slightly above the limit values. Curing was energy efficient at room temperature to reduce the CO₂ footprint. Further testing, including abrasion resistance and freezing in the presence of de-icing salt, will ensure product quality. The establishment of a test field at Termit d.d. is an important step towards the commercial application and long-term evaluation of these innovative paving solutions.

Acknowledgements

This project has received funding from the European Union's AEC EUROCLUSTER Technology adoption under Grant Agreement Number 101074498 (PI-04, WALK - Waste-based alkali-activated paving stones). This research was also funded by bilateral WEAVE project N2-0320: Waste to alkali-activated binders (WIN).

The data presented in this study are openly available from the repository DiRRoS at link: <https://hdl.handle.net/20.500.12556/DiRRoS-20951>

References

- A. Badkul, R. Paswan, S.K. Singh, J.P. Tegar, A comprehensive study on the performance of alkali activated fly ash/GGBFS geopolymer concrete pavement, *Road Mater. Pavement Des.* 23 (2022) 1815-1835. <https://doi.org/10.1080/14680629.2021.1926311>.
- A. Franković, V. Ducman, L. Kriskova, E. Tatsis, P. Petrica, Y. Pontikes, The development and assessment of alkali activated paving blocks, en: 3rd Int. Conf. Technol. Bus. Model. Circ. Econ. December 2020], University of Maribor, University Press, Faculty of Chemistry and Chemical ..., 2022: p. 2-9.
- D. Rambabu, S.K. Sharma, M. Abdul Akbar, A review on suitability of using geopolymer concrete for rigid pavement, *Innov. Infrastruct. Solut.* 2022 75. 7 (2022) 1-25. <https://doi.org/10.1007/S41062-022-00878-W>.
- D. Rambabu, S.K. Sharma, M.A. Akbar, Fatigue analysis of ambient-cured geopolymer concrete for high-traffic pavements, *Environ. Sci. Pollut. Res. Int.* (2024). <https://doi.org/10.1007/S11356-024-34402-7>.
- EN 12457-2:2004: Characterisation of waste - Leaching - Compliance test for leaching of granular waste materials and sludges - Part 2: One stage batch test at a liquid to solid ratio of 10 l/kg for materials with particle size below 4 mm (without or with, s.d.
- F.P. Glasser, Fundamental aspects of cement solidification and stabilisation, *J. Hazard. Mater.* 52 (1997) 151-170. [https://doi.org/https://doi.org/10.1016/S0304-3894\(96\)01805-5](https://doi.org/https://doi.org/10.1016/S0304-3894(96)01805-5).
- I. Phummiphan, S. Horpibulsuk, R. Rachan, A. Arulrajah, S.-L. Shen, P. Chindaprasirt, High calcium fly ash geopolymer stabilized lateritic soil and granulated blast furnace slag blends as a pavement base material, *J. Hazard. Mater.* 341 (2018) 257-267. <https://doi.org/https://doi.org/10.1016/j.jhazmat.2017.07.067>.
- J. V. Bothe, P.W. Brown, Arsenic Immobilization by Calcium Arsenate Formation, *Environ. Sci. Technol.* 33 (1999) 3806-3811. <https://doi.org/10.1021/ES980998M>.
- L. Diaz Caselles, C. Roosz, J. Hot, S. Blotevogel, M. Cyr, Immobilization of molybdenum by alternative cementitious binders and synthetic C-S-H: An experimental and numerical study, *Sci. Total Environ.* 789 (2021) 148069. <https://doi.org/https://doi.org/10.1016/j.scitotenv.2021.148069>.
- L. Wang, D.-W. Cho, D.C.W. Tsang, X. Cao, D. Hou, Z. Shen, D.S. Alessi, Y.S. Ok, C.S. Poon, Green remediation of As and Pb contaminated soil using cement-free clay-based stabilization/solidification, *Environ. Int.* 126 (2019) 336-345. <https://doi.org/https://doi.org/10.1016/j.envint.2019.02.057>.
- M.F. Mohd Tahir, M.M.A.B. Abdullah, S.Z. Abd Rahim, M.R. Mohd Hasan, M. Saafi, R. Putra Jaya, R. Mohamed, Potential of industrial By-Products based geopolymer for rigid concrete pavement application, *Constr. Build. Mater.* 344 (2022) 128190. <https://doi.org/https://doi.org/10.1016/j.conbuildmat.2022.128190>.
- M.G. Girish, K.K. Shetty, A. Rao Raja, Self-Consolidating Paving Grade Geopolymer Concrete, en: IOP Conf. Ser. Mater. Sci. Eng., 2018. <https://doi.org/10.1088/1757-899X/431/9/092006>.
- M.G. Girish, K.K. Shetty, A. Raja Rao, Geopolymer concrete an eco-friendly alternative to portland cement paving grade concrete, *Int. J. Civ. Eng. Technol.* 8 (2017) 886-892. <https://www.scopus.com/inward/record.uri?eid=2-s2.0-85026452553&partnerID=40&md5=b56c123b3053ba67fc5fd8b41b594107>.
- Minocha AK, Goyal MK (2013) Immobilization of Molybdenum in Ordinary Portland Cement. *J Chem Eng Process Technol* 4: 162 doi:10.4172/2157-7048.1000162.

- M. Pavlin, B. Horvat, V. Ducman, Preparation of façade panels based on alkali-activated waste mineral wool, their characterization and durability aspects, *Int. J. Appl. Ceram. Technol.* n/a (2022). <https://doi.org/https://doi.org/10.1111/ijac.13998>.
- M.S. Eisa, E.A. Fahmy, M.E. Basiouny, Using metakaolin-based geopolymer concrete in concrete pavement slabs, *Innov. Infrastruct. Solut.* 7 (2022) 1-11. <https://doi.org/10.1007/S41062-021-00601-1/FIGURES/10>.
- N. Hossiney, H.K. Sepuri, M.K. Mohan, A. H R, S. Govindaraju, J. Chyne, Alkali-activated concrete paver blocks made with recycled asphalt pavement (RAP) aggregates, *Case Stud. Constr. Mater.* 12 (2020) e00322. <https://doi.org/https://doi.org/10.1016/j.cscm.2019.e00322>.
- Official Gazette of Republic Slovenia, Decree on Waste Landfill, Nos. 20/20, 10/14, 54/15, 36/16, 37/18, (2014). <https://www.ecolex.org/details/legislation/decreed-on-the-landfill-of-waste-lex-faoc130542/>.
- Official Gazette of Republic Slovenia, Decree on Waste, Nos. 37/15, 69/15, 129/20 and 77/22), (2022). <https://www.uradni-list.si/1/objava.jsp?sop=2021-01-0302>.
- S. Marathe, T.S. Shetty, B.M. Mithun, A. Ranjith, Strength and durability studies on air cured alkali activated pavement quality concrete mixes incorporating recycled aggregates, *Case Stud. Constr. Mater.* 15 (2021) e00732. <https://doi.org/https://doi.org/10.1016/j.cscm.2021.e00732>.
- Q.Y. Chen, M. Tyrer, C.D. Hills, X.M. Yang, P. Carey, Immobilisation of heavy metal in cement-based solidification/stabilisation: A review, *Waste Manag.* 29 (2009) 390-403. <https://doi.org/https://doi.org/10.1016/j.wasman.2008.01.019>.

SEWAGE SLUDGE DRYING AND HEATING VALORIZATION

TIM TETIČKOVIČ, DUŠAN KLINAR, KLAVDIJA RIŽNAR

ZRS Bistra Ptuj, Ptuj, Slovenija

tim.tetickovic@bistra.si, dusan.klinar@bistra.si, klavdija.riznar@bistra.si

This study explores a sustainable method for converting sewage sludge with 80% water content into reusable biochar through drying and pyrolysis. The drying phase reduces water content to 12-15% using energy from pyrolysis-produced biochar, minimizing external energy requirements. Pyrolysis decomposes organic materials, producing biochar, gases, and oils, which are burned for energy recovery. The biochar can be reused up to eight times, enhancing resource efficiency and sustainability. Heat generated during both drying and pyrolysis is recycled within the system, further improving energy efficiency. The process demonstrates an innovative, closed-loop approach to waste management, minimizing waste and maximizing energy recovery, with significant potential for industrial applications.

DOI

<https://doi.org/10.18690/um.fkkt.1.2025.12>

ISBN

978-961-286-959-5

Keywords:

sewage sludge,
drying,
pyrolysis,
energy recovery,
biochar reuse



University of Maribor Press

1 Introduction to Sewage Sludge Treatment

Sewage sludge is an inevitable byproduct of municipal and industrial wastewater treatment processes. As urban populations and industrial activities grow, the volume of sewage sludge generated also increases, presenting significant challenges for its management and disposal. Typically, sewage sludge consists of a mixture of water, organic materials, microorganisms, and inorganic solids. Its high moisture content, often around 80%, makes it heavy and voluminous, which complicates transportation and disposal. Additionally, the organic content can be a source of energy if properly processed, but it can also pose environmental hazards if not managed correctly.

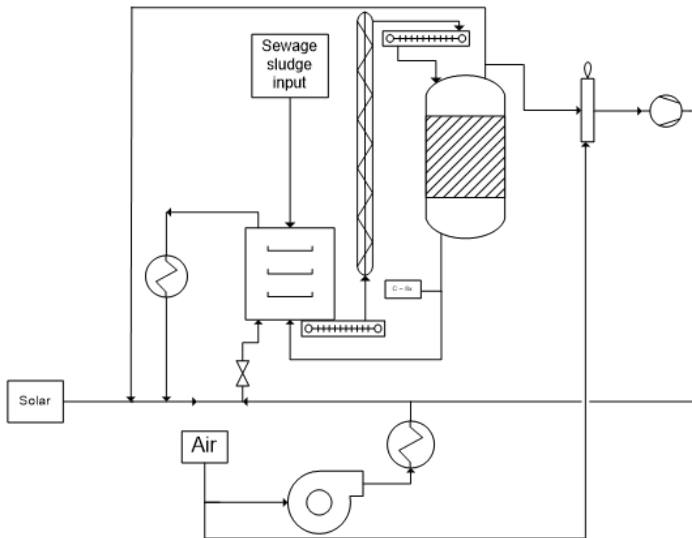


Figure 1: Process of drying and pyrolysis of sewage sludge

Conventional methods of sludge disposal, such as landfilling, incineration, and agricultural use, are facing increasing scrutiny and regulatory constraints due to concerns over environmental contamination, greenhouse gas emissions, and long-term sustainability. As a result, there is a growing interest in innovative treatment technologies that can reduce the volume of sludge, recover valuable resources, and minimize environmental impacts. One such promising approach involves the

integrated process of drying sewage sludge followed by pyrolysis. This method not only reduces the moisture content and volume of the sludge but also converts it into valuable by-products like pyrolysis gas and biochar, thereby enhancing the overall sustainability and economic viability of sludge management.¹

2 Drying Process

2.1 Characteristics of Sewage Sludge

The raw sewage sludge entering the drying process has an input flow rate of 1 tonne per hour (1000 kg/h) with an initial moisture content of 80%, equivalent to 800 kg of water and 200 kg of dry solids. The sludge's initial temperature is 20 °C. Given its high moisture content, substantial drying is required to reduce its weight and volume, making it more manageable for further processing and disposal.

2.1 Heating the Sewage Sludge

The first critical step in the drying process is to raise the temperature of the sewage sludge from 20 °C to 60 °C. This heating is essential to enhance the evaporation rate during the drying phase. The energy required for this temperature increase, considering the specific heat capacity of the sludge, amounts to 55.6 kWh. This heating process ensures that the sludge reaches an optimal temperature for effective moisture removal in the subsequent drying stage.

2.1.1 Air Used for Drying

In addition to heating the sludge, the drying process requires a significant amount of heated air to facilitate the evaporation of water content. The air must be heated from its ambient temperature to the required drying temperature of 60 °C. The input air flow rate is 3000 kg/h, and the final air flow rate after drying is 765 kg/h. The energy required for heating this air is 69 kWh. The moisture content of the air used for drying is 0.003 kg H₂O per kg of dry air. Heated air at 60 °C, with this moisture

¹ Dušan Klinar, 'Universal Model of Slow Pyrolysis Technology Producing Biochar and Heat from Standard Biomass Needed for the Techno-Economic Assessment', *Bioresource Technology*, 206 (2016), pp. 112–20, doi:10.1016/j.biortech.2016.01.053.

content, maximizes the drying process's efficiency by absorbing more moisture from the sludge, thereby accelerating the drying rate.

2.1.2 Detailed Drying Process

The primary objective of the drying process is to reduce the moisture content of the sewage sludge from 80% to 15%. This involves removing a substantial amount of water, which requires precise control of temperature and airflow. The output sewage sludge flow rate is 235.3 kg/h with a final moisture content of 15%, and the energy required for drying is 764.71 kWh. The drying phase involves several key steps:

- **Pre-Heating:** The pre-heated sludge is exposed to hot air, initiating the evaporation of surface moisture.
- **Moisture Removal:** As the process continues, moisture within the sludge gradually moves to the surface and evaporates.
- **Drying Rate:** The drying rate is governed by factors such as temperature, airflow, and the physical characteristics of the sludge.
- **End Point:** The process continues until the sludge reaches the desired final moisture content of 15%.

The enthalpy change associated with drying is critical, as it represents the energy required to evaporate the water content from the sludge. This process is energy-intensive, necessitating efficient energy use and recovery strategies.

2.1.3 Total Energy Requirements for the Drying Process

Summarizing the energy inputs required for the drying process, the energy for heating sewage sludge is 55.6 kWh, the energy for heating air is 69 kWh, and the energy for the drying process is 764.71 kWh, resulting in a total energy requirement of 889 kWh. This comprehensive energy requirement underscores the need for efficient energy recovery and supplementation methods to ensure the process's sustainability.

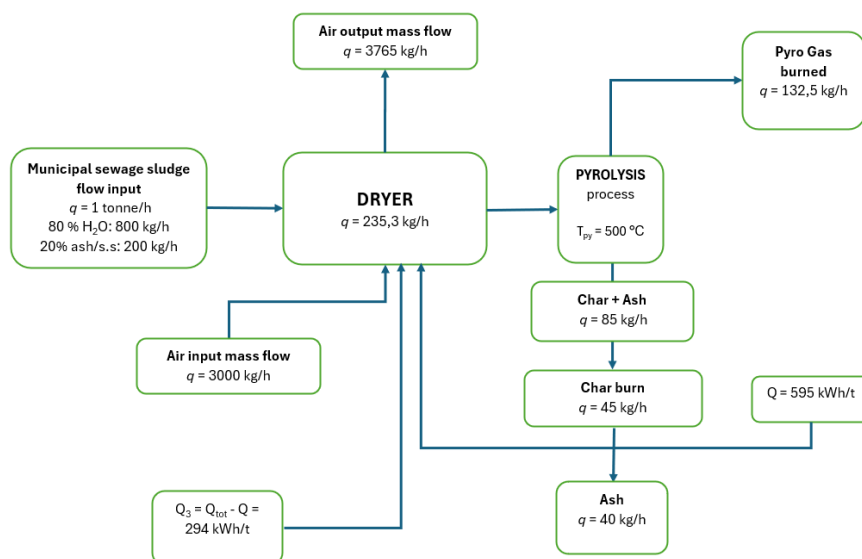


Figure 3: Process mass balances

3 Pyrolysis Process

Post-drying, the sewage sludge undergoes pyrolysis, a thermochemical decomposition process conducted in the absence of oxygen. The pyrolysis in this scenario is a slow pyrolysis method occurring at a temperature of 500 °C. Slow pyrolysis is characterized by a longer residence time, which maximizes the yield of solid char compared to faster pyrolysis processes that favour liquid and gas products.²

Pyrolysis transforms the organic components of the dried sludge into valuable by-products such as pyrolysis gas and biochar. The dried sewage sludge input is 235.3 kg/h, and the pyrolysis gas production is 132.5 kg/h, yielding 232 kWh of energy. Additionally, biochar production is 45 kg/h, which, when burned, provides 363 kWh of energy. Ash production is 47.1 kg/h. The pyrolysis process involves several stages:

² Aida Hosseinian and others, 'Life Cycle Assessment of Sewage Sludge Treatment: Comparison of Pyrolysis with Traditional Methods in Two Swedish Municipalities', *Journal of Cleaner Production*, 455 (2024), doi:10.1016/j.jclepro.2024.142375.

- **Dehydration:** Any remaining water in the dried sludge evaporates.
- **Decomposition:** Organic materials break down into gases, liquids, and solids (biochar).
- **Gas Collection:** The gases produced (pyrolysis gas) are collected and can be used as a fuel source.
- **Char Production:** The remaining solid fraction is converted into biochar, a carbon-rich product with potential energy and soil amendment applications

3.1 Energy Recovery from Pyrolysis

The energy produced from the pyrolysis process can be harnessed to offset the energy requirements of the drying process. The contributions from pyrolysis gas and biochar are substantial, amounting to a total of 595 kWh. This recovered energy plays a crucial role in making the overall process more energy efficient and reducing the reliance on external energy sources.

3.2 Energy Deficit Analysis

Despite the significant energy recovery from pyrolysis, there remains an energy deficit that must be addressed to ensure the process's viability. The total energy required for drying is 889 kWh, while the energy produced from pyrolysis is 595 kWh, resulting in an energy deficit of 294 kWh (missing 33 %). This shortfall highlights the need for additional energy inputs to fully meet the drying process's energy demands.

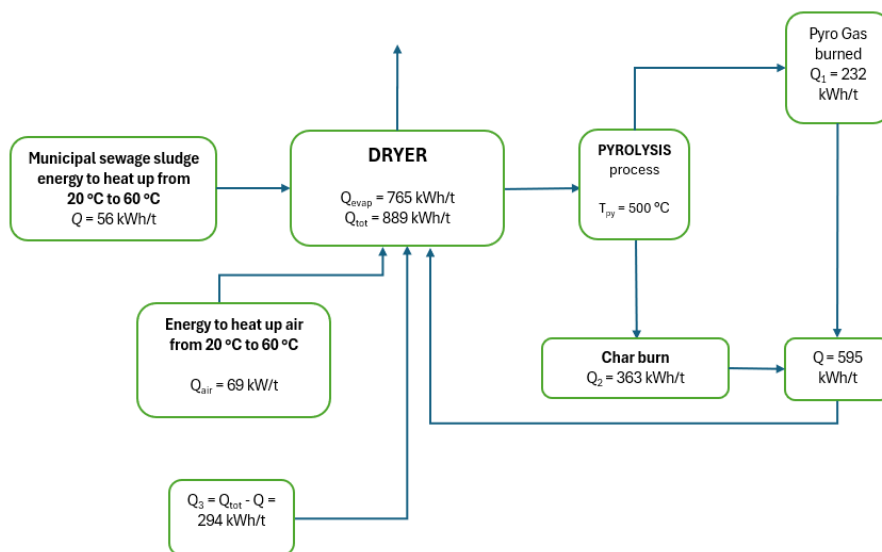


Figure 4: Process energy balances

4 Process Optimization and Reuse of Char

To enhance the efficiency of the drying process, biochar produced during pyrolysis can be reused multiple times. Char has excellent thermal properties and can be used as a heat transfer medium in the drying process. By incorporating biochar back into the drying system, it is possible to optimize the heat transfer rates, thereby reducing the overall energy consumption. Biochar can typically be reused about eight times in the drying process before it needs to be replaced, which contributes to a reduction in operational costs and energy use.

4.1 Environmental and Economic Benefits

The integrated process of sewage sludge drying with char and pyrolysis offers significant environmental and economic benefits:³

³ Salman Raza Naqvi and others, 'Recent Developments on Sewage Sludge Pyrolysis and Its Kinetics: Resources Recovery, Thermogravimetric Platforms, and Innovative Prospects', *Computers and Chemical Engineering* (Elsevier Ltd, 2021), doi:10.1016/j.compchemeng.2021.107325.

- **Volume Reduction:** By reducing the moisture content and converting the organic matter into char and gas, the volume of sewage sludge is significantly reduced, lowering transportation and disposal costs.
- **Resource Recovery:** Pyrolysis gas can be used as a fuel source, and biochar has potential applications as a soil amendment, enhancing soil fertility and carbon sequestration.
- **Energy Efficiency:** The process maximizes energy recovery, reducing the reliance on external energy sources and contributing to a more sustainable operation.
- **Reduced Environmental Impact:** By minimizing the amount of sludge sent to landfills or incinerated, the process reduces greenhouse gas emissions and potential leachate issues.

5 Conclusion

The integrated process of sewage sludge drying with char and pyrolysis represents a forward-thinking approach to managing the complex challenge of sewage sludge disposal. By leveraging the combined benefits of drying and slow pyrolysis at 500°C, this method not only reduces the volume and moisture content of the sludge but also generates valuable by-products such as pyrolysis gas and biochar, which can be used as energy sources. This approach significantly enhances the sustainability and economic viability of sludge management by recovering energy and reducing environmental impact.⁴

Despite the process's efficiency, an energy deficit remains, necessitating the integration of additional renewable energy sources like solar panels or efficient systems such as heat pumps. These supplementary energy sources help bridge the gap, making the overall process more self-sufficient and environmentally friendly.

In summary, the drying and pyrolysis of sewage sludge offer a promising solution to the growing problem of sludge disposal. This integrated approach not only addresses the immediate need for effective sludge management but also contributes to broader

⁴ Xiaoguang Liu and others, 'Pre-Drying Limitedly Affected the Yield, Fuel Properties, Pyrolysis and Combustion Behavior of Sewage Sludge Hydrochar', *Waste Management*, 184 (2024), pp. 63–71, doi:10.1016/j.wasman.2024.05.032.

environmental goals by minimizing waste, recovering energy, and producing useful by-products. As urbanization and industrial activities continue to expand, such innovative and sustainable methods will be essential for managing the by-products of human activity in an environmentally responsible manner.

Acknowledgments

I would like to sincerely thank dr. Dušan Klinar and dr. Klavdija Rižnar for their guidance, support, and expertise throughout this research. Additionally, I would like to express my appreciation to ZRS Bistra Ptuj for providing the necessary resources and a collaborative environment that made this research possible.

References

- Hossainian, Aida, Pedro Brancoli, Naeimeh Vali, Jenni Ylä-Mella, Anita Pettersson, and Eva Pongrácz, 'Life Cycle Assessment of Sewage Sludge Treatment: Comparison of Pyrolysis with Traditional Methods in Two Swedish Municipalities', *Journal of Cleaner Production*, 455 (2024), doi:10.1016/j.jclepro.2024.142375
- Klinar, Dušan, 'Universal Model of Slow Pyrolysis Technology Producing Biochar and Heat from Standard Biomass Needed for the Techno-Economic Assessment', *Bioresource Technology*, 206 (2016), pp. 112–20, doi:10.1016/j.biortech.2016.01.053
- Liu, Xiaoguang, Qingtong Tan, Peisheng Wang, Peiyue Deng, Ling Peng, Yaman Xu, and others, 'Pre-Drying Limitedly Affected the Yield, Fuel Properties, Pyrolysis and Combustion Behavior of Sewage Sludge Hydrochar', *Waste Management*, 184 (2024), pp. 63–71, doi:10.1016/j.wasman.2024.05.032
- Naqvi, Salman Raza, Rumaisa Tariq, Muhammad Shahbaz, Muhammad Naqvi, Muhammad Aslam, Zakir Khan, and others, 'Recent Developments on Sewage Sludge Pyrolysis and Its Kinetics: Resources Recovery, Thermogravimetric Platforms, and Innovative Prospects', *Computers and Chemical Engineering* (Elsevier Ltd, 2021), doi:10.1016/j.compchemeng.2021.107325

DETERMINATION OF THE MAXIMUM CO₂ SEQUESTRATION CAPACITY OF SLOVENIAN WASTE ASHES USING THERMOGRAVIMETRY AND CALCIMETRY

SARA TOMINC, VILMA DUCMAN

Slovenian National Building and Civil Engineering Institute, Ljubljana, Slovenia
sara.tominc@zag.si, vilma.ducman@zag.si

There are several ways to utilize as-received or pre-treated waste ash, one of the most promising is by accelerated mineral carbonation. Ashes with a high content of Ca and Mg compounds, such as ashes from wood biomass, are ideal candidates for sequestration. Due to the shift toward renewable fuels, ash from biomass as a by-product of solid fuel combustion is therefore available in huge quantities. As part of the EU AshCycle project, we have analyzed ashes from different incineration and thermal power plants to determine their carbon sequestration potential. These include various waste ashes from Slovenia, which were subjected to accelerated carbonation in a closed carbonation chamber with a CO₂ concentration of 4% (v/v), 80% relative humidity and a temperature of 40 °C until maximum CO₂ uptake was reached. CO₂ quantification was performed using calcimetry (pressure calcimeter) and thermogravimetry. We have shown that ash from wood biomass and the co-combustion of wood waste and paper sludge have a high CO₂ sequestration potential in comparison to others. The direct use of wood biomass ash for CO₂ sequestration in carbonated building products could significantly benefit the circular economy, especially since 70% of wood biomass ash is still landfilled.

DOI
[https://doi.org/
10.18690/um.fkkt.1.2025.13](https://doi.org/10.18690/um.fkkt.1.2025.13)

ISBN
978-961-286-959-5

Keywords:
CO₂ sequestration capacity,
accelerated carbonation,
waste ashes,
thermogravimetric analysis,
calcimetry



University of Maribor Press

1 Introduction

Mineral sequestration is a carbonation approach, in which CO₂ is captured and stored using alkaline materials consisting of calcium (Ca) and magnesium (Mg) (hydr)oxides and silicates, resulting in the formation of solid, permanently stored carbonate products (Alturki 2022, Koch et al. 2021, Li and Wu 2022). Many different carbonate phases can be detected in waste materials; however, after carbonation, Ca-containing carbonates are the predominant products (Santos et al. 2013, Wang et al. 2021). Alkaline solid waste materials such as steel slag, cement waste and coal fly ash are well suited for mineral carbonation due to their high reaction rates, low energy requirements and superior carbonate conversion efficiency compared to natural minerals where carbonation is slow (Ahmed et al. 2024). Carbonation can be accelerated by increased CO₂ concentration, pressure, relative humidity, temperature or contact time (Ahmed et al. 2024, Capelo-Avilés et al. 2024, Li et al. 2022). To mitigate climate change fast enough, accelerated carbonation is very beneficial compared to natural carbonation. Therefore, a wide range of accelerated curing environments can be found in the literature (Koch et al. 2021, Zajac et al. 2022, Tominc and Ducman 2023, Winnefeld et al. 2022). In recent years, the direct wet carbonation process has been intensively investigated due to the highest carbonation efficiency, while studies on semi-dry carbonation are rare.

The use of CO₂ sequestration for the production of building materials is an economically sustainable industrial process with negative carbon emissions and therefore deserves attention for further development (Lippiatt et al. 2020). Possible sources from waste streams are ashes containing Ca and Mg compounds, as they enable the sequestration of CO₂ in the form of carbonate compounds, for example ash from wood biomass (WBA) (Koch et al. 2021, Tominc and Ducman 2023). This is not only a waste management option, but also has the benefit of reducing CO₂ emissions.

Various methods can be used to quantify the CO₂ sequestration capacity. In thermogravimetric analysis (TGA), the mass of the sample is recorded as a function of time during the decomposition of CaCO₃ into CaO and the release of CO₂ in a controlled (inert) atmosphere. This method accounts for possible hydration and dehydroxylation reactions that contribute to weight loss (Nielsen and Quaghebeur 2023). Using a pressure calcimeter, CaCO₃ reacts with 10% hydrochloric acid (HCl)

in a closed reaction cell to form CaCl₂, CO₂ and H₂O, measuring the pressure of the released CO₂ (Tominc and Ducman 2023). In this regard, comparing different methods for estimating the CO₂ or carbonate content in selected waste materials and determining the measurement uncertainty of each method can be challenging.

As part of the AshCycle project, we have proposed a methodology to assess the CO₂ sequestration potential of waste ashes, as not all ashes are equally suitable for CO₂ sequestration. Wood biomass ash has shown greater potential than coal ash because it contains higher content of Ca oxides and other minerals that react with CO₂ and convert it into stable carbonate minerals (Tominc and Ducman 2023). In this study, we shortened the duration of carbonation by optimizing the conditions, i.e. the temperature, and determined the maximum CO₂ sequestration capacity of selected ashes after 7 days of carbonation at 40 °C, 80% relative humidity and 4% CO₂ (v/v).

2 Materials and methods

We investigated the CO₂ sequestration capacity of seven waste ashes from different Slovenian plants (Figure 1). The first two ashes, fly ash (WA.FA.1) and bottom ash (WA.BA.1) came from a Slovenian combined heat and power plant and were produced during the combustion of wood biomass (wood chips). The next two ashes came from a paper mill industry, where the fuel source for fly ash (CC.FA.2) was coal, biomass and paper sludge, while the fuel source for mixed ash (CC.MA.2) was fibrous paper sludge, waste wood and bark. The next two ashes (CC.FA.3 and CC.BA.3) came from a Slovenian combined heat and power plant, where the fuel source was brown coal and wood biomass-wood chips (15%). The last bottom ash (CC.BA.4) came from a Slovenian heat and power station, where municipal waste (light fraction) and dehydrated sewage sludge were used as fuel. All obtained ashes were first homogenized by quartering (see Figure 1), packed in a PVC bag and stored in a plastic container.

For the chemical analysis, the samples were sieved below 125 µm and dried at 105 °C. The loss on ignition (LOI) was determined at 950 °C. A fused bead was then prepared with a mixture of sample and flux (50% lithium tetraborate/50% lithium metaborate) at a ratio of 1:10 (0.947 g: 9.47 g) and heated at 1100 °C. The chemical composition was determined using an ARL PERFORM'X wavelength dispersive X-ray fluorescence spectrometer (WDXRF; Thermo Fischer Scientific Inc., Ecublens,

Switzerland) with a Rh-target X-ray tube and UniQuant 5 software (Thermo Fisher Scientific Inc., Waltham, MA, USA). Two measurements were performed for each ash. For mineralogical analysis, the ashes were sieved below 63 μm and placed in 27 mm holders (in diameter). Analyzes were performed before and after CO_2 treatment with X-ray diffraction (XRD; Empyrean X-ray Diffractometer, Cu X-ray source; PANalytical, Almelo, The Netherlands) in 0.013° steps from angles of $4\text{--}70^\circ$ under clean room conditions using the external standard corundum NIST SRM 676a. The mineral phases were analyzed with the PANalytical X'Pert High Score Plus diffraction software v.4.8. Fourier transform infrared spectroscopy (FTIR) measurements were performed using an FTIR, PerkinElmer Spectrum Two, ATR mode. All infrared spectra were recorded in a wavenumber range of $4000\text{--}380\text{ cm}^{-1}$.

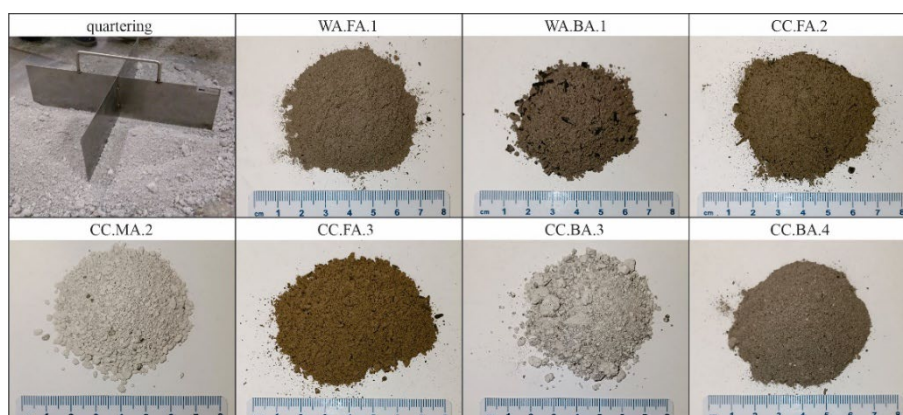


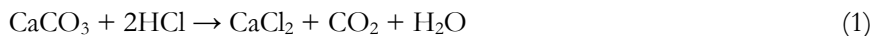
Figure 1: Waste ashes from different sources, homogenized by quartering, source: own.

20 g of each ash with a particle size of less than 125 μm was then placed in a petri dish and exposed to 4% CO_2 (v/v) in a closed carbonation chamber at 80% relative humidity and a temperature of 40° C . Carbonation was completed when a constant mass was reached.

For the determination of carbonate content, as-received and carbonated ashes were analyzed using the pressure calcimeter (OFITE Calcimeter, OFI Testing Equipment Inc., Houston, TX, USA, according to ASTM D 4373) with an analytical error of $<5\%$. Each sample was ground and sieved below 125 μm and dried in an oven at 105° C for 24 hours. Then $1.0 \pm 0.01\text{ g}$ of the sample was weighed and added to the reaction cell. The acid cup was filled with 20 mL of 10% HCl and carefully placed

in the reaction cell. CaCO₃ reacts with 10% HCl in a closed reaction cell and the pressure of the released CO₂ is measured with a manometer. The calcimeter was calibrated before the actual measurements by reacting HCl with pure CaCO₃.

The calculations for the amount of CO₂ released were based on stoichiometry.



$$1\text{ mol} : 2\text{ mol} \text{ ----- } 1\text{ mol} : 1\text{ mol} : 1\text{ mol}$$

$$n(\text{CaCO}_3) = n(\text{CO}_2) = 1:1$$

$$M(\text{CaCO}_3) = 100.0869 \text{ g/mol}; M(\text{CO}_2) = 44.01 \text{ g/mol}$$

$$1 \text{ mol of CaCO}_3 \text{ releases } 44.01 \text{ g of CO}_2.$$

The thermal decomposition of each sample was analyzed before and after the carbonation process using a TGA Q5000IR thermal analyzer (TA Instruments, New Castle, Delaware, USA). Prior to the measurements, the ashes were dried at 105 °C and sieved to a particle size below 63 μm. The analysis included a controlled heating program with a ramp rate of 10 °C per minute, from 25 to 1000 °C. To prevent oxidation during the measurement, the sample chamber was filled with N₂ at a flow rate of 25 mL per minute. Samples were placed in 100 μL Al₂O₃ crucibles. We used TGA to measure the weight loss in the temperature range of decomposition of the carbonate mineral. The results were analyzed with TA Universal Analysis 2000 v.4.5A (TA Instruments, New Castle, Delaware, USA).

3 Results and discussion

First, the characterization of the different ashes before the carbonation reaction was assessed. Their CaO content is particularly important, as this is decisive for the extent of carbonation (Capelo-Avilés et al. 2024). X-ray fluorescence (XRF) analysis of the selected Slovenian ashes shows that they are mainly composed of CaO (20-55%), SiO₂ (6-31%), Al₂O₃ (3-18%), MgO (2-10%), Fe₂O₃ (1-10%) and K₂O (0.3-8%), with lower contents of Na₂O and SO₃. The average values of the primary oxides measured by XRF and LOI at 950 °C are shown in Table 1.

Table 1: Chemical composition of the analyzed Slovenian ashes in terms of primary oxides (wt%), measured by XRF and loss on ignition at 950 °C.

Sample ID	LOI _{950 °C}	Al ₂ O ₃	SiO ₂	CaO	MgO	Fe ₂ O ₃	K ₂ O	Na ₂ O	SO ₃
WA.FA.1	29.91	5.62	19.04	29.27	3.78	1.70	5.65	0.56	1.00
WA.BA.1	26.09	3.35	5.64	44.95	5.88	0.68	8.14	0.48	0.32
CC.FA.2	11.71	11.28	22.90	34.01	5.99	8.53	0.99	0.74	1.70
CC.MA.2	14.55	11.08	14.45	55.40	2.12	0.56	0.25	0.41	0.20
CC.FA.3	16.98	10.87	27.78	19.77	8.21	10.44	2.16	0.28	1.69
CC.BA.3	12.79	7.43	31.17	28.98	10.25	3.56	3.21	0.57	0.07
CC.BA.4	7.21	17.77	27.14	30.59	3.89	3.09	0.48	2.12	0.99

The carbonation reaction of the waste ashes was then studied under the specified conditions (40 °C, 80% RH, 4% CO₂). The reaction was complete after 7 days, indicating a faster reaction rate at elevated temperature, as in our previous study (Tominc and Ducman 2023). With an increase in temperature from 20 to 40 °C, the kinetics of calcium species dissolution can be accelerated (Capelo-Avilés et al. 2024). However, at higher temperatures, the nucleation and growth of CaCO₃ can be hindered due to lower CO₂ solubility, which has a detrimental effect on the carbonation reaction (Capelo-Avilés et al. 2024).

The CO₂ content of each ash (in wt%) was compared using TGA and measured with a pressure calcimeter, as shown in Table 2. The weight loss in the temperature range of CaCO₃ decomposition was between 550-950 °C, based on dry matter at 105 °C (or between 620-950 °C for some samples). The main problem in determining CO₂ content using TGA is that thermal decomposition of carbon species sometimes overlaps with other thermal events (Protić et al. 2021). However, the results obtained with the calcimeter and TGA are very comparable in our case, as they differ by less than 3% (the difference is within the measurement error of the calcimeter, which is up to 5%).

Of the analyzed Slovenian ashes, the ash from wood biomass and the mixed ash from co-combustion showed the highest sequestration potential, as the amount of sequestered CO₂ in 1 kg of sample was 298 g for WA.BA.1 and 274 g for CC.MA.2 (according to the calcimetric measurements).

Table 2: TGA and calcimetric measurements for Slovenian wood and co-combustion ashes.

Sample ID	TGA (weight losses-%)		Calculations (TGA)		Calculations (calcimeter)
	0-150 °C	550-950 °C	% dry matter	%CO ₂ /dry matter	% CO ₂
WA.FA.1	2.0	16.3*	98.0	16.6	13.7
WA.BA.1	2.8	27.9	97.2	28.7	29.8
CC.FA.2	1.3	7.5*	98.7	7.6	8.6
CC.MA.2	2.3	26.2	97.7	26.9	27.4
CC.FA.3	2.2	8.8*	97.8	8.9	8.3
CC.BA.3	1.0	12.2	99.0	12.3	14.8
CC.BA.4	1.9	10.8	98.1	11.0	11.7

*T:620-950 °C

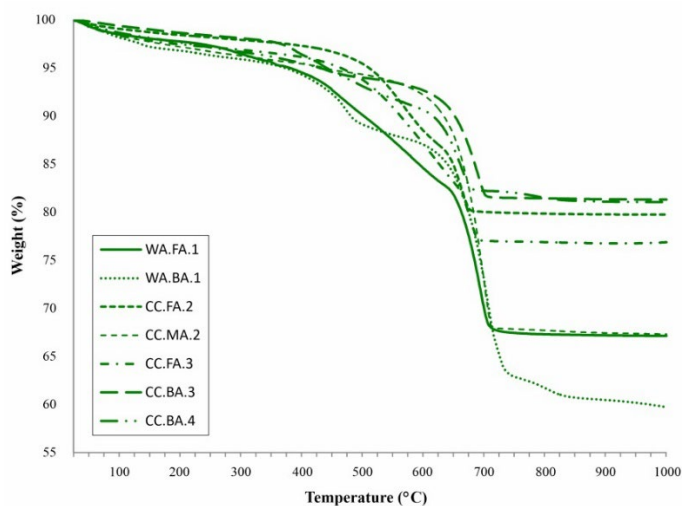


Figure 2: TGA of selected samples after 7 days of carbonation

Source: own.

The presence of carbonates was also observed by FTIR spectra of as-received and carbonated ashes, recorded in the range between 4000 cm⁻¹ and 380 cm⁻¹ (Figure 3). The intense band centered at around 1400 cm⁻¹ corresponds to the ν₃ vibrations of CO₃²⁻ (asymmetric C-O stretching), while the peaks at 872 cm⁻¹ and at 712 cm⁻¹ are associated with out-plane and in-plane bending (ν₂) vibrations of CO₃²⁻, respectively (Capelo-Avilés et al. 2024). The peak at 1795 cm⁻¹ can also be attributed to CaCO₃ (Capelo-Avilés et al. 2024). The increase in intensity of these bands in the carbonated sample indicates that the carbonation of the sample occurred during the CO₂ mineralization process, which was also confirmed by the X-ray diffraction (XRD).

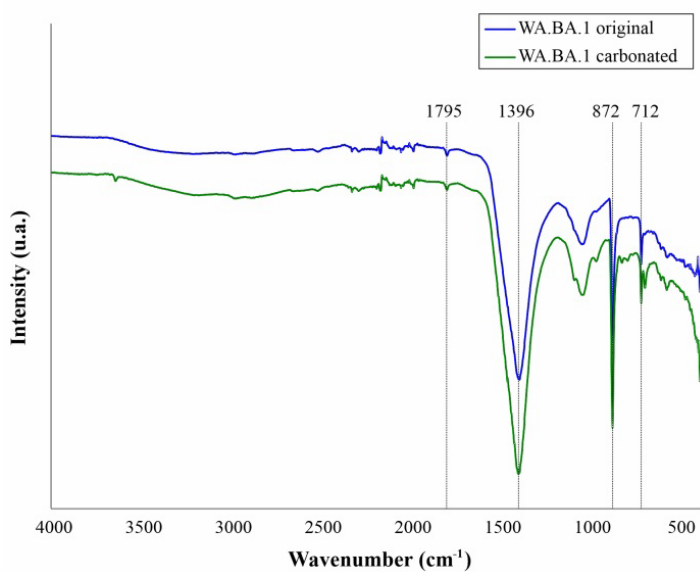


Figure 3: FTIR spectra of original and carbonated WA.BA.1

Source: own.

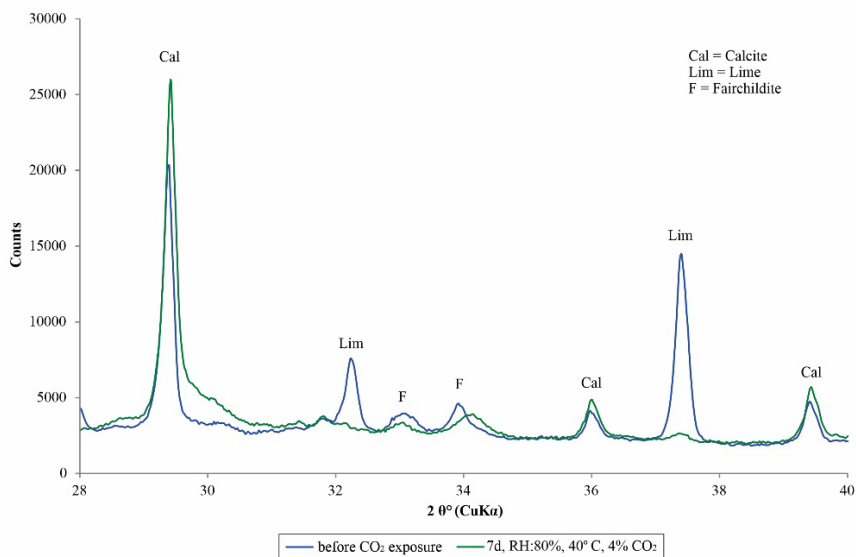


Figure 4: X-ray diffractograms of wood biomass ash (WA.BA.1) before and after 7 days of carbonation.

Source: own.

The XRD analysis enabled us to determine the composition of the crystalline minerals. For example, the main phases detected in sample WA.BA.1 (Figure 4) were calcite (CaCO₃), fairchildite (K₂Ca(CO₃)₂) and lime (CaO). After CO₂ treatment, a clear change in the intensity of the calcite peak can be observed, while the lime peak almost disappeared, indicating that CaO is the main reactant in the mineralization process. In the case of fairchildite, only a slight change in the intensity of the peak can be observed.

4 Conclusions

In this study, seven different waste ashes from Slovenia were subjected to accelerated carbonation to determine their sequestration potential. Depending on their chemical and mineralogical composition, the ashes showed different sequestration capacities. The highest CO₂ sequestration capacity, i.e. 298 g_{CO₂}/kg_{ash}, was measured for ash from wood biomass (WA.BA.1). A high sequestration potential was also found for ash from the co-incineration of wood waste and paper sludge (CC.MA.2), while other waste ashes showed a lower potential. As most waste ashes are still landfilled, the use of these ashes for CO₂ sequestration for carbonated building products would be very beneficial in terms of a circular economy.

Acknowledgments

The authors would like to thank Dr. Lea Žibret for the XRD measurements and Dušica Tauzes and Majda Pavlin for the XRF measurements.

Funding & Data availability

This research was EU-funded by AshCycle project, grant number 101058162.

The data presented in this study are openly available from the repository DiRROS at link: <http://hdl.handle.net/20.500.12556/DiRROS-20544>.

References

- Ahmed, O., Ahmad, S., Adekunle S.K (2024). Carbon dioxide sequestration in cementitious materials: A review of techniques, material performance, and environmental impact. *Journal of CO₂ Utilization*, 83, 102812. doi:10.1016/j.jcou.2024.102812
- Alturki, A. (2022). The Global Carbon Footprint and How New Carbon Mineralization Technologies Can Be Used to Reduce CO₂ Emissions. *ChemEngineering*, 6, 44. doi:10.3390/chemengineering6030044
- Capelo-Avilés, S., Tomazini de Oliveira, R., Gallo Stampino, I.I., Gispert-Guirado, F., Casals-Terré, A., Giancola, S., Galán-Mascarós, J.R. (2024). A thorough assessment of mineral carbonation

- of steel slag and refractory waste. *Journal of CO₂ Utilization*, 82, 102770. doi:10.1016/j.jcou.2024.102770
- Koch, R., Sailer, G., Paczkowski, S., Pelz, S., Poetsch, J., Müller, J. (2021). Lab-Scale Carbonation of Wood Ash for CO₂–Sequestration. *Energies*, 14, 7371. doi:10.3390/en14217371
- Li, L., Wu, M. (2022). An overview of utilizing CO₂ for accelerated carbonation treatment in the concrete industry. *Journal of CO₂ Utilization*, 60, 102000. doi:10.1016/j.jcou.2022.102000
- Lippiatt, N., Ling, T.C., Pan, S.Y. (2020). Towards carbon-neutral construction materials: Carbonation of cement-based materials and the future perspective. *Journal of Building Engineering*, 28, 101062. doi:10.1016/j.jobe.2019.101062
- Nielsen, P., Quaghebeur, M. (2023). Determination of the CO₂ Uptake of Construction Products Manufactured by Mineral Carbonation. *Minerals*, 13, 1079. doi:10.3390/min13081079
- Protić, M., Milojević, A., Zoraja, B., Raos, M., Krstić, I. (2021). Application of Thermogravimetry for Determination of Carbon Content in Biomass Ash as an Indicator of the Efficiency of the Combustion Process. *Tehnički vjesnik*, 28 (5), 1762-1768. <https://doi.org/10.17559/TV-20200508110940>
- Santos, R.M., Van Bouwel, J., Vandeveld, E., Mertens, G., Elsen, J., Van Gerven, T. (2013). Accelerated mineral carbonation of stainless steel slags for CO₂ storage and waste valorization: Effect of process parameters on geochemical properties. *International Journal of Greenhouse Gas Control*, 17, 32–45. doi:10.1016/j.ijggc.2013.04.004
- Tominc, S., Ducman, V. (2023). Methodology for Evaluating the CO₂ Sequestration Capacity of Waste Ashes. *Materials*, 16, 5284. doi:10.3390/ma16155284
- Zajac, M., Skibsted, J., Bullerjahn, F., Skocek, J. (2022). Semi-dry carbonation of recycled concrete paste. *Journal of CO₂ Utilization*, 63, 102111. doi:10.1016/j.jcou.2022.102111
- Wang, X., Ni, W., Li, J., Zhang, S., Li, K. (2021). Study on mineral compositions of direct carbonated steel slag by QXRD, TG, FTIR, and XPS. *Energies*, 14, 4489. doi:10.3390/en14154489
- Winnefeld, F., Leemann, A., German, A., Lothenbach, B. (2022). CO₂ storage in cement and concrete by mineral carbonation. *Current Opinion in Green and Sustainable Chemistry*, 38, 100672. doi:10.1016/j.cogsc.2022.100672

THE CARBON FOOTPRINT OF DIFFERENT CONSTRUCTION AND DEMOLITION WASTE MANAGEMENT METHODS

JANEZ TURK,¹ PATRICIJA OSTRUH,¹ ANJA KODRIČ,¹
TAJDA POTRČ OBRECHT²

¹ Slovenian National Building and Civil Engineering Institute, Ljubljana, Slovenia
janez.turk@zag.si, patricija.ostruh@zag.si, anja.kodric@zag.si

² Graz University of Technology, Graz, Austria
tajda.obrecht@tugraz.at

End-of-life management with three CDW fractions are considered in this study: wood, steel, and broken concrete. The goal of the study is to evaluate the Global Warming Potential (GWP) of different end-of-life management approaches and to benchmark the circular approaches versus the linear approaches. In the case of waste wood, the circular scenario refers to wood recycling and the production of recycled particle board or glue-laminated timber. Waste wood landfilling and the production of particle board/glue-laminated timber from primary wood are considered in the linear scenario. Considering the production of particle board, the circular scenario shows 4 times lower GWP than the linear scenario. Considering the production of glue-laminated timber, the circular scenario shows comparable GWP as the linear scenario. In the case of waste steel, the GWP of two circular scenarios were compared; recycling versus reuse. The reuse scenario shows around 8 times lower GWP than the recycling. In the case of waste concrete, the circular scenario refers to the recycling of broken concrete into recycled aggregate. The linear scenario includes the landfilling of waste concrete and the production of natural aggregate. LCA results show around 2 times lower impact on GWP in the case of the circular scenario.

DOI
[https://doi.org/
10.18690/um.fkkt.1.2025.14](https://doi.org/10.18690/um.fkkt.1.2025.14)

ISBN
978-961-286-959-5

Keywords:

LCA,
Global Warming Potential,
concrete,
steel,
wood



University of Maribor Press

1 Introduction

Construction and Demolition Wastes (CDWs) pose significant environmental challenges, accounting for nearly half of all solid waste sent to landfills worldwide. In the European Union, this share is lower, but still around 38% (Tonini et al., 2023). Moreover, CDWs are among the heaviest and most voluminous waste streams, which is just one of the concerns relating to their landfilling (Zhang et al., 2020). Other concerns refer to problems such as resource efficiency and climate change, the latter is indirectly related to carbon embodied in CDW (Liu et al., 2023).

Construction and demolition waste (CDW) consists of various materials such as concrete, bricks, tiles, plaster, timber, wood, glass, metals, plastic, stones, and others. Given its high potential for recycling or reuse, the European Commission has prioritized CDW as a key waste stream. The waste hierarchy serves as a framework for managing materials at the end of their life cycle, focusing on preserving their economic value in the market wherever feasible and environmentally acceptable. This approach prioritizes waste prevention above all else, followed by re-use, recycling, recovery, and disposal (landfilling) – the latter considered the least favorable option (Stahel and MacArthur, 2019; Kabirifar et al., 2020).

The goal of this study is to compare the environmental performance of different end-of-life management practices for selected fractions of CDW: wood, steel, and broken concrete. Only global warming potential (known also as carbon footprint) was considered in the comparative analysis. Special attention was given to the comparison of linear circular versus linear end-of-life management practices.

2 Material and methods

2.1 Life Cycle Assessment (LCA)

End-of-life (EoL) management practices for selected fractions of CDW are benchmarked with Life Cycle Assessment (LCA) method. This method is commonly used comparatively in order to find among different options the most environmentally sustainable solutions, for instance regarding waste management (Guinée et al., 2002). The end-of-life management scenarios were compared in terms of the impact on global warming potential (GWP), known also as carbon footprint,

expressed in kg CO₂ equivalents. “LCA for experts” professional tool was applied to conduct LCA and to calculate GWPs.

The functional unit in this study refers to the end-of-life management with 1 tone of specific CDW fraction.

Demolition of the building and generation of CDW fractions are not considered in the system boundaries, considering the “cut-off” approach (Potrč Obrecht, 2021). System boundaries of the circular end-of-life management scenarios include processes related to recycling and the production of new products with recycled content. In the case of steel, system boundaries include processes related to reuse. In the case of linear end-of-life management scenarios, processes related to landfilling are included as well as the processes related to the production of products based on primary materials. These products are a functional equivalent to the same products from recycled materials, considered in the system boundaries of the circular end-of-life management scenarios. Transport of waste fractions to the recycling facility or to the landfill is also considered.

2.2 Wood

The most common linear end-of-life management of wood is incineration. Two circular scenarios were taken into account to make a comparison with the linear scenario; the first one is the recycling of waste wood into wood chips, which is further used in the process of particle board production. In the case of the linear scenario, system expansion was considered, which means that the linear scenario includes not only the incineration of waste wood but also the production of particle board from primary wood. Such particle board from primary wood is a functional equivalent of particle board from recycled wood. Life cycle inventory data for the production of particle boards were taken from Hossain and Poon (2018).

The second circular scenario considered in this study is the production of glue-laminated timber from waste wood. For environmental comparison with the linear scenario, system expansion was conducted in the latter scenario; e.g. production of glue-laminated timber from primary wood was accounted to incineration of waste wood. Life cycle inventory data were gathered from the paper of Risse et al (2019).

2.3 Steel

Considering end-of-life management with steel recovered from CDW, recycling is a common end-of-life practice. Steel is a completely recyclable material. It can be continuously recycled without losing its quality or properties (Broadbent, 2016). Some steel components (claddings, beams, columns) recovered from demolished buildings can be reused (Tonini et al., 2023). Both recycling and reuse are circular end-of-life management practices. Landfilling as a linear approach is not practiced, because steel is a valuable and fully recyclable material. Life cycle inventory data for recycling and reusing steel components were taken from the literature (Andersen et al., 2022).

2.4 Broken concrete

The linear end-of-life practice for broken concrete is landfilling. A typical circular end-of-life practice of broken concrete is recycling at a stationary or mobile recycling plant to produce recycled aggregate, which can be used for road construction or even for concrete production – depending on the purity of raw material and consequent quality of produced recycled aggregate (Gruhler and Schiller, 2023). In the case of the linear scenario related to landfilling, system expansion includes the production of natural aggregate in a quarry as a functional equivalent of recycled aggregate produced in a circular scenario. Life cycle inventory data for recycling of broken concrete were taken from the study of Gruhler and Schiller (2023).

3 Results and discussion

3.1 GWP of end-of-life wood

The linear scenario, which considers not only the incineration of EoL wood but also the production of particle board from primary wood, shows a significantly higher impact on GWP than the circular scenario, which deals with the recycling of EoL wood to woodchips and their further utilization in the process of particle board production. GHG emissions associated with incineration of waste wood predominate. For this reason, the linear scenario shows around 4 times higher impact on GWP than the circular scenario (Table 1). In the comparative LCA

analysis, credits related to heat production during waste wood incineration (e.g., benefits beyond the system boundary) are accounted for.

The GWP of particle board produced from EoL wood and the GWP of particle board produced from primary wood are also compared. The one produced from EoL wood yields a lower impact. Both particle boards contain similar amounts of biogenic carbon, contributing to the mitigation of GWP. However, biogenic carbon was excluded from LCA, due to so-called carbon-neutral approach. The lifecycle emissions of CO₂ from bio-based products are offset by equivalent CO₂ absorption during biomass growth. From this point of view, the uptake and release of biogenic CO₂ can be omitted from the LCA (Hoxha et al., 2020).

Excluding biogenic carbon storage in the final product, particle boards produced from primary wood show almost 50% higher impact on the GWP than particle boards produced from EoL wood. Production of primary wood as a raw material is directly related to deforestation, e.g. cutting down trees, which is the main reason for the higher GWP of the particle board produced from primary wood.

Recycling EoL wood to glue-laminated timber shows a relatively low yield considering the literature data; e.g. only 26%. However, the yield (or recycling rate) depends on the contamination of the EoL wood with preservatives. Mechanical cleaning of the surfaces results in a significant share of rejects (shavings, off-cuts) and a relatively low recycling rate (Risse et al., 2019). However, when using primary wood to produce glue-laminated timber, the yield is much higher; 77% considering the literature data (Risse et al., 2019). However, a similar amount of energy is consumed in the production process of glue-laminated timber from the same amount of raw materials whether EoL wood or primary wood. For these reasons, glue-laminated timber produced from EoL wood shows higher GWP than glue-laminated timber produced from primary wood; the difference is around a factor of 6. Accounting credits associated with heat production during the incineration of shavings and off-cuts (e.g. benefits beyond system boundary), the difference in GWP between two benchmarked glue-laminated timbers is reduced to 1 versus 4.5, still in favor of glue-laminated timber produced from EoL wood. A greater amount of shavings and off-cuts is generated when using EoL wood as a raw material. The incineration of rejected parts (shavings, off-cuts) is associated with heat recovery, which results in the reduction of GWP.

When accounting incineration of EoL wood to the linear scenario, in addition to the production of glue-laminated timber from primary wood as a functional equivalent of glue-laminated timber from EoL wood in the circular scenario, the difference in GWP between the two scenarios becomes minor. It is 1 versus 1.2 in favor of the circular scenario (Table 1). The incineration of the EoL wood in the linear scenario is the main contributor to the GWP, making the linear approach relatively less sustainable regarding GWP.

3.2 GWP of end-of-life steel

Recycling of EoL steel takes place in an electric arc furnace (EAF). A 100% recycling rate was assumed in this study. Considering the reuse scenario, it was also assumed that the EoL steel component is completely reusable. The reuse includes sandblasting, landfilling of removed paint, and adding a new protective layer. LCA results showed that reuse yields around 8 times lower impact on GWP than recycling (Table 1). However, the GWP of the reuse is influenced by the surface area of the steel component. The larger the surface area per certain mass of the steel component, the more energy is required for the sandblasting and the higher the GWP.

3.3 GWP of broken concrete

LCA results show that processing pure broken concrete at a recycling plant into recycled aggregate results in a similar impact on GWP as the production of natural aggregate in a quarry. The difference in GWP is in the range of data uncertainty.

When accounting for the landfilling of pure broken concrete alongside the production of natural aggregate in a linear scenario, the difference between the two scenarios becomes significant. The linear scenario shows a double GWP impact compared to the circular scenario (Table 1). Landfilling of broken concrete is associated with the use of machinery (compactor), and the use of sealing materials, causing additional impact on GWP.

Table 1: Global warming potential of benchmarked end-of-life management scenarios, considering wood, steel, and broken concrete

	EoL wood	EoL steel	EoL broken concrete
Circular scenario (recycling)	341* / 803**	542	5.5
Circular scenario (reuse)	-	70	-
Linear scenario	1333* / 1000**	-	10.4

* considering the production of particle board

** considering the production of glue-laminated timber

4 Conclusions

The environmental benefits of circular end-of-life management practices were confirmed compared to linear end-of-life management practices for selected CDW fractions; e.g. broken concrete and waste wood. In the case of the recovered steel component, the reuse was confirmed to yield significantly lower environmental impact than recycling. Attention was given to Global Warming Potential (carbon footprint) expressed in kg of emissions equivalent to CO₂. Further research should consider other CDW fractions and evaluate additional environmental impacts, especially the abiotic depletion of minerals and metals. This is related to another crucial aspect of the circular economy, such as resource efficiency.

Acknowledgments

The research was conducted within the scope of the CirCon4Climate project, financed by the European Climate Initiative (EUKI) of the German Federal Ministry for Economic Affairs and Climate Action. Part of the research was financially supported by the Slovenian Research and Innovation Agency (research core funding No. P2-0273).

References

- Andersen, R., Stokbro Ravn, A., Walbech Ryberg, M. (2022). Environmental benefits of applying selective demolition to buildings: A case study of the reuse of façade steel cladding. *Resources, Conservation and Recycling* 184, 106430. <https://doi.org/10.1016/j.resconrec.2022.106430>.
- Broadbent, C. (2016). Steel's recyclability: demonstrating the benefits of recycling steel to achieve a circular economy. *Int J Life Cycle Assess*, 21, 1658–1665, <https://doi.org/10.1007/s11367-016-1081-1>
- Gruhler, K., Schiller, G. (2023). Grey energy impact of building material recycling – a new assessment method based on process chains. *Resources, Conservation & Recycling Advances* 18, 200139, <https://doi.org/10.1016/j.rcradv.2023.200139>.
- Guinée, J.B., Gorrée, M., Heijungs, R., Huppes, G., Kleijn, R., Koning, A. de, Oers, L. van, Wegener Sleswijk, A., Suh, S., Udo de Haes, H.A., Bruijn, H. de, Duin, R. van, Huijbregts, M.A.J. (2002). Handbook on life cycle assessment. Operational guide to the ISO standards. I: LCA

- in perspective. IIa: Guide. IIb: Operational annex. III: Scientific background. Kluwer Academic Publishers, ISBN 1-4020-0228-9, Dordrecht, 692 pp.
- Hossain, M.U., Poon, C.S. (2018). Comparative LCA of wood waste management strategies generated from building construction activities. *Journal of Cleaner Production* 177, 387-397.
- Hoxha, E., Passer, A., Saade, M.R.M., Trigaux, D., Shuttleworth, A., Pittau, F., Allacker, K., Habert, G. (2020). Biogenic carbon in buildings: a critical overview of LCA methods. *Buildings and Cities*, 1(1), 504–524. <https://doi.org/10.5334/bc.46>.
- Kabirifar, K., Mojtahedi, M., Wang, C., Tam, V. W. Y. (2020). Construction and demolition waste management contributing factors coupled with reduce, reuse, and recycle strategies for effective waste management: A review. *Journal of Cleaner Production*, 263, 121265. <https://doi.org/10.1016/j.jclepro.2020.121265>
- Liu, J., Li, Y., Wang, Z. (2023). The potential for carbon reduction in construction waste sorting: A dynamic simulation. *Energy*, 275, 127477, <https://doi.org/10.1016/j.energy.2023.127477>
- Potrč Obrecht, T., Jordan, S., Legat, A., Ruschi Mendes Saade, M., Passer, A. (2021). An LCA methodology for assessing the environmental impacts of building components before and after refurbishment. *Journal of Cleaner Production*. 327, 129527, <https://doi.org/10.1016/j.jclepro.2021.129527>.
- Risse, M., Weber-Blaschke, G., Richter, K. (2019). Eco-efficiency analysis of recycling recovered solid wood from construction into laminated timber products. *Science of The Total Environment* 661, 107-119. <https://doi.org/10.1016/j.scitotenv.2019.01.117>.
- Stahel, W. R., MacArthur, E. (2019). The Circular Economy: A User's Guide. DOI:10.4324/9780429259203
- Tonini, D., Caro, D., Cristobal, J., Foster, G., Pristera, G. (2023). Techno-economic and environmental assessment of construction and demolition waste management. With a view to support the feasibility assessment of preparation for re-use and recycling targets for individual material fractions. JRC Science for policy report.
- Zhang, C., Hu, M., Yang, X., Xicotencatl, B. M., Sprecher, B., Di Maio, F., Zhong, X., Tukker, A. (2020). Upgrading construction and demolition waste management from downcycling to recycling in the Netherlands. *Journal of Cleaner Production*, 266. <https://doi.org/10.1016/j.jclepro.2020.121718>.

EVALUATION OF THE PERFORMANCE OF CLAY-BASED BRICKS WITH THE ADDITION OF CO-COMBUSTION ASH

LEA ŽIBRET,¹ IVANA CAREVIĆ,² NINA ŠTIRMER,²
IVAN KOLODA,³ MOJCA VRČON MIHELJ,⁴
MIHA KRAGELJ,⁴ VILMA DUCMAN¹

¹ Slovenian National Building and Civil Engineering Institute, Ljubljana, Slovenia
lea.zibret@zag.si, vilma.ducman@zag.si

² University of Zagreb, Faculty of Civil Engineering, Zagreb, Croatia
ivana.carevic@grad.unizg.hr, nina.stirmer@grad.unizg.hr

³ NEXE, Dilj d.o.o., Vinkovci, Croatia
ivan.koloda@nexe.hr

⁴ Goriške opekarne d.o.o., Renče, Slovenia
mojca.vrcon@goriske.si, miha.kragelj@goriske.si

The gradual replacement of coal by local renewable resources leads to an increased production of co-combustion ashes (CC). Their disposal can be limited by their use in the construction sector, where they can partially replace primary raw materials. This study evaluates the incorporation of selected Slovenian CC ash into clay-based fired bricks within the EU AshCycle project. The tests included the measurement of water absorption, porosity, density, weight loss, shrinkage, flexural and compressive strength, and freeze-thaw resistance. Two types of clay were used to compare the influence of the selected ash on the performance of the fired samples. Replacing clay mixtures with 10 wt% CC ash reduced the compressive strength of the fired bricks but it still reached the required 10 MPa as specified in EN 772-1 (2015). The addition of CC ash to fired bricks requires careful planning of the raw mixes, taking into account various parameters that may affect the properties of the products.

DOI
[https://doi.org/
10.18690/um.fkkt.1.2025.15](https://doi.org/10.18690/um.fkkt.1.2025.15)

ISBN
978-961-286-959-5

Keywords:
fired clay bricks,
waste ashes,
raw mixture,
ceramic-technological tests,
freeze-thaw resistance



University of Maribor Press

1 Introduction

Worldwide large amounts of biomass ashes are landfilled (Insam and Knapp 2011). In accordance with the global initiatives on the gradual replacing of the fossil fuels by the renewable resources coal-combustion power plants are introducing a biomass as supplementary fuel (Sahu et al. 2014). The resulting co-combustion (CC) ashes may have various applications. One of the largest global industries, which could consume large amounts of co-combustion ashes, is brick making.

Fired clay bricks are one of the most versatile building materials in the world. Clay for brick production can be at least partially replaced by various secondary raw materials, such as dredged sediments (Božič et al. 2023), sawdust (Cultrone et al. 2020), wastewater treatment sludge (Detho et al. 2024), slags and various ashes (Zhang 2013): coal ash (Zhang 2013), MSWI ash (Haiying et al. 2011; Kirkelund et al. 2020), sewage sludge ash (Ottosen et al. 2020) and biomass ash (Eliche-Quesada et al. 2017; Šantek Bajto and Štirmer 2019). On the other hand clay supplies are limited and already running out in some parts of the world and consequently promoting the circular economy model seems crucial for the future of the brick sector (Zhang 2013). Furthermore, firing the mixture of clay and secondary raw materials at around 1000 °C can significantly reduce the leaching of heavy metals from the secondary raw materials (Ukwatta and Mohajerani 2017) what can be of importance also when utilize waste ash in clay bricks production to avoid disposal to landfills, which leads to a reduction in the cost of ash treatment and brick production (Haiying et al. 2011).

Fired bricks are usually produced by a vacuum extrusion, which ensures a homogeneous and dense structure (Krakowiak et al. 2011; Božič et al. 2023). Extruded brick samples can also be produced on a laboratory scale, which allows a direct comparison of industrial and laboratory samples (Viani et al. 2018). On the other hand, the final properties of fired bricks are strongly influenced by the composition of the raw mix. The high proportion of carbonates in the raw brick mix leads to increased weight loss during firing at temperatures of up to 950 °C and increased porosity of the fired bricks, which weakens their mechanical properties (Božič et al. 2023). Similar to carbonates, biomass ash is known as a pore-forming additive that increases the porosity of fired bricks and can contribute to the deterioration of mechanical properties (Beal et al. 2019).

As part of the EU project AshCycle - *Integration of underutilized ashes into material cycles by Industry-Urban symbiosis*, ashes from various Slovenian incineration plants were tested for their potential use in fired clay bricks. A screening of ash replacement and firing temperature in the production of extruded bricks was carried out by measuring water absorption, porosity, density, weight loss, shrinkage, flexural and compressive strength and freeze-thaw resistance. In this study two different clay mixtures were used to compare the influence of the selected CC ash on the performance of the fired samples.

2 Materials and methods

The raw materials included two types of basic clay mixes: (i) a mixture of marl (50 wt%), clay (48 %) and coal (2 wt%), provided by Goriške opekarne d.o.o. brick factory (GO) (ii) pure clay, provided by NEXE brick factory, Dilj d.o.o. (NA). The replacement of both basic clay mixes by 10 mass percent (ma%) of selected Slovenian biomass ash from the co-combustion of brown coal and wood biomass was investigated.

The particle size distribution (PSD) of ash and clays was measured by laser diffraction granulometry using a Sync+FlowSync laser particle size analyzer (Microtrack MRB) in wet dispersion measurement mode. The dispersion medium for the ash was isopropanol, while the clays were analyzed in distilled water with the addition of a dispersant. The ash was sieved to a particle size of less than 0.25 mm for this measurement.

The chemical composition of the raw materials was determined with an ARL PERFORM'X sequential X-ray fluorescence (XRF) spectrometer (Thermo Fisher Scientific Inc., Ecublens, Switzerland) using UniQuant 5 software (Thermo Fisher Scientific Inc., Waltham, MA, USA). The samples were previously ignited at 950°C for 2 hours and then mixed with Fluxana (Li tetraborate and Li metaborate in a 1:1 mass ratio) at a ratio of 1:10 and melted into discs. LiBr(l) (50 mL H₂O and 7.5 g LiBr(s) from Sigma Aldrich) was added to the mixture to prevent the melt from sticking to the Pt crucible.

The mineralogical composition of raw materials and bricks was performed using a PANalytical Empyrean X-ray diffractometer with CuK α radiation (wavelength CuK α 1 1.54 Å). The samples were ground to a particle size below 63 μ m. Each sample was measured from $2\theta = 4^\circ$ to 70° with an increment of 0.0130° as it was rotated. The X-ray tube was operated at 45 kV and 40 mA. Phase determination was performed using PANalytical X'Pert High Score Plus Diffraction software v. 4.8. using the structures for the phases from the ICDD PDF 4 + 2016 RDB powder diffraction files.

The brick mixtures were prepared according to Table 1. Approximately 20 kg of each mixture was shaped in three main shapes using a laboratory vacuum extruder (Karl Händle & Söhne Mühlacker, type PZVMga): cylinders (mould diameter=56.3 mm; extruded length=55 mm), prisms (mould dimensions: 54.3 mm \times 27.7 mm; extruded length=150 mm) and tiles (mould dimensions: 57.2 mm \times 9.3 mm; extruded length=150 mm). Extruded shapes were fired in a chamber furnace at 950 °C, with a heating rate of 150 °C/h and a dwelling time of 2h.

The compressive strength was measured on fired cylinders using a ToniNORM (ToniTechnik, Berlin, Germany) at a force rate of 0.5 kN/s, while the bending strength was measured on fired prisms using a Gabbrielli tile strength tester (Gabbrielli, s.r.l., Calenzano, Italy). Compressive strength was measured on five specimens and bending strength on seven specimens (both results are average values). Drying and firing shrinkage was calculated from the difference in the length of the 50 mm lines impressed on the fresh prisms before/after firing (seven samples, two measurements for each; the reported result is an average of 14 values). The density of the fired prisms was calculated from the measured dimensions and mass. Water absorption was determined after the prisms had been boiled in water for two hours (the cooled samples were weighed). Freeze-thaw resistance was determined according to SIST EN 539-2 (2013). The samples were dried at (110 ± 5) °C, pre-saturated by gradual immersion in water and subjected to 150 freeze/thaw cycles in a temperature range between (-16 ± 3) °C and $(+13 \pm 3)$ °C.

Extruded tiles were cut into smaller samples (57.2 mm \times 9.3 mm \times 25 mm) for firing in the gradient furnace. The samples were heated to 1134 °C at a heating rate of 150 °C/h and a dwelling time of 20 minutes. The water absorption of the samples fired in the gradient furnace was determined after gradual immersion in distilled water

(immersion of $\frac{1}{4}$ of the length per hour, 4 hours) and subsequent boiling for two hours.

Samples of extruded bricks were cast in epoxy resin and dry polished. The prepared polished cross-sections were coated with a carbon layer of approximately 15 nm thickness and examined by SEM and EDXS using a JEOL IT500 LV SEM equipped with an Ultim Max detector (Oxford Instruments) operated in high vacuum mode with an accelerating voltage of 15 kV. EDXS was performed using Aztec 5.0 SP1 software (Oxford Instruments Nanotechnology Tools Ltd).

Table 1: The extruded mixtures.

sample designation	CC ash (wt%)	clay GO (wt%)	clay NA (wt%)
G-O	-	100	-
G-1	10	90	-
N-0	-	-	100
N-1	10	-	90

3 Results and discussion

3.1 Characterization of the raw materials

Clay GO had the finest granulation with the highest percentage of particles less than $2\ \mu\text{m}$ in diameter. However, the GO clay also had some larger particles, whereas the Našice clay had a unimodal distribution. The CC ash had a similar distribution to the GO clay, but with a lower percentage of particles smaller than $2\ \mu\text{m}$ (Figure 1).

The mineralogical composition of the raw materials is shown in Figure 2. Both clays contained illite/muscovite, chlorite, feldspars and quartz. The NA clay showed higher intensities of clay minerals than the GO clay. Clay mix GO had an intense calcite peak related to the marl content (Figure 2). This was also evident in the chemical composition, namely clay mix GO had a higher CaO content compared to clay mix NA (Table 2). The main crystal phases of CC ash were quartz, calcite, anhydrite, lime, periclase and hematite, with minor amounts of brownmillerite and portlandite.

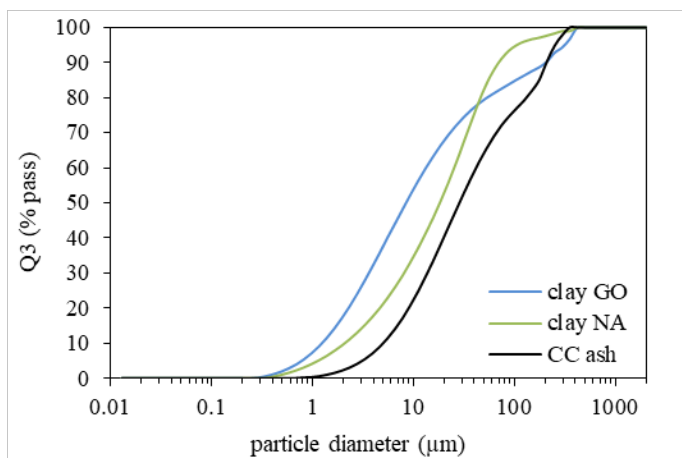


Figure 1: Cumulative particle size distribution (PSD) of clay mixes (clay GO, clay NA) and co-combustion (CC) ash, determined by laser diffraction.

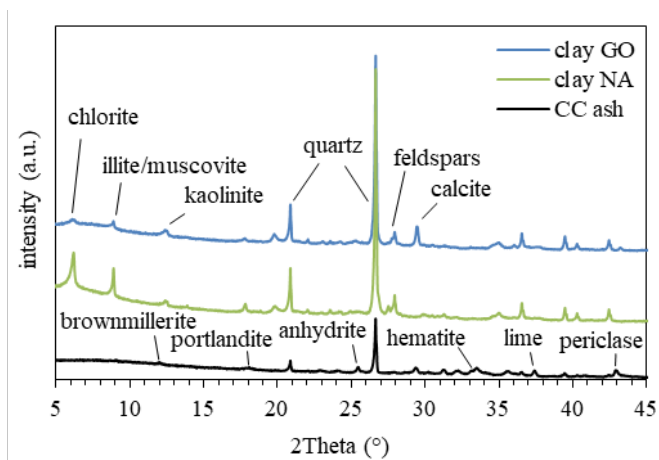


Figure 2: XRD patterns of clay mixes (clay GO, clay NA) and co-combustion (CC) ash.

Table 2: Chemical composition of raw materials measured by XRF (LOI = loss on ignition at 950 °C).

units	LOI	Na ₂ O	MgO	Al ₂ O ₃	SiO ₂	SO ₃	K ₂ O	CaO	TiO ₂	Fe ₂ O ₃	other
	wt%	wt%	wt%	wt%	wt%	wt%	wt%	wt%	wt%	wt%	wt%
clay GO	8.97	0.84	1.71	15.63	59.04	0.20	2.24	4.07	0.70	6.00	0.61
clay NA	6.22	1.07	1.40	16.77	64.35	b.d.l.	2.17	0.84	0.95	5.57	0.66
CC ash	16.30	0.35	8.18	10.70	28.21	1.70	2.22	19.98	0.53	10.57	1.26

3.2 Ceramic technological tests

The physical and mechanical properties of the bricks after drying and firing at 950 °C are shown in Table 3. Mixture N-0 had a higher drying shrinkage than mixture G-0. The 10 wt% replacement of clay GO with ash resulted in a lower drying shrinkage, while for clay Našice a 10 wt % ash did not significantly change the drying shrinkage of the samples, despite the high water demand (moisture content) of mixture N-1 (Table 3).

The effect of the firing temperature on shrinkage and water absorption is shown in Figure 3. The mixtures with clay NA showed a higher water absorption and lower firing shrinkage than mixtures with clay GO. For example, the shrinkage and water absorption of the pure clay NA sample (sample N-0) at 940 °C were 0.0% and 13.9%, while the shrinkage and water absorption of the sample with clay GO (sample G-0) at 940 °C were 1.0% and 13.0%. The water absorption increased significantly when 10 wt % CC ash was incorporated into both mixtures. Thus, the water absorption of the clay NA sample (sample N-1) at 940 °C was 23.2%, while the water absorption of the sample with clay GO (sample G-1) at 940 °C was 20.5%. The firing shrinkage was only slightly lower the when clay mixtures were replaced by 10 wt % CC ash.

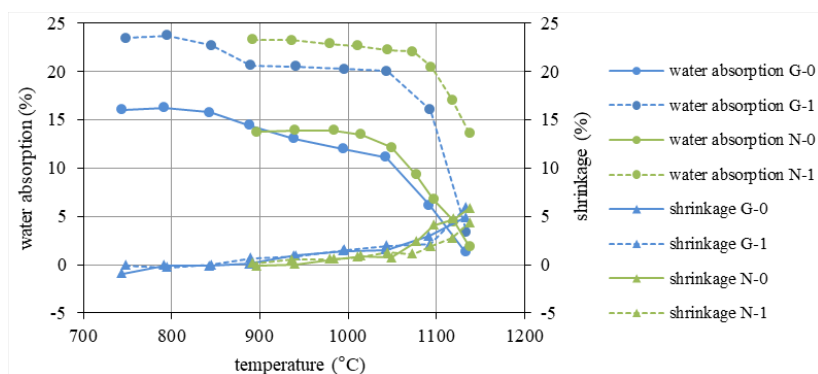


Figure 3: Water absorption and shrinkage of the samples, fired in gradient kiln.

The fired sample G-0 (with marl) had a higher compressive and flexural strength than the fired sample N-0, which did not contain marl. However, when clay mixes were replaced by 10 wt % CC ash, the G-1 bricks (with marl) had a slightly lower

compressive strength than the N-1 bricks. Incorporated ash reduced the density of the fired products, regardless of the clay type (Table 3).

Table 3: Properties of bricks after drying and firing at 950 °C and freeze-thaw resistance.

	CC ash (wt %)	moist. per wet mass during extrusion (%)	drying shrink. by length (%)	firing shrink. by length (%)	water absorption (%)	density (g/cm ³)	bending strength (MPa)	compressive strength (MPa)	freeze/thaw resistance
G-0	0	18.8	7.8	0.2	11.8	1.89	17	72.6	yes
G-1	10	21.6	5.6	0.2	21.5	1.63	6.9	27.3	yes
N-0	0	20.4	9.2	0.7	13.3	1.88	12.7	42.1	yes
N-1	10	25.8	9.3	0.1	23.2	1.6	5.6	34.7	no

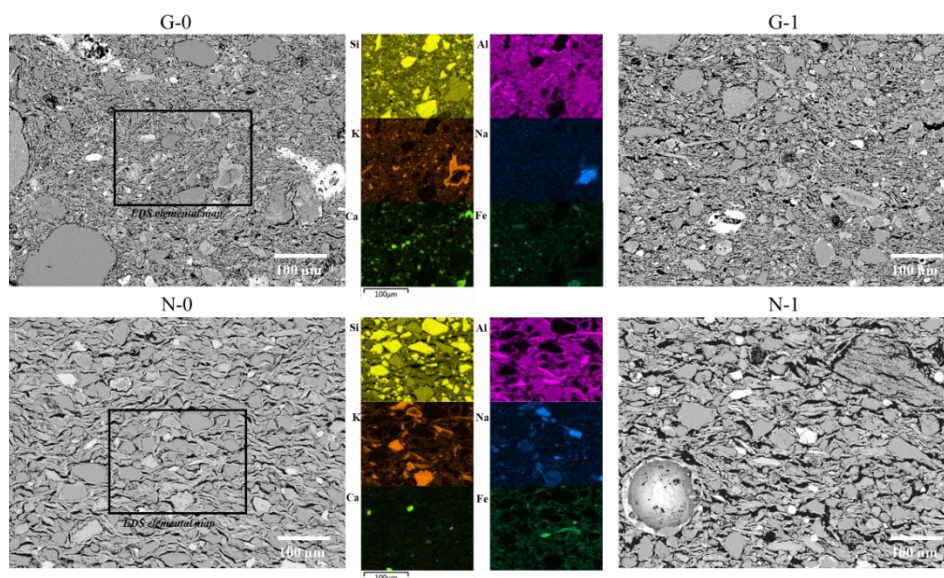


Figure 4: SEM micrographs of the fired bricks and EDXS elemental maps for the selected areas.

The fired bricks N-0 and N-1 showed a higher open porosity than G-0 and G-1 (Figure 4). Electron microscopy confirmed the increased porosity of the sample N-0 and N-1 compared to samples G-0 and G-1 (Figure 4). The homogeneously distributed elongated pores in N-0 and N-1 are most likely due to the higher clay mineral content in the clay mixture NA (Figure 2) and the shrinkage associated with the evaporation of physically bound water in clay. Sample N-1 had the highest open porosity (Table 3). As a result, the thinnest N-1 specimens (tiles) cracked during

room drying and were the source of new surface cracks during the freeze/thaw test (Table 3, Figure 5). In addition, the clay mix NA with 10 wt% ash (N-1) was very difficult to knead and required high moisture (Table 3), as the ash content of 10 wt% is too high for this type of clay. Nevertheless, the compressive strengths of all samples exceeded the 10 MPa limit specified in EN 772-1(2015).

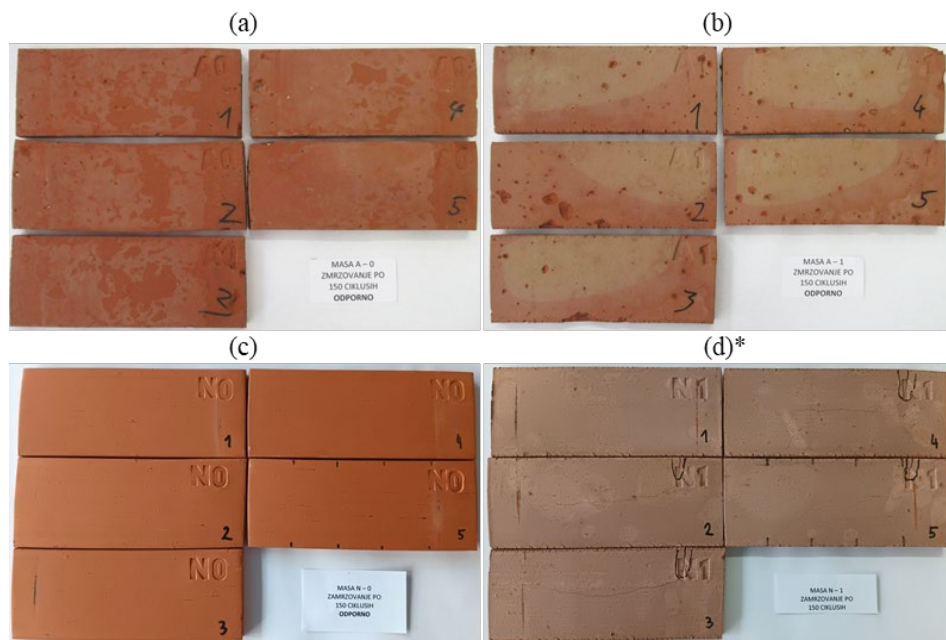


Figure 5: Bricks, fired at 950 °C, after 150 freeze/thaw cycles: (a) G-0, (a) G-1, (c) N-0, (d) N-1. * The circled cracks were formed during drying and are not related to freeze/thaw deformation.

4 Conclusions

Although the replacement of pure clay or clay with marl by 10 wt% CC ash reduced the compressive strength of the fired bricks, it was still above the 10 MPa limit specified in EN 772-1 (2015). The reduction in strength was less when pure clay was used than when clay with marl was used. However, the mixture of pure clay with 10 wt% ash was very difficult to knead as the ash content of 10 wt% is too high for this type of clay. Higher clay mineral content promoted shrinkage associated with evaporation of physically bound water in the clay. This resulted in cracking during

drying and poorer freeze-thaw resistance. The incorporation of CC ash into fired bricks requires careful design of the raw mixtures, taking into account various factors that can affect the properties of the products.

Acknowledgments

This research has received funding from the European Union under the AshCycle project, grant agreement no. 101058162, and partial support from the Slovenian Research and Innovation Agency (ARIS) under research core grant no. P2-0273.

Data availability

The data presented in this study are openly available from the repository DiRRROS at link: <http://hdl.handle.net/20.500.12556/DiRRROS-20922>.

References

- Beal, B., Selby, A., Atwater, C., James, C., Viens, C., Almquist, C. (2019). A Comparison of Thermal and Mechanical Properties of Clay Bricks Prepared with Three Different Pore-Forming Additives: Vermiculite, Wood Ash, and Sawdust. *Environmental Progress and Sustainable Energy* 38, 13150. <https://doi.org/10.1002/ep.13150>
- Božič, M., Žibret, L., Kvočka, D., Pranjic, A. M., Gregorc, B., Ducman, V. (2023). Drava river sediment in clay brick production: Characterization, properties, and environmental performance. *Journal of Building Engineering* 71, 106470. <https://doi.org/10.1016/j.jobee.2023.106470>
- Cultrone, G., Aurrekoetxea, I., Casado, C., Arizzi, A. (2020). Sawdust recycling in the production of lightweight bricks: How the amount of additive and the firing temperature influence the physical properties of the bricks. *Construction and Building Materials* 235, 117436. <https://doi.org/10.1016/j.conbuildmat.2019.117436>
- Detho, A., Kadir, A. A., Ahmad, S. (2024). Utilization of wastewater treatment sludge in the production of fired clay bricks: An approach towards sustainable development. *Results in Engineering* 21, 101708. <https://doi.org/10.1016/j.rineng.2023.101708>
- Eliche-Quesada, D., Felipe-Sesé, M. A., Martínez-Martínez, S., Pérez-Villarejo, L. (2017). Comparative Study of the Use of Different Biomass Bottom Ash in the Manufacture of Ceramic Bricks. *Journal of Materials in Civil Engineering* 29, 04017238. [https://doi.org/10.1061/\(ASCE\)MT.1943-5533.0002078](https://doi.org/10.1061/(ASCE)MT.1943-5533.0002078)
- Haiying, Z., Youcai, Z., Jingyu, Q. (2011). Utilization of municipal solid waste incineration (MSWI) fly ash in ceramic brick: Product characterization and environmental toxicity. *Waste Management* 31, 331–341. <https://doi.org/10.1016/j.wasman.2010.10.017>
- Insam, H., Knapp, B. A. (eds) (2011). Recycling of Biomass Ashes. *Springer Berlin Heidelberg, Berlin, Heidelberg*
- Kirkelund, G. M., Skevi, L., Ottosen, L. M. (2020). Electrodialytically treated MSWI fly ash use in clay bricks. *Construction and Building Materials* 254, 119286. <https://doi.org/10.1016/j.conbuildmat.2020.119286>
- Krakowiak, K. J., Lourenço, P. B., Ulm, F. J. (2011). Multitechnique Investigation of Extruded Clay Brick Microstructure. *Journal of the American Ceramic Society* 94, 3012–3022. <https://doi.org/10.1111/j.1551-2916.2011.04484.x>

- Ottosen, L. M., Bertelsen, I. M. G., Jensen, P. E., Kirkelund, G. M. (2020). Sewage sludge ash as resource for phosphorous and material for clay brick manufacturing. *Construction and Building Materials* 249, 118684. <https://doi.org/10.1016/j.conbuildmat.2020.118684>
- Sahu, S. G., Chakraborty, N., Sarkar, P. (2014). Coal–biomass co-combustion: An overview. *Renewable and Sustainable Energy Reviews* 39, 575–586. <https://doi.org/10.1016/j.rser.2014.07.106>
- Šantek Bajto, J., Štirmer, N. (2019). Possibilities of wood biomass ash use in brick production. In: *5th Symposium on Doctoral Studies in Civil Engineering, University of Zagreb Faculty of Civil Engineering*, pp 81–93
- Ukwatta, A., Mohajerani, A. (2017). Leachate analysis of green and fired-clay bricks incorporated with biosolids. *Waste Management* 66, 134–144. <https://doi.org/10.1016/j.wasman.2017.04.041>
- Viani, A., Ševčík, R., Appavou, M. S., Radulescu, A. (2018). Evolution of fine microstructure during firing of extruded clays: A small angle neutron scattering study. *Applied Clay Science* 166, 1–8. <https://doi.org/10.1016/j.clay.2018.09.002>
- Zhang, L. (2013). Production of bricks from waste materials – A review. *Construction and Building Materials* 47, 643–655. <https://doi.org/10.1016/j.conbuildmat.2013.05.043>
- (2013) SIST EN 539-2. Clay roofing tiles for discontinuous laying-Determination of physical characteristics-Part 2: Test for frost resistance
- (2015) SIST EN 772-1. Methods of test for masonry units Determination of compressive strength





7TH INTERNATIONAL CONFERENCE ON TECHNOLOGIES & BUSINESS MODELS FOR CIRCULAR ECONOMY: CONFERENCE PROCEEDINGS

SANJA POTRČ, MILOŠ BOGATAJ, ZDRAVKO KRAVANJA,
ZORKA NOVAK PINTARIČ (EDS.)

University of Maribor, Faculty of Chemistry and Chemical Engineering, Maribor,
Slovenija

sanja.potrc@um.si, milos.bogataj@um.si, zdravko.kravanja@um.si, zorka.novak@um.si

The 7th International Conference on Technologies & Business Models for Circular Economy (TBMCE) was organized by the Faculty of Chemistry and Chemical Engineering of the University of Maribor in collaboration with the Strategic Research and Innovation Partnership – Networks for the transition into circular economy (SRIP – Circular economy), managed by the Chamber of Commerce and Industry of the Štajerska. The event took place from September 4 to 6, 2024 in Portorož, Slovenia, at the Grand Hotel Bernardin. The conference focused on the current challenges and opportunities related to technological development and society's responsibility in the transition to a more sustainable and circular management of resources. The conference program included a round table on "Circular Economy Transition in the South-East Europe", 5 panel discussions, plenary and 2 keynote speeches as well as oral and poster presentations. The conference was held under the patronage of the Ministry of the Economy, Tourism and Sport and the Ministry of Cohesion and Regional Development. EIT RawMaterials RIS Hub Adria, SPIRIT Slovenia Business Development Agency, and Pomurje Technology Park (as part of the GREENE 4.0 and CI-Hub projects) joined us as co-organizers.

DOI
[https://doi.org/
10.18690/um.fkkt.1.2025](https://doi.org/10.18690/um.fkkt.1.2025)

ISBN
978-961-286-959-5

Keywords:
circular economy,
sustainable development,
processes and
technologies,
circular business models,
research and development



University of Maribor Press



University of Maribor

Faculty of Chemistry and
Chemical Engineering



2024

September

4 - 6

Grand Hotel Bernardin
Portorož, Slovenia